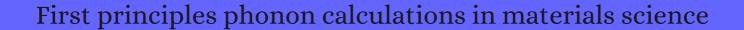
CITATION REPORT List of articles citing



DOI: 10.1016/j.scriptamat.2015.07.021 Scripta Materialia, 2015, 108, 1-5.

Source: https://exaly.com/paper-pdf/62690220/citation-report.pdf

Version: 2024-04-09

This report has been generated based on the citations recorded by exaly.com for the above article. For the latest version of this publication list, visit the link given above.

The third column is the impact factor (IF) of the journal, and the fourth column is the number of citations of the article.

#	Paper	IF	Citations
2230	An Alternative Strategy to Polymorph Recognition at Work: The Emblematic Case of Coronene.		
2229	Significant Lanthanoid Substitution Effect on the Redox Reactivity of the Oxygen-Storage Material BaYMn2O5+.		
2228	Determining and Controlling the Stoichiometry of Cu2ZnSnS4 Photovoltaics: The Physics and Its Implications.		
2227	•		
2226	Stable Ordered Phases of Cuprous Iodide with Complexes of Copper Vacancies.		
2225	•		
2224			
2223	On the Functionality of Complex Intermetallics: Frustration Chemical Pressure Relief, and Potential Rattling Atoms in Y11Ni60C6.		
2222	Understanding the Structural and Electronic Properties of Bismuth Trihalides and Related Compounds.		
2221	Anharmonic Origin of Giant Thermal Displacements in the MetalOrganic Framework UiO-67.		
2220	First-Principles Investigation of Native Interstitial Diffusion in Cr2O3.		
2219	Accelerated Discovery of New 8Electron Half-Heusler Compounds as Promising Energy and Topological Quantum Materials.		
2218	Compression Behavior of Copper Hydroxyfluoride CuOHF as a Case Study of the High-Pressure Responses of the Hydrogen-Bonded Two-Dimensional Layered Materials.		
2217	Accurate Neural Network Description of Surface Phonons in Reactive GasSurface Dynamics: N2 + Ru(0001).		
2216	Two-Dimensional Lattices of VN: Emergence of Ferromagnetism and Half-Metallicity on Nanoscale.		
2215	Interlayer-Decoupled Sc-Based Mxene with High Carrier Mobility and Strong Light-Harvesting Ability.		
2214	Revealing the Spectrum of Unknown Layered Materials with Superhuman Predictive Abilities.		

2197

2196

Non-graphene-like 12-Borophene.

Organometallic Lattices.

2213 Two-Dimensional Carbon-Based Auxetic Materials for Broad-Spectrum Metal-Ion Battery Anodes. Lone-Pair Electron-Driven Thermoelectrics at Room Temperature. Ballistic Phonons in Ultrathin Nanowires. Enhancing the Photocatalytic Performance of MXenes via Stoichiometry Engineering of Their 2210 Electronic and Optical Properties. 2209 Insight into Sodium Insertion and the Storage Mechanism in Hard Carbon. 2208 Optical Properties of Lead-Free Double Perovskites by Ab Initio Excited-State Methods. Thermal Transport in Quasi-1D van der Waals Crystal Ta2Pd3Se8 Nanowires: Size and Length 2207 Dependence. Phonon and Thermal Properties of Quasi-Two-Dimensional FePS3 and MnPS3 Antiferromagnetic 2206 Semiconductors. 2205 . 2204 Asynchronous Photoexcited Electronic and Structural Relaxation in Lead-Free Perovskites. 2203 . 2202 Above Room Temperature Ferromagnetism in Gd2B2 Monolayer with High Magnetic Anisotropy. 2201 Mechanism for Solid-State Ion Exchange of Cu+ into Zeolites. Room-Temperature Electrodeposition of Aluminum via Manipulating Coordination Structure in AlCl3 Solutions. 2199 DFT-Assisted Polymorph Identification from Lattice Raman Fingerprinting. Two-Dimensional Stoichiometric Boron Oxides as a Versatile Platform for Electronic Structure 2198 Engineering.

Design of Two-Dimensional Graphene-like Dirac Materials 12-XBeB5 (X = H, F, Cl) from

Toward Room-Temperature Magnetic Semiconductors in Two-Dimensional Ferrimagnetic

2195	Room-Temperature Ferromagnetism in Transition Metal Embedded Borophene Nanosheets.	
2194	Quantum Confined TomonagaLuttinger Liquid in Mo6Se6 Nanowires Converted from an Epitaxial MoSe2 Monolayer.	
2193	Harnessing Hot Phonon Bottleneck in Metal Halide Perovskite Nanocrystals via Interfacial ElectronPhonon Coupling.	
2192	Bottom-up Design of Three-Dimensional Carbon-Honeycomb with Superb Specific Strength and High Thermal Conductivity.	
2191	Engineering Magnetic Phases in Two-Dimensional Non-van der Waals Transition-Metal Oxides.	
2190	Magnetic Order-Induced Polarization Anomaly of Raman Scattering in 2D Magnet CrI3.	
2189	PhononGrain-Boundary-Interaction-Mediated Thermal Transport in Two-Dimensional Polycrystalline MoS2.	
2188	Unraveling Oxygen Evolution on Iron-Doped Nickel Oxyhydroxide: The Key Role of Highly Active Molecular-like Sites.	
2187	High-Pressure Synthesis of Magnetic Neodymium Polyhydrides.	
2186	Shining Light on Growth-Dependent Surface Chemistry of Organic Crystals: A Polarized Raman Spectroscopic and Computational Study of Aspirin.	
2185	Hydrogen Bonding versus Entropy: Revealing the Underlying Thermodynamics of the Hybrid OrganicInorganic Perovskite [CH3NH3]PbBr3.	
2184	Dirac points with giant spin-orbit splitting in the electronic structure of two-dimensional transition-metal carbides. 2015 , 92,	47
2183	Tuning thermal conductivity of crystalline polymer nanofibers by interchain hydrogen bonding. 2015 , 5, 87981-87986	42
2182	Thin-Shell Thickness of Two-Dimensional Materials. 2015 , 82,	34
2181	First-Principles Study of Lithiation of Type I Ba-Doped Silicon Clathrates. 2015 , 119, 28247-28257	18
2180	Pressure-Induced Phase Transition and Mechanical Properties of MgBr Intermetallics. 2016, 9,	1
2179	A New Superhard Phase and Physical Properties of ZrBIfrom First-Principles Calculations. 2016, 9,	17
2178	Multiple Dirac cones in BN co-doped Egraphyne. 2016 , 4, 7339-7344	11

Thermal Properties of EGa2O3 from First Principles. 2016 , 1, 109-114	3
2176 Ab initio lattice dynamics and thermochemistry of layered bismuth telluride (Bi2Te3). 2016 , 28, 115401	13
A First-Principles Study on the Electronic, Vibrational, and Thermodynamic Properties of Jadeite and its Tentative Low-Density Polymorph. 2016 , 642, 590-596	3
On the relationship between chemical expansion and hydration thermodynamics of proton conducting perovskites. 2016 , 4, 5917-5924	34
2173 Ground state of the U2Mo compound: Physical properties of the Ephase. 2016 , 479, 59-66	5
On the electrical properties of the Bi2Br Ir2O7 pyrochlore solid solution: Quantum ab initio and classic calculations. 2016 , 241, 173-179	
Polymorphism and electronic structure of polyimine and its potential significance for prebiotic chemistry on Titan. 2016 , 113, 8121-6	24
2170 e-TiO, a Novel Stable Polymorph of Titanium Monoxide. 2016 , 128, 1684-1689	2
2169 Electromagnon dispersion probed by inelastic X-ray scattering in LiCrO. 2016 , 7, 13547	18
2168 Creating new layered structures at high pressures: SiS. 2016 , 6, 37694	16
2167 Candidate Elastic Quantum Critical Point in LaCu_{6-x}Au_{x}. 2016 , 117, 235701	9
2166 Chapter 1 Discovery and Design of New Thermoelectric Materials. 2016 , 1-38	2
2165 Impacts of first principles calculations in engineering ceramics. 2016 , 124, 791-795	3
2164 Topological Phase in Non-centrosymmetric Material NaSnBi. 2016 , 33, 127301	6
2163 Complex optimization for big computational and experimental neutron datasets. 2016 , 27, 484002	2
Lattice thermal expansion and anisotropic displacements in ?-sulfur from diffraction experiments and first-principles theory. 2016 , 145, 234512	17
Temperature-dependent elastic and thermodynamic properties of Fe3Ga (DO3, L12, and DO19) alloys from first-principles calculations. 2016 , 253, 2236-2244	2
Phonon anharmonicity, lifetimes, and thermal transport in CH3NH3PbI3 from many-body perturbation theory. 2016 , 94,	101

2159	Determination of the basic physical properties of semiconductor chalcopyrite type MgSnT2 (T = P, As, Sb) from first-principles calculations. 2016 , 31, 1518-1531	6
2158	Coupling and competition between ferroelectricity, magnetism, strain, and oxygen vacancies in AMnO3 perovskites. 2016 , 6, 182-191	42
2157	Beyond Perturbation: Role of Vacancy-Induced Localized Phonon States in Thermal Transport of Monolayer MoS2. 2016 , 120, 29324-29331	26
2156	Novel Stable Compounds in the C-H-O Ternary System at High Pressure. 2016 , 6, 32486	19
2155	Band Gap Engineering of Two-Dimensional Nitrogene. 2016 , 6, 34177	11
2154	Tinselenidene: a Two-dimensional Auxetic Material with Ultralow Lattice Thermal Conductivity and Ultrahigh Hole Mobility. 2016 , 6, 19830	119
2153	Electric field dependence of optical phonon frequencies in wurtzite GaN observed in GaN high electron mobility transistors. 2016 , 120, 155104	8
2152	Raman signatures of inversion symmetry breaking and structural phase transition in type-II Weyl semimetal MoTe. 2016 , 7, 13552	77
2151	A new structure of two-dimensional allotropes of group V elements. 2016 , 6, 25423	32
2150	Correlated structural and electronic phase transformations in transition metal chalcogenide under high pressure. 2016 , 119, 135901	2
2149	Stable single-layer structure of group-V elements. 2016 , 94,	88
2148	Identification and properties of the non-cubic phases of Mg2Pb. 2016 , 6, 125108	1
2147	Characteristic length of phonon transport within periodic nanoporous thin films and two-dimensional materials. 2016 , 120, 065101	20
2146	Persistence of polar distortion with electron doping in lone-pair driven ferroelectrics. 2016 , 94,	38
2145	Lattice dynamics and thermal conductivity of calcium fluoride via first-principles investigation. 2016 , 119, 095103	10
2144	Hybrid crystals of cuprates and iron-based superconductors. 2016 , 25, 077402	3
2143	First-principles study of thermodynamic and stability properties of TiC-SiC alloys. 2016,	0
2142	Density-functional theory computer simulations of CZTS0.25Se0.75 alloy phase diagrams. 2016 , 145, 064704	10

(2016-2016)

2141	Importance of the Hubbard correction on the thermal conductivity calculation of strongly correlated materials: a case study of ZnO. 2016 , 6, 36875	13
2140	Ultrafast Band Engineering and Transient Spin Currents in Antiferromagnetic Oxides. 2016 , 6, 25121	5
2139	A single-volume approach for vacancy formation thermodynamics calculations. 2016 , 116, 16001	3
2138	Suppression of lattice thermal conductivity by mass-conserving cation mutation in multi-component semiconductors. 2016 , 4, 104809	8
2137	Free energy model for solid high-pressure phases of carbon. 2016 , 28, 145401	2
2136	Strain-modulated electronic and thermal transport properties of two-dimensional O-silica. 2016 , 27, 265706	13
2135	Thermal properties and thermoelasticity of L12 ordered Al3RE (RE = Er, Tm, Yb, Lu) phases: A first-principles study. 2016 , 102, 100-105	10
2134	Low-density superhard materials: computational study of Li-inserted B-substituted closo-carboranes LiBC11 and Li2B2C10. 2016 , 6, 52695-52699	2
2133	A model for understanding the formation energies of nanolamellar phases in transition metal carbides and nitrides. 2016 , 24, 055004	14
2132	Structural stability and electronic properties of AgInS2 under pressure. 2016 , 89, 1	4
2131	The electronic, optical, and thermodynamic properties of borophene from first-principles calculations. 2016 , 4, 3592-3598	250
2130	Thermoelectric properties of SnSe nanoribbons: a theoretical aspect. 2016 , 3, 035013	10
2129	Hydrostatic pressure driven spin, volume and band gap collapses in SmFeO3: a GGA + U study. 2016 , 96, 1613-1622	4
2128	Quantum Phase Transition in Germanene and Stanene Bilayer: From Normal Metal to Topological Insulator. 2016 , 7, 1919-24	26
2127	Development of n-body expansion interatomic potentials and its application for V. 2016 , 121, 67-78	17
2126	Strain-induced enhancement in the thermoelectric performance of a ZrS2 monolayer. 2016 , 4, 4538-4545	130
2125	Electronic structure and topological features of tin-based binary nanosheets and their hydrogenated/fluorinated derivatives: A first-principles study. 2016 , 382, 1-9	8
2124	An efficient ab-initio quasiharmonic approach for the thermodynamics of solids. 2016 , 120, 84-93	43

2123	Catenation of carbon in LaC2 predicted under high pressure. 2016 , 18, 14286-91	5
2122	Diffusive nature of thermal transport in stanene. 2016 , 18, 14257-63	27
2121	Few-Layer Tin Sulfide: A New Black-Phosphorus-Analogue 2D Material with a Sizeable Band Gap, Odd E ven Quantum Confinement Effect, and High Carrier Mobility. 2016 , 120, 22663-22669	94
2120	High-throughput prediction of finite-temperature properties using the quasi-harmonic approximation. 2016 , 125, 82-91	38
2119	Hydrogenated borophene as a stable two-dimensional Dirac material with an ultrahigh Fermi velocity. 2016 , 18, 27284-27289	136
2118	Tunable Negative Thermal Expansion in Layered Perovskites from Quasi-Two-Dimensional Vibrations. 2016 , 117, 115901	20
2117	Metallic and Magnetic 2D Materials Containing Planar Tetracoordinated C and N. 2016 , 120, 21685-21690	10
2116	Intrinsic magnetism in penta-hexa-graphene: A first-principles study. 2016 , 94,	11
2115	Strong correlation effect on the thermodynamic and mechanical properties of ytterbium dihydride. 2016 , 41, 21286-21292	1
2114	Strain-induced chiral symmetry breaking leads to large Dirac cone splitting in graphene/graphane heterostructure. 2016 , 94,	14
2113	Isotropic Conduction Network and Defect Chemistry in Mg Sb -Based Layered Zintl Compounds with High Thermoelectric Performance. 2016 , 28, 10182-10187	259
2112	Stable monolayer honeycomb-like structures of RuX2 (X=S,Se). 2016 , 94,	28
2111	Evolutionary design of interfacial phase change van der Waals heterostructures. 2016 , 8, 18212-18220	25
2110	First-principles study of relative stability of rutile and anatase TiO using the random phase approximation. 2016 , 18, 29914-29922	40
2109	Characterization of Few-Layer 1T' MoTe by Polarization-Resolved Second Harmonic Generation and Raman Scattering. 2016 , 10, 9626-9636	104
2108	Auxetic Black Phosphorus: A 2D Material with Negative Poisson's Ratio. 2016 , 16, 6701-6708	135
2107	Superhard Semiconducting Phase of Osmium Tetraboride Stabilizing at 11 GPa. 2016 , 120, 23165-23171	10
2106	Direct Observation of Dynamic Symmetry Breaking above Room Temperature in Methylammonium Lead Iodide Perovskite. 2016 , 1, 880-887	177

(2016-2016)

2105	Insight into the collective vibrational modes driving ultralow thermal conductivity of perovskite solar cells. 2016 , 94,	41
2104	Lattice dynamics and electronic structures of Ti3C2O2 and Mo2TiC2O2 (MXenes): The effect of Mo substitution. 2016 , 124, 8-14	69
2103	Estimates of crystalline LiF thermal conductivity at high temperature and pressure by a Green-Kubo method. 2016 , 94,	13
2102	Evolution of lattice dynamics in ferroelectric hexagonal REInO3(RE = Ho, Dy, Tb, Gd, Eu, Sm) perovskites. 2016 , 3, 075703	11
2101	Ab initio study of the effect of vacancies on the thermal conductivity of boron arsenide. 2016 , 94,	53
2100	Topological ferroelectricity in layered perovskite LaTaO4: A first principles study. 2016 , 247, 31-35	6
2099	Modeling non-harmonic behavior of materials from experimental inelastic neutron scattering and thermal expansion measurements. 2016 , 28, 385201	4
2098	Chemical Pressure-Driven Incommensurability in CaPd5: Clues to High-Pressure Chemistry Offered by Complex Intermetallics. 2016 , 55, 6781-93	11
2097	Hosting of La3+ guest ions in type-I Ge clathrates: A first-principles characterization for thermoelectric applications. 2016 , 122, 46-56	3
2096	Anharmonicity in the High-Temperature Cmcm Phase of SnSe: Soft Modes and Three-Phonon Interactions. 2016 , 117, 075502	104
2096		104
	Interactions. 2016, 117, 075502 Anisotropic thermal motion in transition-metal carbonyls from experiments and ab initio theory.	
2095	Interactions. 2016, 117, 075502 Anisotropic thermal motion in transition-metal carbonyls from experiments and ab initio theory. 2016, 45, 13680-5 Carbon-rich icosahedral boron carbides beyond B4C and their thermodynamic stabilities at high	14
2095	Anisotropic thermal motion in transition-metal carbonyls from experiments and ab initio theory. 2016 , 45, 13680-5 Carbon-rich icosahedral boron carbides beyond B4C and their thermodynamic stabilities at high temperature and pressure from first principles. 2016 , 94,	14
2095 2094 2093	Anisotropic thermal motion in transition-metal carbonyls from experiments and ab initio theory. 2016, 45, 13680-5 Carbon-rich icosahedral boron carbides beyond B4C and their thermodynamic stabilities at high temperature and pressure from first principles. 2016, 94, Static and Dynamical Properties of heavy actinide Monopnictides of Lutetium. 2016, 6, 29309	14 16 14
2095 2094 2093 2092	Anisotropic thermal motion in transition-metal carbonyls from experiments and ab initio theory. 2016, 45, 13680-5 Carbon-rich icosahedral boron carbides beyond B4C and their thermodynamic stabilities at high temperature and pressure from first principles. 2016, 94, Static and Dynamical Properties of heavy actinide Monopnictides of Lutetium. 2016, 6, 29309 Revealing the hidden structural phases of FeRh. 2016, 94, The stability of aluminium oxide monolayer and its interface with two-dimensional materials. 2016,	14 16 14 21
2095 2094 2093 2092 2091 2090	Anisotropic thermal motion in transition-metal carbonyls from experiments and ab initio theory. 2016, 45, 13680-5 Carbon-rich icosahedral boron carbides beyond B4C and their thermodynamic stabilities at high temperature and pressure from first principles. 2016, 94, Static and Dynamical Properties of heavy actinide Monopnictides of Lutetium. 2016, 6, 29309 Revealing the hidden structural phases of FeRh. 2016, 94, The stability of aluminium oxide monolayer and its interface with two-dimensional materials. 2016, 6, 29221 Activation of New Raman Modes by Inversion Symmetry Breaking in Type II Weyl Semimetal	14 16 14 21 39

2087	Thermal transport in van der Waals solids from first-principles calculations. 2016, 94,	67
2086	Mechanism of polysulfide immobilization on defective graphene sheets with N-substitution. 2016 , 110, 207-214	68
2085	Crystal structures and dynamical properties of dense CO2. 2016 , 113, 11110-11115	23
2084	Design of Li1+2xZn1⊠PS4, a new lithium ion conductor. 2016 , 9, 3272-3278	81
2083	Investigation of novel crystal structures of Bi-Sb binaries predicted using the minima hopping method. 2016 , 18, 29771-29785	28
2082	Phonon transport in the ground state of two-dimensional silicon and germanium. 2016 , 6, 69956-69965	12
2081	Organised chaos: entropy in hybrid inorganic-organic systems and other materials. 2016 , 7, 6316-6324	49
2080	Emergence of Dirac and quantum spin Hall states in fluorinated monolayer As and AsSb. 2016 , 93,	25
2079	Estimates of the thermal conductivity and the thermoelectric properties of PbTiO3 from first principles. 2016 , 93,	13
2078	Two competing soft modes and an unusual phase transition in the stuffed tridymite-type oxide BaAl2O4. 2016 , 93,	11
2077	Orthogonal tight-binding model for the thermal conductivity of Si. 2016 , 93,	11
2076	Mermin-Wagner theorem, flexural modes, and degraded carrier mobility in two-dimensional crystals with broken horizontal mirror symmetry. 2016 , 93,	55
2075	First-principles calculation and experimental investigation of lattice dynamics in the rare-earth pyrochlores R2Ti2O7 (R=Tb,Dy,Ho). 2016 , 93,	20
2074	Charge transfer and electron-phonon coupling in monolayer FeSe on Nb-doped SrTiO3. 2016 , 93,	30
2073	Second-order structural transition in the superconductor La3Co4Sn13. 2016 , 93,	13
2072	Electronic properties of 8Pmmn borophene. 2016 , 93,	87
2071	Strain-Mediated Modification of Phagraphene Dirac Cones. 2016 , 120, 17101-17105	11
2070	Single and bilayer bismuthene: Stability at high temperature and mechanical and electronic properties. 2016 , 94,	224

2069	Anomalous Temperature Dependence of the Band Gap in Black Phosphorus. 2016 , 16, 5095-101	64
2068	Tailoring Vacancies Far Beyond Intrinsic Levels Changes the Carrier Type and Optical Response in Monolayer MoSe2-x Crystals. 2016 , 16, 5213-20	85
2067	The hydrogen-induced structural stability and promising electronic properties of molybdenum and tungsten dinitride nanosheets: a first-principles study. 2016 , 4, 7485-7493	24
2066	Elastic and Thermodynamic Properties of Complex Mg-Al Intermetallic Compounds via Orbital-Free Density Functional Theory. 2016 , 5,	20
2065	Effect of thermal lattice expansion on the stacking fault energies of fcc Fe and Fe75Mn25 alloy. 2016 , 93,	15
2064	Stability of the Btructure of transition elements. 2016 , 93,	15
2063	Origin of ferroelectric polarization in tetragonal tungsten-bronze-type oxides. 2016 , 93,	30
2062	Phonon-Assisted Resonant Tunneling of Electrons in Graphene-Boron Nitride Transistors. 2016 , 116, 186603	63
2061	Dimensionality-driven phonon softening and incipient charge density wave instability in TiS 2. 2016 , 115, 47001	31
2060	An atomically thin layer of Ru/MoS heterostructure: structural, electronic, and magnetic properties. 2016 , 18, 32528-32533	6
2059	Ab initio study of the phononic origin of negative thermal expansion. 2016 , 94,	7
2058	The thermodynamic scale of inorganic crystalline metastability. 2016 , 2, e1600225	352
2057	Density functional theory study of bulk and single-layer magnetic semiconductor CrPS4. 2016 , 94,	36
2056	Superconductivity of novel tin hydrides (Sn(n)H(m)) under pressure. 2016 , 6, 22873	29
2055	Bonding-restricted structure search for novel 2D materials with dispersed C2 dimers. 2016 , 6, 29531	13
2054	Microscopic origin of entropy-driven polymorphism in hybrid organic-inorganic perovskite materials. 2016 , 94,	39
2053	Evaluation of Shear-Slip Transitions in Crystalline Aspirin by Density-Functional Theory. 2016 , 16, 6867-6873	11
2052	Structures of Nanoalloy Clusters AunAln (n = 1110) and the Growth Patterns to the Bulk Phase. 2016 , 120, 25588-25595	8

2051	Phononic Structure Engineering: the Realization of Einstein Rattling in Calcium Cobaltate for the Suppression of Thermal Conductivity. 2016 , 6, 30530	1
2050	Heptagraphene: Tunable Dirac Cones in a Graphitic Structure. 2016 , 6, 33220	3
2049	Unravelling the fundamentals of thermal and chemical expansion of BaCeO from first principles phonon calculations. 2016 , 18, 31296-31303	7
2048	Comparative study of phonon spectrum and thermal expansion of graphene, silicene, germanene, and blue phosphorene. 2016 , 94,	61
2047	Ising-Type Magnetic Ordering in Atomically Thin FePS. 2016 , 16, 7433-7438	412
2046	Ultrafast carrier dynamics in BiVO4 thin film photoanode material: interplay between free carriers, trapped carriers and low-frequency lattice vibrations. 2016 , 4, 18516-18523	45
2045	Direct calculation of the linear thermal expansion coefficients of MoS2 via symmetry-preserving deformations. 2016 , 94,	34
2044	A general forcefield for accurate phonon properties of metal-organic frameworks. 2016 , 18, 29316-29329	26
2043	Two-dimensional shape memory graphene oxide. 2016 , 7, 11972	26
2042	First-principles approach to thin superconducting slabs and heterostructures. 2016 , 94,	3
2041	Extent of hydrogen coverage of Si(001) under chemical vapor deposition conditions from ab initio approaches. 2016 , 144, 204706	9
2040	Giant Phonon Anharmonicity and Anomalous Pressure Dependence of Lattice Thermal Conductivity in Y2Si2O7 silicate. 2016 , 6, 29801	16
2039	Boundary scattering effect on the thermal conductivity of nanowires. 2016 , 31, 074004	7
2038	Control change cause analysis for engine fault diagnosis. 2016 ,	1
2037	Investigation of the bipolar effect in the thermoelectric material CaMg2Bi2 using a first-principles study. 2016 , 18, 16566-74	47
2036	First-principles investigation of LaGaO3 and LaInO3 lanthanum perovskite oxides. 2016 , 96, 2040-2058	13
2035	FeO2 and FeOOH under deep lower-mantle conditions and Earth's oxygen-hydrogen cycles. 2016 , 534, 241-4	169
2034	A first-principles study of stable few-layer penta-silicene. 2016 , 18, 18486-92	38

2033	New opportunities for materials informatics: Resources and data mining techniques for uncovering hidden relationships. 2016 , 31, 977-994	133
2032	A Honeycomb BeN2 Sheet with a Desirable Direct Band Gap and High Carrier Mobility. 2016 , 7, 2664-70	72
2031	Ammonothermal Synthesis, Crystal Structure, and Properties of the Ytterbium(II) and Ytterbium(III) Amides and the First Two Rare-Earth-Metal Guanidinates, YbC(NH)3 and Yb(CN3H4)3. 2016 , 55, 6161-8	13
2030	Strain enhancement of acoustic phonon limited mobility in monolayer TiS3. 2016 , 18, 14434-41	24
2029	Istructure in steel: A first-principles study. 2016 , 684, 624-627	16
2028	Large Spin-Valley Polarization in Monolayer MoTe2 on Top of EuO(111). 2016 , 28, 959-66	183
2027	e-TiO, a Novel Stable Polymorph of Titanium Monoxide. 2016 , 55, 1652-7	35
2026	Tuning band inversion symmetry of buckled III-Bi sheets by halogenation. 2016 , 27, 055704	30
2025	Thermochemical properties of rare-earth oxyhydrides from first principles phonon calculations. 2016 , 6, 9822-9826	4
2024	Computational searching for new stable graphyne structures and their electronic properties. 2016 , 98, 404-410	29
2023	Neutron powder diffraction and theory-aided structure refinement of rubidium and cesium ureate. 2016 , 71, 431-438	5
2022	New nanostructured phases with reversible hydrogen storage capability in immiscible magnesium girconium system produced by high-pressure torsion. 2016 , 108, 293-303	54
2021	Effect of Cu doping on Ba0.5Sr0.5Fe1⊠CuxO3□perovskites for solid oxide fuel cells: A first-principles study. 2016 , 311, 13-20	14
2020	Interlayer Interactions in van der Waals Heterostructures: Electron and Phonon Properties. 2016 , 8, 6286-92	53
2019	Magnetostructural phase transition assisted by temperature in Ag-MnO2: a density functional theory study. 2016 , 18, 7442-8	4
2018	Enhanced piezoelectricity and half-metallicity of fluorinated AlN nanosheets and nanoribbons: a first-principles study. 2016 , 4, 1517-1526	16
2017	The influence of liquid Pb-Bi on the anti-corrosion behavior of Fe3O4: a first-principles study. 2016 , 18, 7789-96	4
2016	Insight into the Vibrational and Thermodynamic Properties of Layered Lithium Transition-Metal Oxides LiMO2 (M = Co, Ni, Mn): A First-Principles Study. 2016 , 120, 5876-5882	20

2015	H-Bond Isomerization in Crystalline Cellulose IIII: Proton Hopping versus Hydroxyl Flip-Flop. 2016 , 5, 50-54	6
2014	Kinetics stabilized doping: computational optimization of carbon-doped anatase TiO2 for visible-light driven water splitting. 2016 , 18, 2776-83	13
2013	Two-Dimensional SiS Layers with Promising Electronic and Optoelectronic Properties: Theoretical Prediction. 2016 , 16, 1110-7	110
2012	Understanding the thermodynamic pathways of SnO-to-SnO x phase transition. 2016 , 111, 359-365	19
2011	A new interatomic pair potential for the modeling of crystalline Li2SiO3. 2017 , 118, 218-225	7
2010	Computational Search for Novel Hard Chromium-Based Materials. 2017, 8, 755-764	50
2009	Design of Lead-Free Inorganic Halide Perovskites for Solar Cells via Cation-Transmutation. 2017 , 139, 2630-2638	490
2008	Lattice dynamics and thermal conductivity of cesium chloride via first-principles investigation. 2017 , 254, 31-36	11
2007	Electronic characteristics of p-type transparent SnO monolayer with high carrier mobility. 2017 , 401, 114-119	28
2006	Vacancies and Vacancy-Mediated Self Diffusion in Cr2O3: A First-Principles Study. 2017 , 121, 1817-1831	20
2005	Atomistic Modeling-Based Design of Novel Materials . 2017 , 19, 1600688	10
2004	Dehydrogenation of goethite in Earth's deep lower mantle. 2017 , 114, 1498-1501	63
2003	Tetrel Bonds in Infinite Molecular Chains by Electronic Structure Theory and Their Role for Crystal Stabilization. 2017 , 121, 1381-1387	13
2002	Calculation of Phonon Spectra of Two-Dimensional Crystals of Molybdenum Disulfide and Ditelluride. 2017 , 83, 1035-1038	
2001	Lattice thermal conductivity of TixZryHf1\(\mathbb{D}\) NiSn half-Heusler alloys calculated from first principles: Key role of nature of phonon modes. 2017 , 95,	59
2000	Thermodynamic modelling of Ti-Zr-N system. 2017 , 56, 102-107	16
1999	Estimating carrier relaxation times in the BaGaGe clathrate in the extrinsic regime. 2017 , 19, 3010-3018	8
1998	A possible new family of unconventional high temperature superconductors. 2017 , 62, 212-217	10

1997	Novel hybrid C/BN two-dimensional heterostructures. 2017 , 28, 085205	3
1996	Anomalously low electronic thermal conductivity in metallic vanadium dioxide. 2017 , 355, 371-374	208
1995	First-principles study on structural, thermal, mechanical and dynamic stability of T'-MoS. 2017 , 29, 095702	11
1994	Raman signature and phonon dispersion of atomically thin boron nitride. 2017 , 9, 3059-3067	104
1993	Structural, electrical, phonon, and optical properties of Ti- and V-doped two-dimensional MoS2. 2017 , 674, 157-163	23
1992	Two-Dimensional Excitonic Photoluminescence in Graphene on a Cu Surface. 2017 , 11, 3207-3212	9
1991	Prediction of thermodynamically stable Li-B compounds at ambient pressure. 2017 , 19, 8471-8477	5
1990	Lattice dynamics calculations based on density-functional perturbation theory in real space. 2017 , 215, 26-46	27
1989	First-principles calculations on elastic and entropy properties in FeRh alloys. 2017 , 195, 156-158	4
1988	Ti3BN monolayer: the MXene-like material predicted by first-principles calculations. 2017 , 7, 11834-11839	5
1987	Extracting Crystal Chemistry from Amorphous Carbon Structures. 2017 , 18, 873-877	63
1986	Bismuth based half-Heusler alloys with giant thermoelectric figures of merit. 2017 , 5, 6131-6139	42
1985	Atypically small temperature-dependence of the direct band gap in the metastable semiconductor copper nitride Cu3N. 2017 , 95,	27
1984	Reinvestigation of Mechanical Properties and Shear-Induced Atomic Deformation of Tetragonal Superhard Semiconducting OsB4. 2017 , 121, 6290-6299	5
1983	Antiferroelectric instability in the kagome francisites Cu3Bi(SeO3)2O2X (X=Cl,Br). 2017 , 95,	19
1982	Novel bonding patterns and optoelectronic properties of the two-dimensional SixCy monolayers. 2017 , 5, 3561-3567	29
1981	Small compressive strain-induced semiconductor the taltransition and tensile strain-enhanced thermoelectric properties in monolayer PtTe2. 2017 , 32, 055004	19
1980	Role of orbital filling on nonlinear ionic Raman scattering in perovskite titanates. 2017 , 95,	10

1979	First-principles study of the effect of (111) strain on octahedral rotations and structural phases of LaAlO3. 2017 , 95,	14
1978	Thermodynamic stability and properties of boron subnitrides from first principles. 2017 , 95,	10
1977	Two-dimensional topological crystalline quantum spin Hall effect in transition metal intercalated compounds. 2017 , 95,	8
1976	Prediction of Two-Dimensional Phase of Boron with Anisotropic Electric Conductivity. 2017 , 8, 1224-1228	32
1975	New type of quantum spin Hall insulators in hydrogenated PbSn thin films. 2017 , 7, 42410	2
1974	Modulation of the electronic and mechanical properties of phagraphene via hydrogenation and fluorination. 2017 , 19, 11771-11777	32
1973	Thermodynamics of Phase Selection in MnO Framework Structures through Alkali Intercalation and Hydration. 2017 , 139, 2672-2681	114
1972	The microscopic origin of low thermal conductivity for enhanced thermoelectric performance of Yb doped MgAgSb. 2017 , 128, 227-234	30
1971	A computational assessment of the electronic, thermoelectric, and defect properties of bournonite (CuPbSbS) and related substitutions. 2017 , 19, 6743-6756	30
1970	Unerwartete Ge-Ge-Kontakte in der zweidimensionalen Phase Ge4Se3Te und Analyse ihres chemischen Ursprungs mittels Energiedichte(DOE)-Funktion. 2017 , 129, 10338-10342	1
1969	Thermal transport in novel carbon allotropes with sp2 or sp3 hybridization: An ab initio study. 2017 , 95,	32
1968	Ultrafast Structure Switching through Nonlinear Phononics. 2017 , 118, 054101	51
1967	Stability, electronic and thermodynamic properties of aluminene from first-principles calculations. 2017 , 409, 85-90	40
1966	Prediction of Single-Wall Boron Nanotube Structures and the Effects of Hydrogenation. 2017 , 121, 5841-5847	8
1965	Thermal transport across metal silicide-silicon interfaces: An experimental comparison between epitaxial and nonepitaxial interfaces. 2017 , 95,	20
1964	Chemical and Lattice Stability of the Tin Sulfides. 2017 , 121, 6446-6454	52
1963	Thermal transport and anharmonic phonons in strained monolayer hexagonal boron nitride. 2017 , 7, 43956	15
1962	Unexpected Ge-Ge Contacts in the Two-Dimensional Ge Se Te Phase and Analysis of Their Chemical Cause with the Density of Energy (DOE) Function. 2017 , 56, 10204-10208	45

1961	Tuning Electronic Properties of Monolayer Hexagonal Boron Phosphide with Group III I V I V Dopants. 2017 , 121, 4583-4592	38
1960	High Thermoelectric Performance in n-Doped Silicon-Based Chalcogenide Si2Te3. 2017 , 29, 3723-3730	29
1959	Engineering the strongly correlated properties of bulk Ruddlesden-Popper transition metal oxides via self-doping. 2017 , 19, 11373-11379	4
1958	Transformation of monolayer MoS2 into multiphasic MoTe2: Chalcogen atom-exchange synthesis route. 2017 , 10, 2761-2771	11
1957	Cu-In Halide Perovskite Solar Absorbers. 2017 , 139, 6718-6725	226
1956	Improved Electrochemical Phase Diagrams from Theory and Experiment: The NiWater System and Its Complex Compounds. 2017 , 121, 9782-9789	92
1955	Chemical Bonding at High Pressure. 2017 , 1-41	1
1954	Insights into the thermoelectric properties of SnSe from ab initio calculations. 2017 , 19, 12804-12815	32
1953	Theoretical Study on the Negative Thermal Expansion Perovskite LaCuFeO: Pressure-Triggered Transition of Magnetism, Charge, and Spin State. 2017 , 56, 6371-6379	7
1952	Thermo-elastic behavior of grossular garnet at high pressures and temperatures. 2017 , 102, 851-859	26
1951	Intrinsic ferromagnetism and quantum anomalous Hall effect in a CoBr monolayer. 2017 , 19, 13432-13437	23
1950	Neutron diffraction study of superconductingLa3Ni2B112N3E 2017, 716, 251-258	
1949	Phase evolution of lithium intercalation dynamics in 2H-MoS. 2017 , 9, 7533-7540	58
1948	Atomic motions in the layered copper pseudochalcogenide CuNCN indicative of a quantum spin-liquid scenario. 2017 , 29, 235701	5
1947	Persistence of Mixed and Non-intermediate Valence in the High-Pressure Structure of Silver(I,III) Oxide, AgO: A Combined Raman, X-ray Diffraction (XRD), and Density Functional Theory (DFT) Study. 2017 , 56, 5804-5812	16
1946	On the influence of junction structures on the mechanical and thermal properties of carbon honeycombs. 2017 , 119, 278-286	44
1945	Lattice dynamics of the tin sulphides SnS, SnS and SnS: vibrational spectra and thermal transport. 2017 , 19, 12452-12465	108
1944	Borophane as a Benchmate of Graphene: A Potential 2D Material for Anode of Li and Na-Ion Batteries. 2017 , 9, 16148-16158	101

1943	Understanding the electronic and phonon transport properties of a thermoelectric material BiCuSeO: a first-principles study. 2017 , 19, 12913-12920	29
1942	Accurate Neural Network Description of Surface Phonons in Reactive Gas-Surface Dynamics: N + Ru(0001). 2017 , 8, 2131-2136	103
1941	Ground-State Structure of YN2 Monolayer Identified by Global Search. 2017 , 121, 10258-10264	26
1940	Bottom-up Design of Three-Dimensional Carbon-Honeycomb with Superb Specific Strength and High Thermal Conductivity. 2017 , 17, 179-185	65
1939	Intrinsically low thermal conductivity from a quasi-one-dimensional crystal structure and enhanced electrical conductivity network via Pb doping in SbCrSe3. 2017 , 9, e387-e387	26
1938	Defect segregation to grain boundaries in BaZrO3 from first-principles free energy calculations. 2017 , 5, 13421-13429	21
1937	Sn2Se3: A conducting crystalline mixed valent phase change memory compound. 2017 , 121, 225106	8
1936	Hydrogen-Bonding Evolution during the Polymorphic Transformations in CH3NH3PbBr3: Experiment and Theory. 2017 , 29, 5974-5981	51
1935	Ternary Gold Hydrides: Routes to Stable and Potentially Superconducting Compounds. 2017 , 139, 8740-8751	32
1934	Structural stability and the electronic properties of a (SiH)O-formed siloxene sheet: a computational study. 2017 , 19, 18030-18035	5
1933	Two-dimensional honeycomb hafnene monolayer: stability and magnetism by structural transition. 2017 , 9, 10038-10043	5
1932	First-principles investigation of intrinsic defects and self-diffusion in ordered phases of VC. 2017 , 29, 245403	10
1931	Universal Method for Large-Scale Synthesis of Layered Transition Metal Dichalcogenides. 2017 , 23, 10177-101	8166
1930	Oxygen-Rich Lithium Oxide Phases Formed at High Pressure for Potential Lithium-Air Battery Electrode. 2017 , 4, 1600453	17
1929	First Principles Theory of the hcp-fcc Phase Transition in Cobalt. 2017 , 7, 3778	57
1928	How Chemical Composition Alone Can Predict Vibrational Free Energies and Entropies of Solids. 2017 , 29, 6220-6227	69
1927	Structural properties and mechanical stability of lithium-ion based materials. A theoretical study. 2017 , 136, 271-279	6
1926	Computational Dissection of Two-Dimensional Rectangular Titanium Mononitride TiN: Auxetics and Promises for Photocatalysis. 2017 , 17, 4466-4472	71

(2017-2017)

1925	Electronic and thermoelectric properties of Mg 2 Ge x Sn 1 $\frac{1}{2}$ k (x = 0.25, 0.50, 0.75) solid solutions by first-principles calculations. 2017 , 26, 066103	4
1924	The investigation of electronic, mechanical and lattice dynamical properties of PdCoX (X = Si and Ge) half-Heusler metallics in ⊞and ßtructural phases: an ab initio study. 2017 , 97, 2237-2254	8
1923	Modeling ferroelectric film properties and size effects from tetragonal interlayer in Hf1⊠ZrxO2 grains. 2017 , 121, 205304	38
1922	First principles study of electronic, phonon and elastic properties of rock-salt-phase MTe (M´=´Mg, Ca, Sr, Ba). 2017 , 11, 69-76	2
1921	Pressure-induced phase transition and electronic properties of MgB2C2. 2017 , 121, 195102	3
1920	The investigation of electronic, magnetic, mechanical, and lattice dynamical properties of PdMX(M = Cr, Fe andX = Si and Ge) ferromagnetic half-Heusler metallics: anab initiostudy. 2017 , 4, 066504	11
1919	A scheme for the generation of Fe P networks to search for low-energy LiFePO4 crystal structures. 2017 , 5, 14611-14618	9
1918	First-principles study on structural, electronic, vibrational and thermodynamic properties of $Sr10(PO4)6X2$ (X = F, Cl, Br). 2017 , 7, 30310-30319	3
1917	Mechanical, elastic and thermodynamic properties of crystalline lithium silicides. 2017, 134, 48-57	4
1916	Double-layer ice from first principles. 2017 , 95,	20
1915	Stability and strength of atomically thin borophene from first principles calculations. 2017, 5, 399-407	109
1914	Theoretical prediction of a graphene-like structure of indium nitride: A promising excellent material for optoelectronics. 2017 , 7, 169-178	16
1913	Nb-H system at high pressures and temperatures. 2017 , 95,	27
1912	Composition and temperature-dependent phase transition in miscible MoWTe single crystals. 2017 , 7, 44587	41
1911	Investigation of a Quantum Monte Carlo Protocol To Achieve High Accuracy and High-Throughput	
1911	Materials Formation Energies. 2017 , 13, 1943-1951	17
		23
	Materials Formation Energies. 2017 , 13, 1943-1951 Mode decomposition based on crystallographic symmetry in the band-unfolding method. 2017 , 95,	

1907	Structural, Electronic, and Optical Properties of Cu2NiSnS4: A Combined Experimental and Theoretical Study toward Photovoltaic Applications. 2017 , 29, 3133-3142	61
1906	Lattice dynamics and ferroelectric properties of the nitride perovskite LaWN3. 2017 , 95,	20
1905	Structural Complexity and Phonon Physics in 2D Arsenenes. 2017 , 8, 1375-1380	34
1904	High accuracy and transferability of a neural network potential through charge equilibration for calcium fluoride. 2017 , 95,	48
1903	On-the-fly parameterization of internal coordinate force constants for quasi-Newton geometry optimization in atomistic calculations. 2017 , 133, 71-81	4
1902	Neutron filter efficiency of beryllium and magnesium fluorides. 2017 , 50, 441-450	3
1901	Metastable cubic tin sulfide: A novel phonon-stable chiral semiconductor. 2017 , 5, 036101	36
1900	Structural phase transition, electronic, elastic, and vibrational properties of LiAl intermetallic compound: insights from first-principles calculations. 2017 , 95, 691-698	1
1899	Carbon-rich carbon nitride monolayers with Dirac cones: Dumbbell C4N. 2017 , 118, 285-290	30
1898	Embedded and DFT Calculations on the Crystal Structures of Small Alkanes, Notably Propane. 2017 , 17, 1636-1646	15
1897	First-Principles Calculations on the Crystal/Electronic Structure and Phase Stability of H-Doped SrFeO2. 2017 , 121, 7478-7484	1
1896	Quartic Dispersion, Strong Singularity, Magnetic Instability, and Unique Thermoelectric Properties in Two-Dimensional Hexagonal Lattices of Group-VA Elements. 2017 , 17, 2589-2595	24
1895	Large gap two dimensional topological insulators: the bilayer triangular lattice TlM (M = N, P, As, Sb). 2017 , 5, $4268-4274$	5
1894	Competing Structural Instabilities in the Ruddlesden P opper Derivatives HRTiO4 (R = Rare Earths): Oxygen Octahedral Rotations Inducing Noncentrosymmetricity and Layer Sliding Retaining Centrosymmetricity. 2017 , 29, 656-665	19
1893	Electronic properties and stability phase diagrams for cubic BN surfaces. 2017 , 43, 267-275	4
1892	Rational Design of Two-Dimensional Metallic and Semiconducting Spintronic Materials Based on Ordered Double-Transition-Metal MXenes. 2017 , 8, 422-428	115
1891	Pressure-Induced Multiferroics via Pseudo Jahn¶eller Effects and Novel Couplings. 2017, 27, 1604513	22
1890	Electronic and vibrational properties of transition metal-oxides: Comparison of GGA, GGA + U, and hybrid approaches. 2017 , 669, 1-8	6

1889	Lattice thermal conductivities and thermoelectric performances of binary tin-based sheets: A computational study. 2017 , 396, 1164-1169	6
1888	Interatomic potential that describes martensitic phase transformations in pure lithium. 2017 , 129, 202-210	6
1887	Few-layer arsenic trichalcogenides: Emerging two-dimensional semiconductors with tunable indirect-direct band-gaps. 2017 , 699, 554-560	23
1886	Stability and electronic properties of two-dimensional indium iodide. 2017 , 95,	7
1885	Dataset on the structure and thermodynamic and dynamic stability of MoScAlC from experiments and first-principles calculations. 2017 , 10, 576-582	2
1884	Impact of Vacancies on the Mechanical Properties of Ultraincompressible, Hard Rhenium Subnitrides: Re2N and Re3N. 2017 , 29, 2542-2549	15
1883	A first-principle study of the structural, elastic, lattice dynamical and thermodynamic properties of #Fe16C2 and #Fe16N2 phases. 2017 , 128, 278-286	13
1882	Electrolyte-controlled discharge product distribution of Na-O batteries: a combined computational and experimental study. 2017 , 19, 2940-2949	13
1881	First-principles modeling of molecular crystals: structures and stabilities, temperature and pressure. 2017 , 7, e1294	108
1880	The Interplay of Long Range Interactions and Electron Density Distributions in Polar and Strongly Correlated Materials. 2017 , 30, 91-96	4
1879	Quantifying Thermal Disorder in Metal-Organic Frameworks: Lattice Dynamics and Molecular Dynamics Simulations of Hybrid Formate Perovskites. 2017 , 121, 421-429	12
1878	What will freestanding borophene nanoribbons look like? An analysis of their possible structures, magnetism and transport properties. 2017 , 19, 1054-1061	28
1877	Exchange-Hole Dipole Dispersion Model for Accurate Energy Ranking in Molecular Crystal Structure Prediction. 2017 , 13, 441-450	47
1876	Surface functionalization of molybdenum dinitride nanosheets by halogen and alkali atoms: a first-principles study. 2017 , 5, 683-689	8
1875	Electronic and Optical Properties of Two-Dimensional GaN from First-Principles. 2017, 17, 7345-7349	101
1874	A two-dimensional TiB monolayer exhibits planar octacoordinate Ti. 2017 , 9, 17983-17990	28
1873	Silicon clathrates for photovoltaics predicted by a two-step crystal structure search. 2017 , 111, 173904	8
1872	Atomic Reconfiguration of van der Waals Gaps as the Key to Switching in GeTe/SbTe Superlattices. 2017 , 2, 6223-6232	48

1871	Superconductivity in ultra-thin carbon nanotubes and carbyne-nanotube composites: An ab-initio approach. 2017 , 125, 509-515	11
1870	Benzene-like N6 rings in a Be2N6 monolayer: a stable 2D semiconductor with high carrier mobility. 2017 , 5, 11515-11521	10
1869	Coupling of quantum well states and phonons in thin multilayer Pb films on Si(111). 2017 , 96,	5
1868	Exchange-Hole Dipole Dispersion Model for Accurate Energy Ranking in Molecular Crystal Structure Prediction II: Nonplanar Molecules. 2017 , 13, 5332-5342	24
1867	Compressive strain induced dynamical stability of monolayer 1T-MX2 ($M = Mo, W; X = S, Se$). 2017 , 4, 115018	8
1866	Soft phonon mode dynamics in Aurivillius-type structures. 2017 , 96,	12
1865	Prediction for electronic, vibrational and thermoelectric properties of chalcopyrite AgX(X=In,Ga)Te: PBE + U approach. 2017 , 4, 170750	10
1864	N-Functionalized MXenes: ultrahigh carrier mobility and multifunctional properties. 2017 , 19, 28710-28717	34
1863	Abnormal negative thermal expansion of sodium: A first-principles discovery at high pressures. 2017 , 96,	6
1862	Theoretical investigation on electronic and mechanical properties of ternary actinide (U, Np, Pu) nitrides. 2017 , 122, 115109	7
1861	Electronic, Magnetic, and Catalytic Properties of Thermodynamically Stable Two-Dimensional Transition-Metal Phosphides. 2017 , 29, 8892-8900	49
1860	Pseudo-topotactic conversion of carbon nanotubes to T-carbon nanowires under picosecond laser irradiation in methanol. 2017 , 8, 683	130
1859	Theoretical design of solid electrolytes with superb ionic conductivity: alloying effect on Li+transportation in cubic Li6PA5X chalcogenides. 2017 , 5, 21846-21857	55
1858	Novel Multiferroic Phases and Phenomena in Epitaxial (111) BiFeO3 Films. 2017 , 3, 1700332	4
1857	Exploration of Stable Strontium Phosphide-Based Electrides: Theoretical Structure Prediction and Experimental Validation. 2017 , 139, 15668-15680	57
1856	Nanostructured topological state in bismuth nanotube arrays: inverting bonding-antibonding levels of molecular orbitals. 2017 , 9, 16638-16644	4
1855	Anab initiostudy on the investigation of structural, electronic, mechanical and lattice dynamical properties of theM2AXtypeMAXphases Sc2AlB0.5C0.5, Sc2AlB0.5N0.5and Sc2AlC0.5N0.5compounds. 2017 , 4, 106520	9
1854	Doping-controlled phase transitions in single-layer MoS2. 2017 , 96,	47

(2017-2017)

1853	High Thermoelectric Performance of Ag9GaSe6 Enabled by Low Cutoff Frequency of Acoustic Phonons. 2017 , 1, 816-830	142
1852	Accelerated ageing of molybdenum oxide. 2017 , 4, 115502	1
1851	Fragment approach to the electronic structure of Eboron allotrope. 2017 , 95,	5
1850	Thermal conductivity of thermoelectric material ECu2Se: Implications on phonon thermal transport. 2017 , 111, 163903	9
1849	Epicycle method for elasticity limit calculations. 2017 , 95,	8
1848	Thermodynamic foundations of applications of ab initio methods for determination of the adsorbate equilibria: hydrogen at the GaN(0001) surface. 2017 , 19, 29676-29684	13
1847	Hydrogen functionalization induced two-dimensional ferromagnetic semiconductor in Mn di-halide systems. 2017 , 19, 29516-29524	5
1846	Lattice thermal expansion and anisotropic displacements in urea, bromomalonic aldehyde, pentachloropyridine, and naphthalene. 2017 , 147, 074112	15
1845	Raman Spectra of Polycrystalline CeO2: A Density Functional Theory Study. 2017 , 121, 20834-20849	157
1844	Elastic, vibrational, and thermodynamic properties of Sr 10 (PO 4) 6 F 2 and Ca 10 (PO 4) 6 F 2 from first principles. 2017 , 26, 086301	1
1843	Orientation-dependent properties of epitaxially strained perovskite oxide thin films: Insights from first-principles calculations. 2017 , 95,	16
1842	New phases of 3d-transition metalderium binary compounds: an extensive structural search. 2017 , 7, 40486-40498	10
1841	Creation of half-metallic f-orbital Dirac fermion with superlight elements in orbital-designed molecular lattice. 2017 , 96,	9
1840	Magnetic domain configuration of (111)-oriented LaFeO3 epitaxial thin films. 2017 , 5, 086107	4
1839	Structural, mechanical and electronic properties of CaB 2 C 2 at high pressure. 2017 , 118, 66001	2
1838	Prediction and synthesis of a family of atomic laminate phases with Kagomlike and in-plane chemical ordering. 2017 , 3, e1700642	104
1837	The structural phases and vibrational properties of MoWTe alloys. 2017, 4,	49
1836	Hopping processes explain linear rise in temperature of thermal conductivity in thermoelectric clathrates with off-center guest atoms. 2017 , 96,	11

1835	Intrinsic magnetism and electronic structure of graphene-like Be3C2 nanoribbons and their Si, Ge analogues: a computational study. 2017 , 5, 10728-10736	9
1834	Three-dimensional topological critical Dirac semimetal in AMgBi(A= K, Rb, Cs). 2017 , 96,	26
1833	Two-Dimensional Graphene-Gold Interfaces Serve as Robust Templates for Dielectric Capacitors. 2017 , 9, 34213-34220	20
1832	Two-Dimensional Magnetic Semiconductor in Feroxyhyte. 2017 , 9, 35368-35375	10
1831	Correlation of Fe-Based Superconductivity and Electron-Phonon Coupling in an FeAs/Oxide Heterostructure. 2017 , 119, 107003	17
1830	Emergence of charge density waves and a pseudogap in single-layer TiTe. 2017 , 8, 516	63
1829	Ab initio phonon thermal transport in monolayer InSe, GaSe, GaS, and alloys. 2017 , 28, 455706	39
1828	Prediction of Green Phosphorus with Tunable Direct Band Gap and High Mobility. 2017 , 8, 4627-4632	79
1827	Spontaneous Octahedral Tilting in the Cubic Inorganic Cesium Halide Perovskites CsSnX and CsPbX (X = F, Cl, Br, I). 2017 , 8, 4720-4726	126
1826	Strain-phonon coupling in (111)-oriented perovskite oxides. 2017 , 96,	4
	Strain-phonon coupling in (111)-oriented perovskite oxides. 2017 , 96, Theoretical study of stability and superconductivity of ScHn (n=4B) at high pressure. 2017 , 96,	31
1825		
1825	Theoretical study of stability and superconductivity of ScHn (n=4B) at high pressure. 2017 , 96,	31
1825 1824	Theoretical study of stability and superconductivity of ScHn (n=4B) at high pressure. 2017 , 96, The curious case of two dimensional Si2BN: A high-capacity battery anode material. 2017 , 41, 251-260	31 68
1825 1824 1823	Theoretical study of stability and superconductivity of ScHn (n=48) at high pressure. 2017, 96, The curious case of two dimensional Si2BN: A high-capacity battery anode material. 2017, 41, 251-260 The Ternary Post-transition Metal Carbodiimide SrZn(NCN)2. 2017, 643, 1456-1461 Strong Local-Field Enhancement of the Nonlinear Soft-Mode Response in a Molecular Crystal. 2017,	31 68 12
1825 1824 1823	Theoretical study of stability and superconductivity of ScHn (n=48) at high pressure. 2017, 96, The curious case of two dimensional Si2BN: A high-capacity battery anode material. 2017, 41, 251-260 The Ternary Post-transition Metal Carbodiimide SrZn(NCN)2. 2017, 643, 1456-1461 Strong Local-Field Enhancement of the Nonlinear Soft-Mode Response in a Molecular Crystal. 2017, 119, 097404 Comparison of approximations in density functional theory calculations: Energetics and structure of binary oxides. 2017, 96,	31 68 12 16
1825 1824 1823 1822	Theoretical study of stability and superconductivity of ScHn (n=48) at high pressure. 2017, 96, The curious case of two dimensional Si2BN: A high-capacity battery anode material. 2017, 41, 251-260 The Ternary Post-transition Metal Carbodiimide SrZn(NCN)2. 2017, 643, 1456-1461 Strong Local-Field Enhancement of the Nonlinear Soft-Mode Response in a Molecular Crystal. 2017, 119, 097404 Comparison of approximations in density functional theory calculations: Energetics and structure of binary oxides. 2017, 96,	31 68 12 16 58

1817	First-principles prediction of stabilities and instabilities of compounds and alloys in the ternary B-As-P system. 2017 , 96,	14
1816	Tunable Magnetism and Extraordinary Sunlight Absorbance in Indium Triphosphide Monolayer. 2017 , 139, 11125-11131	187
1815	Molecular simulations of cement based materials: A comparison between first principles and classical force field calculations. 2017 , 138, 392-402	21
1814	High-throughput Identification and Characterization of Two-dimensional Materials using Density functional theory. 2017 , 7, 5179	122
1813	Structures, phase transitions, and magnetic properties of Co3Si from first-principles calculations. 2017 , 96,	6
1812	Metric for strong intrinsic fourth-order phonon anharmonicity. 2017 , 95,	19
1811	Universal two-dimensional characteristics in perovskite-type oxyhydrides ATiOH (A = Li, Na, K, Rb, Cs). 2017 , 147, 034507	О
1810	Impeding phonon transport through superlattices of organic[horganic halide perovskites. 2017, 7, 37015-370	20-2
1809	Thermal conductivity of hexagonal Si and hexagonal Si nanowires from first-principles. 2017, 111, 032107	19
1808	Comparative first-principles studies of prototypical ferroelectric materials by LDA, GGA, and SCAN meta-GGA. 2017 , 96,	96
1807	Influence of Antisite Defects on the Thermoelectric Properties of Fe2VAl. 2017 , 21, 237-246	13
1806	Cage disorder and gas encapsulation as routes to tailor properties of inorganic clathrates. 2017 , 131, 475-481	5
1805	Lattice Thermal Conductivity of MgSiO Perovskite from First Principles. 2017 , 7, 5417	13
1804	Carrier-Induced Band-Gap Variation and Point Defects in Zn3N2 from First Principles. 2017 , 8,	25
1803	Representation of compounds for machine-learning prediction of physical properties. 2017, 95,	158
1802	Effect of the accuracy of interatomic force constants on the prediction of lattice thermal conductivity. 2017 , 138, 368-376	9
1801	Structural and spectroscopic comparison between polycrystalline, nanocrystalline and quantum dot visible light photo-catalyst Bi2WO6. 2017 , 254, 82-89	13
1800	Computational Prediction and Evaluation of Solid-State Sodium Superionic Conductors Na7P3X11 (X = O, S, Se). 2017 , 29, 7475-7482	43

1799	Two-Dimensional Intrinsic Half-Metals With Large Spin Gaps. 2017 , 17, 5251-5257	111
1798	Accurate and precise ab initio anharmonic free-energy calculations for metallic crystals: Application to hcp Fe at high temperature and pressure. 2017 , 96,	20
1797	The stabilization of the rocksalt structured tantalum nitride. 2017 , 122, 045109	7
1796	The pressure-temperature phase diagram of pure Co based on first-principles calculations. 2017 , 19, 22061-22068	2
1795	Properties of B4C in the shocked state for pressures up to 1.5 TPa. 2017 , 95,	10
1794	Two-Dimensional Hexagonal Sheet of TiO2. 2017 , 29, 8594-8603	51
1793	Single-layer metal halides MX2 ($X = Cl$, Br, I): stability and tunable magnetism from first principles and Monte Carlo simulations. 2017 , 5, 8734-8741	140
1792	Anomalous vibrational modes in few layer WTe 2 revealed by polarized Raman scattering and first-principles calculations. 2017 , 4, 035024	21
1791	First-principles prediction of Si-doped Fe carbide as one of the possible constituents of Earth's inner core. 2017 , 44, 8776-8784	7
1790	Atomistic Origin of Phase Stability in Oxygen-Functionalized MXene: A Comparative Study. 2017 , 121, 18947-18953	34
1789	The importance of polarizability in the modeling of ionic diffusion in ceria. 2017 , 169, 012002	0
1788	Anisotropic carrier mobility in buckled two-dimensional GaN. 2017 , 19, 23492-23496	14
1787	Energy landscape of ZnO clusters and low-density polymorphs. 2017 , 96,	18
1786	Potential thermoelectric material open framework Si24 from a first-principles study. 2017 , 50, 425501	11
1785	First-principles study of thermoelectric transport properties of monolayer gallium chalcogenides. 2017 , 50, 405301	14
1784	Monolayer BC: an ultrahigh capacity anode material for Li ion batteries. 2017 , 19, 24230-24239	17
1783	First-principles investigation of quantum emission from hBN defects. 2017 , 9, 13575-13582	122
1782	Large magnetic anisotropy and strain induced enhancement of magnetic anisotropy in monolayer TaTe. 2017 , 19, 24341-24347	27

1781	Observation of magnetoelastic effects in a quasi-one-dimensional spiral magnet. 2017, 96,	4
1780	Electronic origin of the spin-phonon coupling effect in transition-metal perovskites. 2017 , 96,	2
1779	Atomate: A high-level interface to generate, execute, and analyze computational materials science workflows. 2017 , 139, 140-152	142
1778	Structural properties and strain engineering of a BeB2 monolayer from first-principles. 2017 , 7, 38410-38414	11
1777	Structure and properties of hydrogrossular mineral series. 2017 , 100, 4317-4330	15
1776	The structural, electronic, mechanical, lattice dynamics and thermodynamic properties of Rh5B4: First-principles calculations. 2017 , 31, 1750245	
1775	Phase stability and thermodynamic properties of FeS polymorphs. 2017, 111, 317-323	6
1774	Lattice stability and the effect of Co and Re on the ideal strength of Ni: First-principles study of uniaxial tensile deformation. 2017 , 26, 093106	4
1773	Computational methods for 2D materials: discovery, property characterization, and application design. 2017 , 29, 473001	39
1772	Superhard and superconducting B6C. 2017 , 3, 76-84	9
1771	Low-temperature structure and the ferroelectric phase transitions in the CdTiO3 perovskite. 2017 , 96,	10
1770	Thermodynamic characterization of lithium monosilicide (LiSi) by means of calorimetry and DFT-calculations. 2017 , 108, 942-958	5
1769	Phase stability and mechanical properties of Mo1-xNx with 0 িk 🖟 . 2017 , 122, 195101	29
1768	Ultrafast dynamics of vibrational symmetry breaking in a charge-ordered nickelate. 2017 , 3, e1600735	8
1767	Ultrafast non-radiative dynamics of atomically thin MoSe. 2017 , 8, 1745	35
1766	High-Pressure Behavior of Silver Fluorides up to 40 GPa. 2017 , 56, 14651-14661	21
1765	Absorption and Mid-IR SHG in Two-Dimensional Halogen and Hydrogen Saturated Silicene Series. 2017 , 121, 27139-27146	10
1764	Controlling the H to T' structural phase transition via chalcogen substitution in MoTe monolayers. 2017 , 19, 31874-31882	12

1763	Hydrogen-bearing iron peroxide and the origin of ultralow-velocity zones. 2017 , 551, 494-497	78
1762	Two-Dimensional CoS monolayer with robust ferromagnetism. 2017 , 7, 15993	19
1761	Mono- and Bilayer ZnSnN2 Sheets for Visible-Light Photocatalysis: First-Principles Predictions. 2017 , 121, 26063-26068	15
1760	Fe-Cluster Compounds of Chalcogenides: Candidates for Rare-Earth-Free Permanent Magnet and Magnetic Nodal-Line Topological Material. 2017 , 56, 14577-14583	3
1759	Strain engineering of phonon thermal transport properties in monolayer 2H-MoTe. 2017 , 19, 32072-32078	45
1758	Origin of Negative Longitudinal Piezoelectric Effect. 2017 , 119, 207601	33
1757	Metal phosphides as potential thermoelectric materials. 2017 , 5, 12441-12456	35
1756	Rattling of Oxygen Ions in a Sub-Nanometer-Sized Cage Converts Terahertz Radiation to Visible Light. 2017 , 11, 12358-12364	11
1755	Two-dimensional multilayer M2CO2 (M = Sc, Zr, Hf) as photocatalysts for hydrogen production from water splitting: a first principles study. 2017 , 5, 24972-24980	53
1754	Tunable band structures in digital oxides with layered crystal habits. 2017 , 96,	
1754 1753	Tunable band structures in digital oxides with layered crystal habits. 2017 , 96, Thermal conductivity changes across a structural phase transition: The case of high-pressure silica. 2017 , 96,	9
	Thermal conductivity changes across a structural phase transition: The case of high-pressure silica.	9
	Thermal conductivity changes across a structural phase transition: The case of high-pressure silica. 2017, 96, Unusual Twisting Phonons and Breathing Modes in Tube-Terminated Phosphorene Nanoribbons	
1753 1752	Thermal conductivity changes across a structural phase transition: The case of high-pressure silica. 2017 , 96, Unusual Twisting Phonons and Breathing Modes in Tube-Terminated Phosphorene Nanoribbons and Their Effects on Thermal Conductivity. 2017 , 27, 1702776	17
1753 1752 1751	Thermal conductivity changes across a structural phase transition: The case of high-pressure silica. 2017, 96, Unusual Twisting Phonons and Breathing Modes in Tube-Terminated Phosphorene Nanoribbons and Their Effects on Thermal Conductivity. 2017, 27, 1702776 Orientational Glass Formation in Substituted Hybrid Perovskites. 2017, 29, 10168-10177	17 26
1753 1752 1751 1750	Thermal conductivity changes across a structural phase transition: The case of high-pressure silica. 2017, 96, Unusual Twisting Phonons and Breathing Modes in Tube-Terminated Phosphorene Nanoribbons and Their Effects on Thermal Conductivity. 2017, 27, 1702776 Orientational Glass Formation in Substituted Hybrid Perovskites. 2017, 29, 10168-10177 Tension-Tailored Electronic and Magnetic Switching of 2D Ti2NO2. 2017, 121, 25729-25735	17 26 24
1753 1752 1751 1750 1749	Thermal conductivity changes across a structural phase transition: The case of high-pressure silica. 2017, 96, Unusual Twisting Phonons and Breathing Modes in Tube-Terminated Phosphorene Nanoribbons and Their Effects on Thermal Conductivity. 2017, 27, 1702776 Orientational Glass Formation in Substituted Hybrid Perovskites. 2017, 29, 10168-10177 Tension-Tailored Electronic and Magnetic Switching of 2D Ti2NO2. 2017, 121, 25729-25735 Novel III-Tegraphene van der Waals heterojunctions for optoelectronic devices. 2017, 7, 32383-32390	17 26 24 6

1745	Role of Lone Pair Cations in Ferroelectric Tungsten Bronzes. 2017 , 29, 6414-6424	11
1744	Three-dimensional buckled honeycomb boron lattice with vacancies as an intermediate phase on the transition pathway from \oplus to \oplus . 2017 , 9, e400-e400	4
1743	Origins of the structural phase transitions in MoTe2 and WTe2. 2017 , 95,	71
1742	Superhard three-dimensional carbon with metallic conductivity. 2017 , 123, 311-317	45
1741	almaBTE: A solver of the spacelime dependent Boltzmann transport equation for phonons in structured materials. 2017 , 220, 351-362	124
1740	Systematic First-Principles Study of Binary Metal Hydrides. 2017 , 19, 513-523	19
1739	New group-V elemental bilayers: A tunable structure model with four-, six-, and eight-atom rings. 2017 , 96,	12
1738	Theoretical search for possible Au-Si crystal structures using a genetic algorithm. 2017 , 95,	7
1737	Phonon thermal transport in transition-metal and rare-earth nitride semiconductors from first principles. 2017 , 95,	9
1736	Anharmonic interatomic force constants and thermal conductivity from GrEeisen parameters: An application to graphene. 2017 , 96,	15
1735	Computational design of a robust two-dimensional antiferromagnetic semiconductor. 2017, 96,	13
1734	GeAs2: A IV☑ Group Two-Dimensional Semiconductor with Ultralow Thermal Conductivity and High Thermoelectric Efficiency. 2017 , 29, 6261-6268	57
1733	Finite-temperature properties of nonmagnetic transition metals: Comparison of the performance of constraint-based semilocal and nonlocal functionals. 2017 , 95,	32
1732	First-principles description of van der Waals bonded spin-polarized systems using the vdW-DF+U method: Application to solid oxygen at low pressure. 2017 , 95,	5
1731	Ab initio prediction of the high-pressure phase diagram of BaBiO3. 2017 , 96,	5
1730	Predicted Realization of Cubic Dirac Fermion in Quasi-One-Dimensional Transition-Metal Monochalcogenides. 2017 , 7,	44
1729	Combined Computational and in Situ Experimental Search for Phases in an Open Ternary system, Ba R u B . 2017 , 29, 5841-5849	6
1728	The Preferable F2dd Phase for Ca(BH4)2 Crystal Under Hydrostatic Pressures. 2017 , 46, 3479-3483	

1727	Frustrated magnetism and caloric effects in Mn-based antiperovskite nitrides: Ab initio theory. 2017 , 95,	32
1726	First-principles investigation on crystal structure and physical properties of HfB4. 2017 , 723, 802-810	14
1725	Theoretical prediction of thermal transport in BC 2 N monolayer. 2017 , 38, 249-256	32
1724	Periodic Arrays of Phosphorene Nanopores as Antidot Lattices with Tunable Properties. 2017 , 11, 7494-7507	29
1723	Nonlinear Electron-Phonon Coupling in Doped Manganites. 2017 , 118, 247601	23
1722	EGraphene: A New Metallic Allotrope of Planar Carbon with Potential Applications as Anode Materials for Lithium-Ion Batteries. 2017 , 8, 3234-3241	109
1721	Lattice thermal transport in La3Cu3X4 compounds (X=P,As,Sb,Bi): Interplay of anharmonicity and scattering phase space. 2017 , 95,	11
1720	Oxysulfide LiAlSO: A Lithium Superionic Conductor from First Principles. 2017 , 118, 195901	46
1719	Adsorption of alkali and alkaline earth metal atoms and dimers on monolayer germanium carbide. 2017 , 97, 155-167	11
1718	Two-Dimensional Boron Crystals: Structural Stability, Tunable Properties, Fabrications and Applications. 2017 , 27, 1603300	93
1717	Effects of Fe substitution by Nb on physical properties of BaFeO3: A DFT+U study. 2017 , 126, 491-502	5
1716	Design of Mg alloys: The effects of Li concentration on the structure and elastic properties in the Mg-Li binary system by first principles calculations. 2017 , 691, 15-25	28
1715	Two-dimensional hexagonal CrN with promising magnetic and optical properties: A theoretical prediction. 2017 , 9, 621-630	48
1714	Thermoelectric properties of SnSe monolayer. 2017 , 29, 015001	62
1713	Two-dimensional As 1-x P x binary compounds: Highly tunable electronic structure and optical properties. 2017 , 17, 186-191	6
1712	When water meets iron at Earth's core than the boundary. 2017 , 4, 870-878	51
1711	Dynamic instabilities in strongly correlated VSe2 monolayers and bilayers. 2017 , 96,	51
1710	Prediction and characterization of an Mg-Al intermetallic compound with potentially improved ductility via orbital-free and Kohn-Sham density functional theory. 2017 , 25, 075002	7

, ,	Vibrational Properties of Metal Phosphorus Trichalcogenides from First-Principles Calculations. 2017 , 121, 27207-27217	36
1708	Single-bonded allotrope of nitrogen predicted at high pressure. 2017 , 96,	27
1707	Class of diatomic ferroelectrics with multifunctional properties: IV-VI compounds in the distorted NiAs-type structure. 2017 , 96,	4
1706	Pressure-Induced Phase Transition in Weyl Semimetallic WTe. 2017 , 13, 1701887	20
1705	Lattice Dynamics and Thermochemistry of Solid-State Materials from First-Principles Quantum-Chemical Calculations. 2017 , 491-526	1
1704	New Approaches to Computational Materials Science Using First Principles Methods. 2017 , 56, 234-237	
1703	Neutron total cross section calculation within the framework of quasi-harmonic approximation. 2017 , 19, 103027	2
1702	Synthesis, Crystal Structure, Polymorphism, and Magnetism of Eu(CN3H4)2 and First Evidence of EuC(NH)3. 2017 , 5, 10	12
1701	Phonon broadening in high entropy alloys. 2017 , 3,	61
1700	First-Principles Study on the Stability and STM Image of Borophene. 2017 , 12, 514	11
1699	First-principles study of the stability of NbC-SiC solid solutions. 2017,	Ο
1699 1698	First-principles study of the stability of NbC-SiC solid solutions. 2017 , Discovering charge density functionals and structure-property relationships with PROPhet: A general framework for coupling machine learning and first-principles methods. 2017 , 7, 1192	79
	Discovering charge density functionals and structure-property relationships with PROPhet: A	
1698	Discovering charge density functionals and structure-property relationships with PROPhet: A general framework for coupling machine learning and first-principles methods. 2017 , 7, 1192 Complex interplay of interatomic bonding in a multi-component pyrophosphate crystal: KMg	79
1698 1697	Discovering charge density functionals and structure-property relationships with PROPhet: A general framework for coupling machine learning and first-principles methods. 2017 , 7, 1192 Complex interplay of interatomic bonding in a multi-component pyrophosphate crystal: KMg (HPO)I2HO. 2017 , 4, 170982 First-Principles Calculations of Ti2N and Ti2NT2 (T = O, F, OH) Monolayers as Potential Anode	79 9
1698 1697 1696 1695	Discovering charge density functionals and structure-property relationships with PROPhet: A general framework for coupling machine learning and first-principles methods. 2017 , 7, 1192 Complex interplay of interatomic bonding in a multi-component pyrophosphate crystal: KMg (HPO)IDHO. 2017 , 4, 170982 First-Principles Calculations of Ti2N and Ti2NT2 (T = O, F, OH) Monolayers as Potential Anode Materials for Lithium-Ion Batteries and Beyond. 2017 , 121, 13025-13034	79 9 99
1698 1697 1696 1695	Discovering charge density functionals and structure-property relationships with PROPhet: A general framework for coupling machine learning and first-principles methods. 2017, 7, 1192 Complex interplay of interatomic bonding in a multi-component pyrophosphate crystal: KMg (HPO)IDHO. 2017, 4, 170982 First-Principles Calculations of Ti2N and Ti2NT2 (T = O, F, OH) Monolayers as Potential Anode Materials for Lithium-Ion Batteries and Beyond. 2017, 121, 13025-13034 Temperature-dependent infrared optical properties of 3C-, 4H- and 6H-SiC. 2018, 537, 194-201	79 9 99 13

1691	A controllable robust multiferroic GaTeCl monolayer with colossal 2D ferroelectricity and desirable multifunctionality. 2018 , 10, 5990-5996	34
1690	New two-dimensional V-V binary compounds with a honeycomb-like structure: a first-principles study. 2018 , 5, 035903	21
1689	Bandgap Engineering of Stable Lead-Free Oxide Double Perovskites for Photovoltaics. 2018 , 30, e1705901	38
1688	Vibrational and thermodynamic properties of LiBH4 polymorphs from first-principles calculations. 2018 , 43, 6625-6631	5
1687	Complementary evaluation of structure stability of perovskite oxides using bond-valence and density-functional-theory calculations. 2018 , 19, 101-107	18
1686	Entanglement entropy and entanglement spectrum of Bi Sb (1 1 1) bilayers. 2018 , 30, 125501	1
1685	Tip-induced local strain on MoS2/graphite detected by inelastic electron tunneling spectroscopy. 2018 , 97,	4
1684	Prediction of manganese trihalides as two-dimensional Dirac half-metals. 2018 , 97,	64
1683	Elemental Ferroelectricity and Antiferroelectricity in Group-V Monolayer. 2018, 28, 1707383	86
1682	The Role of Semilabile Oxygen Atoms for Intercalation Chemistry of the Metal-Ion Battery Polyanion Cathodes. 2018 , 140, 3994-4003	20
1681	Novel elastic, lattice dynamics and thermodynamic properties of metallic single-layer transition metal phosphides: 2H-M P (MoP, WP, NbP and TaP). 2018 , 30, 135701	4
1680	Structural predictions for Correlated Electron Materials Using the Functional Dynamical Mean Field Theory Approach. 2018 , 87, 041005	24
1679	Electronic Structure, Mechanical and Dynamical Stability of Hexagonal Subcarbides M2C (M = Tc, Ru, Rh, Pd, Re, Os, Ir, and Pt): Ab Initio Calculations. 2018 , 60, 213-224	11
1678	Epitaxial Growth of Honeycomb Monolayer CuSe with Dirac Nodal Line Fermions. 2018, 30, e1707055	72
1677	Popgraphene: a new 2D planar carbon allotrope composed of 585 carbon rings for high-performance lithium-ion battery anodes from bottom-up programming. 2018 , 6, 6815-6821	145
1676	First-principles calculations on elastic, magnetoelastic, and phonon properties of Ni 2 FeGa magnetic shape memory alloys. 2018 , 27, 016201	1
1675	Ab-initio thermodynamic and elastic properties of AlNi and AlNi3 intermetallic compounds. 2018 , 32, 1850129	13
1674	Observation of soft phonon mode in TbFe3(BO3)4 by inelastic neutron scattering. 2018 , 97,	6

2
12
23
35
4
37
102
65
12
28
18
6
61
11
11
19
4

1655	The influence of surface functionalization on thermal transport and thermoelectric properties of MXene monolayers. 2018 , 10, 8859-8868	72
1654	Resonant phonon scattering in semiconductors. 2018 , 6, 4691-4697	13
1653	Strain and ferroelectric soft-mode induced superconductivity in strontium titanate. 2018 , 97,	22
1652	Tunable ferroelectricity and anisotropic electric transport in monolayer EGeSe. 2018, 97,	49
1651	First-principles investigation of the thermodynamic stability of MB2 materials surfaces (M´=´Ti/Zr/Hf). 2018 , 101, 4118-4127	7
1650	The intrinsic low lattice thermal conductivity in the rock salt SnSe. 2018 , 148, 54-59	10
1649	A theoretical investigation of structural, electronic and optical properties of bulk copper nitrides. 2018 , 753, 576-585	7
1648	Magnetically-driven phase transformation strengthening in high entropy alloys. 2018 , 9, 1363	174
1647	Highly negative Poisson's ratio in a flexible two-dimensional tungsten carbide monolayer. 2018 , 20, 18924-18	39 30
1646	Chemical vapor deposition and phase stability of pyrite on SiO2. 2018 , 6, 4753-4759	2
1646 1645	Chemical vapor deposition and phase stability of pyrite on SiO2. 2018 , 6, 4753-4759 Lattice stability and thermal properties of Fe2VAl and Fe2TiSn Heusler compounds. 2018 ,	2
1645		92
1645	Lattice stability and thermal properties of Fe2VAl and Fe2TiSn Heusler compounds. 2018,	
1645 1644	Lattice stability and thermal properties of Fe2VAl and Fe2TiSn Heusler compounds. 2018, Highly In-Plane Optical and Electrical Anisotropy of 2D Germanium Arsenide. 2018, 28, 1707379	92
1645 1644 1643	Lattice stability and thermal properties of Fe2VAl and Fe2TiSn Heusler compounds. 2018, Highly In-Plane Optical and Electrical Anisotropy of 2D Germanium Arsenide. 2018, 28, 1707379 The High-Pressure Superconducting Phase of Arsenic. 2018, 8, 3026 Strong anharmonic phonon scattering induced giant reduction of thermal conductivity in PbTe	92
1645 1644 1643	Lattice stability and thermal properties of Fe2VAl and Fe2TiSn Heusler compounds. 2018, Highly In-Plane Optical and Electrical Anisotropy of 2D Germanium Arsenide. 2018, 28, 1707379 The High-Pressure Superconducting Phase of Arsenic. 2018, 8, 3026 Strong anharmonic phonon scattering induced giant reduction of thermal conductivity in PbTe nanotwin boundary. 2018, 97, Exploring the intrinsic ductile metastable Fe-C compounds: Complex chemical bonds, anisotropic	92 9
1645 1644 1643 1642	Lattice stability and thermal properties of Fe2VAl and Fe2TiSn Heusler compounds. 2018, Highly In-Plane Optical and Electrical Anisotropy of 2D Germanium Arsenide. 2018, 28, 1707379 The High-Pressure Superconducting Phase of Arsenic. 2018, 8, 3026 Strong anharmonic phonon scattering induced giant reduction of thermal conductivity in PbTe nanotwin boundary. 2018, 97, Exploring the intrinsic ductile metastable Fe-C compounds: Complex chemical bonds, anisotropic elasticity and variable thermal expansion. 2018, 745, 196-211 Computational prediction of a high ZT of n-type MgSb-based compounds with isotropic	92 9 23 21

(2018-2018)

Piezospectroscopy and first-principles calculations of the nitrogen-vacancy center in gallium arsenide. 2018 , 123, 161583	1
1636 Structural properties of barium stannate. 2018 , 262, 142-148	4
TiO2(B) and Anatase Angstrom-Scale Wires: A Theoretical Study. 2018 , 122, 3363-3370	4
Iron Superhydrides FeH5 and FeH6: Stability, Electronic Properties, and Superconductivity. 2018 , 122, 4731-4736	33
1633 Highly Surface-Active Ca(OH) Monolayer as a CO Capture Material. 2018 , 18, 1786-1793	17
1632 Ultrahigh Storage and Fast Diffusion of Na and K in Blue Phosphorene Anodes. 2018 , 10, 8630-8639	96
Two-Dimensional Fluorinated Boron Sheets: Mechanical, Electronic, and Thermal Properties. 2018 , 3, 1815-1822	38
1630 Solid-state electron spin lifetime limited by phononic vacuum modes. 2018 , 17, 313-317	36
Theoretical aspects in structural distortion and the electronic properties of lithium peroxide under high pressure. 2018 , 20, 9488-9497	2
1628 Magnetoelectric and Raman spectroscopic studies of monocrystalline MnCr2O4. 2018 , 97,	13
Stability, elastic and electronic properties of a novel BN sheet with extended hexagons with N-N bonds. 2018 , 30, 135002	3
1626 A new series of two-dimensional silicon crystals with versatile electronic properties. 2018 , 5, 025013	8
Ab initio calculations of ideal strength and lattice instability in W-Ta and W-Re alloys. 2018 , 97,	4
1624 Descriptors for Machine Learning of Materials Data. 2018 , 3-23	26
Understanding the Interactions between Vibrational Modes and Excited State Relaxation in Y3\(\mathbb{L}\)CexAl5O12: Design Principles for Phosphors Based on 5d\(\mathbb{L}\)f Transitions. 2018 , 30, 1865-1877	49
1622 Beyond a phenomenological description of magnetostriction. 2018 , 9, 388	33
1621 Completely flat 2D ZnO monolayer with triangle and pentangle coordinated networks. 2018 , 30, 095	301 1
Topological behaviour of ternary non-symmorphic crystals KZnX (X = P, As, Sb) under pressure and strain: a first principles study. 2018 , 20, 5084-5102	5

1619	Borophene hydride: a stiff 2D material with high thermal conductivity and attractive optical and electronic properties. 2018 , 10, 3759-3768	83
1618	Nonsymmorphic-symmetry-protected hourglass Dirac loop, nodal line, and Dirac point in bulk and monolayer X3SiTe6 ($X = Ta$, Nb). 2018 , 97,	71
1617	Quasiballistic heat removal from small sources studied from first principles. 2018 , 97,	7
1616	Theoretical potential for low energy consumption phase change memory utilizing electrostatically-induced structural phase transitions in 2D materials. 2018 , 4,	24
1615	Nature of the octahedral tilting phase transitions in perovskites: A case study of CaMnO3. 2018, 97,	21
1614	Unusual strain response of thermal transport in dimerized three-dimensional graphene. 2018 , 10, 5229-5238	15
1613	Unique Zigzag-Shaped Buckling ZnC Monolayer with Strain-Tunable Band Gap and Negative Poisson Ratio. 2018 , 57, 1958-1963	17
1612	Symmetry and structure of carbon-nitrogen complexes in gallium arsenide from infrared spectroscopy and first-principles calculations. 2018 , 123, 161553	1
1611	Novel stable structure of Li3PS4 predicted by evolutionary algorithm under high-pressure. 2018 , 8, 015008	5
1610	First-Principles Study of the Thermoelectric Properties of the Zintl Compound KSnSb. 2018 , 122, 4217-4223	16
1609	Influence of defects on the thermal conductivity of compressed LiF. 2018 , 97,	2
1608	First-principles calculations of thermal properties of the mechanically unstable phases of the PtTi and NiTi shape memory alloys. 2018 , 147, 296-303	16
1607	ZrSi: an antiferromagnetic Dirac MXene. 2018 , 20, 3946-3952	10
1606	Anion Order and Spontaneous Polarization in LaTiO_{2}N Oxynitride Thin Films. 2018, 120, 046001	20
1605	Antimony-induced heterogeneous microstructure of Mg2Si0.6Sn0.4 thermoelectric materials and their thermoelectric properties. 2018 , 739, 129-138	9
1604	Multifunctional Interlayer Based on Molybdenum Diphosphide Catalyst and Carbon Nanotube Film for Lithium-Sulfur Batteries. 2018 , 14, 1702853	108
1603	Quasi-2D silicon structures based on ultrathin Me2Si (Me = Mg, Ca, Sr, Ba) films. 2018 , 670, 51-57	8
1602	Searching for Entropically Stabilized Phases: The Case of Silver Iodide. 2018 , 122, 1786-1790	12

(2018-2018)

1601	High Seebeck Coefficient and Unusually Low Thermal Conductivity Near Ambient Temperatures in Layered Compound Yb2\(\mathbb{B}\)EuxCdSb2. 2018 , 30, 484-493	27
1600	Hidden spin polarization in the 1 T -phase layered transition-metal dichalcogenides MX 2 ($M=Zr$, Hf; $X=S$, Se, Te). 2018 , 63, 85-91	16
1599	NaCl-CsCl structural transition in Sr2PdO3 and Sr2TiO4. 2018 , 737, 230-237	1
1598	Tunable electronic and magnetic properties of graphene-like XYBe (XY = BN, AlN, SiC, GeC) nanosheets with carrier doping: a first-principles study. 2018 , 20, 6830-6837	5
1597	Bulk and surface properties of the Ruddlesden-Popper oxynitride SrTaON. 2018 , 20, 2771-2776	16
1596	Lattice dynamics of ultrathin FeSe films on SrTiO3. 2018 , 97,	21
1595	Unraveling Hidden Mg-Mn-H Phase Relations at High Pressures and Temperatures by in Situ Synchrotron Diffraction. 2018 , 57, 1614-1622	8
1594	A first-principles study of a real energetically stable MoN2 nanosheet and its tunable electronic structure. 2018 , 6, 2245-2251	16
1593	Combined experimental and ab initio based determination of the thermal expansion of La0.5Sr0.5Co0.25Fe0.75O3. 2018 , 101, 3086-3093	2
1592	Interplay of Structural and Bonding Characters in Thermal Conductivity and Born-Effective Charge of Transition Metal Dichalcogenides. 2018 , 122, 2521-2527	7
1591	Novel titanium nitride halide TiNX ($X = F$, Cl, Br) monolayers: potential materials for highly efficient excitonic solar cells. 2018 , 6, 2073-2080	51
1590	Collective-Goldstone-mode-induced ultralow lattice thermal conductivity in Sn-filled skutterudite SnFe4Sb12. 2018 , 97,	6
1589	Exotic ferromagnetism in the two-dimensional quantum material C3N. 2018 , 13, 1	7
1588	Momentum-resolved observations of the phonon instability driving geometric improper ferroelectricity in yttrium manganite. 2018 , 9, 15	18
1587	Double-Weyl Phonons in Transition-Metal Monosilicides. 2018 , 120, 016401	124
1586	Cyclopropenium (C3H3)+ as an Aromatic Alternative A-Site Cation for Hybrid Halide Perovskite Architectures. 2018 , 122, 2041-2045	9
1585	Coexistence of open and closed type nodal line topological semimetals in two dimensional B2C. 2018 , 6, 1206-1214	43
1584	Zeolite structure determination using genetic algorithms and geometry optimisation. 2018 , 211, 103-115	4

1583	First-principles study of mechanical and magnetic properties of transition metal (M) nitrides in the cubic M4N structure. 2018 , 120, 197-206	23
1582	Thermal Conductivity of Solids from First-Principles Molecular Dynamics Calculations. 2018 , 122, 10682-10690	14
1581	Ultralow Thermal Conductivity in Diamond-Like Semiconductors: Selective Scattering of Phonons from Antisite Defects. 2018 , 30, 3395-3409	16
1580	Prediction of two-dimensional nodal-line semimetals in a carbon nitride covalent network. 2018 , 6, 11252-1125	19 1
1579	Over-Stoichiometry in Heavy Metal Oxides: The Case of Iono-Covalent Tantalum Trioxides. 2018 , 57, 6057-6064	5
1578	First-principles study of lattice thermal conductivity in ZrTe5 and HfTe5. 2018 , 123, 175104	14
1577	Phonon Softening due to Melting of the Ferromagnetic Order in Elemental Iron. 2018 , 120, 187203	14
1576	Stability, Electronic and Optical Properties of M4M?X4 (M = Ga or In, M? = Si, Ge, or Sn, X = Chalcogen) Photovoltaic Absorbers. 2018 , 122, 10360-10364	3
1575	Theoretical calculation of equilibrium Mg isotope fractionations between minerals and aqueous solutions. 2018 , 488, 62-75	18
1574	EGraphyne analogues based on As and Sb elements. 2018 , 150, 325-328	
1573	Material-genome perspective towards tunable thermal expansion of rare-earth di-silicates. 2018 , 38, 3547-3554	11
1572	Role of zero-point effects in stabilizing the ground state structure of bulk FeP. 2018 , 30, 215401	3
1571	Predicting thermoelectric performance of eco-friendly intermetallic compound p-type CaMgSi from first-principles investigation. 2018 , 752, 85-92	7
1570	The ground state of two-dimensional silicon. 2018 , 5, 035010	21
1569	Mechanical strength and origin of the strengthening effect of tantalum in superhard W 0.5 Ta 0.5 B monoboride. 2018 , 44, 10463-10469	14
1568	Reproducibility of vibrational free energy by different methods. 2018 , 150, 47-53	14
1567	Independently tuning the power factor and thermal conductivity of SnSe via Ag2S addition and nanostructuring. 2018 , 6, 7959-7966	17
1566	The phonon confinement effect in two-dimensional nanocrystals of black phosphorus with anisotropic phonon dispersions. 2018 , 10, 8704-8711	12

1565	Rare earth indates (RE: La-Yb): influence of the synthesis route and heat treatment on the crystal structure. 2018 , 47, 6787-6799	8
1564	Thermal Expansion in Layered Na MO. 2018 , 8, 3988	8
1563	Identifying pragmatic quasi-harmonic electronic structure approaches for modeling molecular crystal thermal expansion. 2018 , 211, 181-207	24
1562	AI3 (A = As, Sb) Single Layers and Their vdW Heterostructure for Photocatalysis and Solar Cell Applications. 2018 , 122, 7656-7663	25
1561	Actinium Hydrides AcH, AcH, and AcH as High-Temperature Conventional Superconductors. 2018 , 9, 1920-192	26 70
1560	Electronic, magnetic, catalytic, and electrochemical properties of two-dimensional Janus transition metal chalcogenides. 2018 , 6, 8021-8029	36
1559	Robust ferroelectricity in two-dimensional SbN and BiP. 2018 , 10, 7984-7990	52
1558	Stability of the 1144 phase in iron pnictides. 2018 , 97,	11
1557	Probing lattice dynamics and electron-phonon coupling in the topological nodal-line semimetal ZrSiS. 2018 , 97,	17
1556	Relative stability of FeS2 polymorphs with the random phase approximation approach. 2018 , 6, 6606-6616	18
1555	Finite-temperature lattice dynamics and superionic transition in ceria from first principles. 2018 , 97,	9
1554	Designing Two-Dimensional KBBF Family Second-Harmonic Generation Monolayers. 2018 , 122, 7992-7996	12
1553	Rocksalt or cesium chloride: Investigating the relative stability of the cesium halide structures with random phase approximation based methods. 2018 , 97,	12
1552	A New Anisotropic Dirac Cone Material: A BS Honeycomb Monolayer. 2018 , 9, 1815-1820	49
1551	First-principles study of lithium-ion diffusion in £Li3PS4 for solid-state electrolytes. 2018 , 18, 541-545	9
1550	Exploring new two-dimensional monolayers: pentagonal transition metal borides/carbides (penta-TMB/Cs). 2018 , 6, 10226-10232	56
1549	High-capacity cathodes for magnesium lithium chlorine tri-ion batteries through chloride intercalation in layered MoS2: a computational study. 2018 , 6, 6830-6839	26
1548	Antiferromagnetic monolayer MnC with density functional theory prediction. 2018 , 30, 175301	3

1547	Origin of ultra-low lattice thermal conductivity in Cs2BiAgX6 (X=Cl, Br) and its impact on thermoelectric performance. 2018 , 748, 63-72	38
1546	Photocatalytic Activity of Phosphorene Derivatives: Coverage, Electronic, Optical, and Excitonic Properties. 2018 , 122, 7194-7202	7
1545	Finite-temperature property-maps of LiMnNiD cathode materials from ab initio calculations. 2018 , 6, 5687-5694	3
1544	Anisotropic vacancy-mediated phonon mode softening in Sm and Gd doped ceria. 2018 , 20, 10048-10059	9
1543	Two-dimensional ferroelectricity and switchable spin-textures in ultra-thin elemental Te multilayers. 2018 , 5, 521-528	68
1542	2D carbon sheets with negative Gaussian curvature assembled from pentagonal carbon nanoflakes. 2018 , 20, 9123-9129	3
1541	Effect of pressure on the Raman-active modes of zircon (ZrSiO4): a first-principles study. 2018 , 45, 173-184	8
1540	Solubility in Zr-Nb alloys from first-principles. 2018 , 144, 21-30	16
1539	Mechanical failure of graphene and the anharmonic phonon coupling mechanisms. 2018, 126, 404-409	4
1538	Phonon instability and charge density wave in U2Ti. 2018 , 730, 36-41	1
1537	Pressure-induced influence on the crystal structure, electronic structure and thermoelectric properties of NaB3: A first-principles study. 2018 , 731, 323-331	4
1536	The effect of the flexibility of hydrogen bonding network on low-frequency motions of amino acids. Evidence from Terahertz spectroscopy and DFT calculations. 2018 , 191, 8-15	12
1535	High Temperature Stability of BaZrO3: An Ab Initio Thermodynamic Study. 2018 , 255, 1700398	3
1534	Experimental and theoretical study on the structural, electrical and optical properties of tantalum-doped ZnO nanoparticles prepared via sol-gel acetate route. 2018 , 44, 703-711	13
1533	Efficient technique for computational design of thermoelectric materials. 2018 , 222, 152-157	20
1532	Physical Properties of Superhard Diamond-Like BC5 from a First-Principles Study. 2018 , 47, 272-284	4
1531	Towards band structure and band offset engineering of monolayer Mo (1 $\bar{l}k$) W (x) S 2 via Strain. 2018 , 5, 015008	19
1530	Phase stability, elastic, anisotropic properties, lattice dynamical and thermodynamic properties of B12M (M=Th, U, Np, Pu) dodecaborides. 2018 , 44, 128-135	27

1529	Fluorine-graphite intercalation compound (C4F)n at high pressure: Experimental and theoretical study. 2018 , 127, 384-391	11
1528	Impact of bi-axial strain on the structural, electronic and optical properties of photo-catalytic bulk bismuth oxyhalides. 2017 , 20, 103-111	12
1527	High-throughput search for caloric materials: the CaloriCool approach. 2018 , 51, 024002	32
1526	Unexpected ground-state structures and properties of carbon nitride C3N at ambient and high pressures. 2018 , 140, 45-53	2
1525	Recycling of zincite (ZnO) via uptake of hydrogen halides. 2018 , 20, 1221-1230	16
1524	Two-dimensional stoichiometric boron carbides with unexpected chemical bonding and promising electronic properties. 2018 , 6, 1651-1658	23
1523	Impact of Phonon Dispersion on Nonlocal Electron P honon Couplings in Organic Semiconductors: The Naphthalene Crystal as a Case Study. 2018 , 122, 44-49	10
1522	Stability and electronic structure of two-dimensional arsenic phosphide monolayer. 2018 , 228, 206-212	14
1521	Impact of Four-Valent Doping on the Crystallographic Phase Formation for Ferroelectric HfO2 from First-Principles: Implications for Ferroelectric Memory and Energy-Related Applications. 2018 , 1, 254-264	39
1520	Phonon Hydrodynamic Heat Conduction and Knudsen Minimum in Graphite. 2018 , 18, 638-649	54
1519	Electronic Structure and Thermoelectric Properties of Transition Metal Monosilicides. 2018 , 47, 3277-3281	14
1518	Ultralow and anisotropic thermal conductivity in semiconductor AsSe. 2018 , 20, 1809-1816	10
1517	Influence of water intercalation and hydration on chemical decomposition and ion transport in methylammonium lead halide perovskites. 2018 , 6, 1067-1074	64
1516	Electronic and magnetic properties of monolayer RuCl: a first-principles and Monte Carlo study. 2018 , 20, 997-1004	42
1515	Stabilizing benzene-like planar N rings to form a single atomic honeycomb BeN sheet with high carrier mobility. 2018 , 10, 949-957	13
1514	Thermo-mechanical properties of cubic titanium nitride. 2018 , 44, 415-423	7
1513	Re-exchange of Fe and Cu at the interface in sintered NdHeB magnets: A method to eliminate Fe precipitation at grain boundaries. 2018 , 382, 135-138	1
1512	Graphene hot-electron light bulb: incandescence from hBN-encapsulated graphene in air. 2018 , 5, 011006	29

1511	Tunable thermal properties in yttrium silicates switched by anharmonicity of low-frequency phonons. 2018 , 38, 2043-2052	10
1510	Strain-induced enhancement of thermoelectric performance of TiS monolayer based on first-principles phonon and electron band structures. 2018 , 29, 015204	31
1509	Lithium halide monolayer sheets: First-principles many-body calculations. 2018, 143, 103-111	20
1508	Thermodynamic Stability of Mg-Based Laves Phases. 2018 , 59, 890-896	4
1507	Directional detection of light dark matter with polar materials. 2018 , 98,	55
1506	Large magnetic anisotropy and its strain modulation in two-dimensional intrinsic ferromagnetic monolayer RuO and OsO. 2018 , 20, 28162-28168	14
1505	Phonon mode contributions to thermal conductivity of pristine and defective EGaO. 2018 , 20, 29236-29242	11
1504	Transparent Amorphous Oxide Semiconductor as Excellent Thermoelectric Materials. 2018 , 8, 462	5
1503	Vibrational properties of isotopically enriched materials: the case of calcite 2018 , 8, 33985-33992	4
1502	Thermal and thermoelectric properties of monolayer indium triphosphide (InP3): a first-principles study. 2018 , 6, 21532-21541	58
1501	Dynamical stabilization in delafossite nitrides for solar energy conversion. 2018 , 6, 20852-20860	13
1500	Hexagonal M2C3 (M = As, Sb, and Bi) monolayers: new functional materials with desirable band gaps and ultrahigh carrier mobility. 2018 , 6, 12689-12697	30
1499	Geometric structures and electronic properties of the Bi2X2Y (X, Y = 0 , S, Se, and Te) ternary compound family: a systematic DFT study. 2018 , 6, 13241-13249	13
1498	Structural search for stable Mg-Ca alloys accelerated with a neural network interatomic model. 2018 , 20, 27545-27557	10
1497	Onset of vertical bonds in new GaN multilayers: beyond van der Waals solids. 2018 , 10, 21842-21850	8
1496	First-principles calculations and experimental studies of XYZ2 thermoelectric compounds: detailed analysis of van der Waals interactions. 2018 , 6, 19502-19519	15
1495	Emergence of high piezoelectricity along with robust electron mobility in Janus structures in semiconducting Group IVB dichalcogenide monolayers. 2018 , 6, 24885-24898	70
1494	First principles study of the structural, stability properties and lattice thermal conductivity of bulk ReSe2. 2018 , 5, 10424-10430	7

1493	Chemical bonding origin of the unexpected isotropic physical properties in thermoelectric MgSb and related materials. 2018 , 9, 4716	54
1492	Unique Gap Structure and Symmetry of the Charge Density Wave in Single-Layer VSe_{2}. 2018 , 121, 196402	90
1491	Atomistic Simulations of Pure Tin Based on a New Modified Embedded-Atom Method Interatomic Potential. 2018 , 8, 900	9
1490	Dialkali-Metal Monochalcogenide Semiconductors with High Mobility and Tunable Magnetism. 2018 , 9, 6695-6701	12
1489	An Ab Initio Study of Connections between Tensorial Elastic Properties and Chemical Bonds in B(210) Grain Boundaries in NiBi. 2018 , 11,	3
1488	Prediction of novel high-pressure H2O-NaCl and carbon oxide compounds with a symmetry-driven structure search algorithm. 2018 , 98,	4
1487	Pressure Effect of the Vibrational and Thermodynamic Properties of Chalcopyrite-Type Compound AgGaSEA First-Principles Investigation. 2018 , 11,	3
1486	Electrically tunable valleytronics in quantum anomalous Hall insulating transition metal trihalides. 2018 , 98,	13
1485	Single-layer antiferromagnetic semiconductor CoS2 with pentagonal structure. 2018 , 98,	14
1484	Interlayer-Decoupled Sc-Based Mxene with High Carrier Mobility and Strong Light-Harvesting Ability. 2018 , 9, 6915-6920	23
1483	Carbon network evolution from dimers to sheets in superconducting ytrrium dicarbide under pressure. 2018 , 1,	8
1482	Heterogeneous reactions of SO on the hematite(0001) surface. 2018 , 149, 194703	6
1481	Catalytic de-halogenation of alkyl halides by copper surfaces. 2018 , 6, 7214-7224	3
1480	Recipe for Dirac Phonon States with a Quantized Valley Berry Phase in Two-Dimensional Hexagonal Lattices. 2018 , 18, 7755-7760	26
1479	Tuning the balance between dispersion and entropy to design temperature-responsive flexible metal-organic frameworks. 2018 , 9, 4899	65
1478	Electronic exchange-correlation, many-body effect issues on first-principles calculations of bulk SiC polytypes. 2018 , 32, 1850328	
1477	Metastable silica high pressure polymorphs as structural proxies of deep Earth silicate melts. 2018 , 9, 4789	24
1476	High-throughput ab initio calculations on dielectric constant and band gap of non-oxide dielectrics. 2018 , 8, 14794	10

1475	Phonon anharmonic frequency shift induced by four-phonon scattering calculated from first principles. 2018 , 124, 145101	13
1474	Electronic and Vibrational Properties of TiS2, ZrS2, and HfS2: Periodic Trends Studied by Dispersion-Corrected Hybrid Density Functional Methods. 2018 , 122, 26835-26844	21
1473	First principles calculations of the thermoelectric properties of \(\text{HMnO2}\) and \(\text{EMnO2}\). 2018 , 91, 1	5
1472	Ab initio calculation of the spin lattice relaxation time T1 for nitrogen-vacancy centers in diamond. 2018 , 98,	7
1471	Temperature effect on the phonon dispersion stability of zirconium by machine learning driven atomistic simulations. 2018 , 98,	22
1470	Hybrid Density Functional Study of Au2Cs2I6, Ag2GeBaS4, Ag2ZnSnS4, and AgCuPO4 for the Intermediate Band Solar Cells. 2018 , 11, 3457	3
1469	Ab initio inspection of thermophysical experiments for molybdenum near melting. 2018 , 8, 125012	8
1468	Ideal intersecting nodal-ring phonons in bcc C8. 2018 , 98,	27
1467	An Ab Initio Study of Pressure-Induced Reversal of Elastically Stiff and Soft Directions in YN and ScN and Its Effect in Nanocomposites Containing These Nitrides. 2018 , 8,	1
1466	First-principles investigations on structural stability, mechanical, and thermodynamic properties of La T 2 Al 20 (T = Ti, V, Cr, Nb, and Ta) intermetallic cage compounds. 2018 , 27, 126201	1
1465	Survey of ab initio phonon thermal transport. 2018 , 7, 106-120	66
1464	Machine Learning a General-Purpose Interatomic Potential for Silicon. 2018 , 8,	122
1463	Semiconducting defect-free polymorph of borophene: Peierls distortion in two dimensions. 2018 , 98,	13
1462	High-Temperature Superconductivity in a Th-H System under Pressure Conditions. 2018 , 10, 43809-43816	55
1461	Decoupling Carrier Concentration and Electron-Phonon Coupling in Oxide Heterostructures Observed with Resonant Inelastic X-Ray Scattering. 2018 , 121, 236802	14
1460	High Thermoelectric Figure of Merit via Tunable Valley Convergence Coupled Low Thermal Conductivity in AIIBIVC2V Chalcopyrites. 2018 , 122, 29150-29157	21
1459	Thermoelectric properties of four typical silicon allotropes. 2018 , 26, 085006	4
1458	Difluorophosphorane-Flattened Phosphorene through Difluorination. 2018 , 9, 6963-6966	6

1457	Spontaneous Frenkel pair formation in zirconium carbide. 2018 , 98,	3
1456	High capacity sodium-rich layered oxide cathode for sodium-ion batteries. 2018 , 27, 118801	3
1455	Predicting Dirac semimetals based on sodium ternary compounds. 2018 , 4,	9
1454	Anharmonicity-induced first-order isostructural phase transition of zirconium under pressure. 2018 , 98,	11
1453	Melting properties from ab initio free energy calculations: Iron at the Earth's inner-core boundary. 2018 , 98,	22
1452	Lattice Thermal Conductivity Calculation of Sb2Te3 using Molecular Dynamics Simulations. 2018 , 73, 1541-1545	3
1451	Bond ordering and phase transitions in Na2IrO3 under high pressure. 2018 , 98,	9
1450	Ferroelectric Problem beyond the Conventional Scaling Law. 2018 , 121, 135702	8
1449	Using the Callaway Model to Deduce Relevant Phonon Scattering Processes: The Importance of Phonon Dispersion. 2018 , 255, 1800208	4
1448	Structure Dependent Phase Stability and Thermal Expansion of Ruddlesden Popper Strontium Titanates. 2018 , 30, 7100-7110	10
1447	Cluster-Assembled Semiconductor CdO Polymorph with Good Ductility, High Carrier Mobility, and Promising Optical Properties. 2018 , 122, 24287-24294	4
1446	Optimized symmetry functions for machine-learning interatomic potentials of multicomponent systems. 2018 , 149, 124106	11
1445	Two-Dimensional Janus Transition Metal Oxides and Chalcogenides: Multifunctional Properties for Photocatalysts, Electronics, and Energy Conversion. 2018 , 10, 35289-35295	77
1444	Tunable ideal strength of ZrSe2 monolayer by charge doping. 2018 , 124, 115101	4
1443	Tuning Thermal Transport in C3N Monolayers by Adding and Removing Carbon Atoms. 2018, 10,	16
1442	High-Throughput Screening of Magnetic Antiperovskites. 2018 , 30, 6983-6991	19
1441	Hydrogen storage in MgX (X = Cu and Ni) systems - is there still news?. 2018 , 402, 394-401	11
1440	Ab initio study of the structure, isotope effects, and vibrational properties in KDP crystals. 2018 , 98,	8

1439	Saddle-Point Excitons and Their Extraordinary Light Absorption in 2D EPhase Group-IV Monochalcogenides. 2018 , 28, 1804581	18
1438	CuTe-AgTe lateral topological insulator heterojunction: stability and properties. 2018 , 29, 505711	1
1437	Tunable Electronic Structures of Hydrogenated Zigzag and Armchair Dumbbell Silicene Nanosheets: A Computational Study. 2018 , 122, 23208-23216	8
1436	Phonon transport properties of two-dimensional electride Ca2NA first-principles study. 2018 , 113, 131902	7
1435	Comparing the Descriptors for Investigating the Influence of Lattice Dynamics on Ionic Transport Using the Superionic Conductor NaPSSe. 2018 , 140, 14464-14473	86
1434	Ab initio phase diagram of PbSe crystals calculated with the random phase approximation. 2018 , 98,	2
1433	Anharmonic effect driven topological phase transition in PbO2 predicted by first-principles calculations. 2018 , 98,	4
1432	Intrinsic Carrier Mobility of Cesium Lead Halide Perovskites. 2018 , 10,	41
1431	D-carbon: study of a novel carbon allotrope. 2018 , 149, 114702	25
1430	First-principles study of the electronic structure, magnetism, and phonon dispersions for CaX (X´= C, N) compounds. 2018 , 17, e00336	11
1429	Role of temperature and Coulomb correlation in the stabilization of the CsCl-type phase in FeS under pressure. 2018 , 98,	5
1428	First-principles quantitative prediction of the lattice thermal conductivity in random semiconductor alloys: The role of force-constant disorder. 2018 , 98,	24
1427	Structural and electrochemical properties of Na2FeSiO4 polymorphs for sodium-ion batteries. 2018 , 292, 190-198	13
1426	Communication: First-principles evaluation of alkali ion adsorption and ion exchange in pure silica LTA zeolite. 2018 , 149, 131102	5
1425	Apical Charge Flux-Modulated In-Plane Transport Properties of Cuprate Superconductors. 2018 , 121, 157001	14
1424	LiCrS and LiMnS Cathodes with Extraordinary Mixed Electron-Ion Conductivities and Favorable Interfacial Compatibilities with Sulfide Electrolyte. 2018 , 10, 36941-36953	14
1423	Physical descriptor for the Gibbs energy of inorganic crystalline solids and temperature-dependent materials chemistry. 2018 , 9, 4168	80
1422	Computational prediction of two-dimensional monolayer B6C2P2 by the global optimization method. 2018 , 32, 1850370	1

1421	A theoretical investigation of structural, mechanical, electronic and thermoelectric properties of orthorhombic CH3NH3PbI3. 2018 , 91, 1	11
1420	Pressure effect on the mechanical and electronic properties of orthorhombic-C20. 2018 , 32, 1850380	1
1419	Hydrogen Bonding versus Entropy: Revealing the Underlying Thermodynamics of the Hybrid OrganicIhorganic Perovskite [CH3NH3]PbBr3. 2018 , 30, 8782-8788	19
1418	KAgSe: A New Two-Dimensional Efficient Photovoltaic Material with Layer-Independent Behaviors. 2018 , 10, 41670-41677	25
1417	Heat capacity of Mg3Sb2, Mg3Bi2, and their alloys at high temperature. 2018 , 6, 83-88	44
1416	Uncovering a Stable Phase in Group V Transition-metal Dinitride (MN2, M = Ta, Nb, V) Nanosheets and Their Electronic Properties via First-principles Investigations. 2018 , 122, 26748-26755	15
1415	Properties of Novel Non-Silicon Materials for Photovoltaic Applications: A First-Principle Insight. 2018 , 11,	5
1414	Hybrid Improper Ferroelectricity in (Sr,Ca)SnO and Beyond: Universal Relationship between Ferroelectric Transition Temperature and Tolerance Factor in n = 2 Ruddlesden-Popper Phases. 2018 , 140, 15690-15700	45
1413	Superconductivity of Bi-III phase of elemental bismuth: Insights from muon-spin rotation and density functional theory. 2018 , 98,	10
1412	Uranium polyhydrides at moderate pressures: Prediction, synthesis, and expected superconductivity. 2018 , 4, eaat9776	52
1411	Bonding Hierarchy Gives Rise to High Thermoelectric Performance in Layered Zintl Compound BaAu2P4. 2018 , 30, 7760-7768	21
1410	Parity-breaking in single-element phases: ferroelectric-like elemental polar metals. 2018 , 30, 415504	3
1409	Using coherent phonons for ultrafast control of the Dirac node of SrMnSb2. 2018 , 98,	8
1408	Relative energies and electronic structures of CoO polymorphs through ab initio diffusion quantum Monte Carlo. 2018 , 98,	12
1407	Effect of a Rare-Earth Ion on the Structural Instability in RFe3(BO3)4 Crystals. 2018, 108, 116-120	3
1406	Physical Properties and Photovoltaic Application of Semiconducting PdBelMonolayer. 2018, 8,	10
1405	Novel Solar Cell Materials: Insights from First-Principles. 2018 , 122, 27107-27126	19
1404	Ab initio calculations of carbon and boron nitride allotropes and their structural phase transitions using periodic coupled cluster theory. 2018 , 98,	19

1403	Possible High-TC Layered Ferromagnetic Insulator Sr2NiRuO4: An Ab Initio Study. 2018 , 122, 25589-25594	1
1402	Insight into Sodium Insertion and the Storage Mechanism in Hard Carbon. 2018 , 3, 2851-2857	89
1401	Computational predictions of stable phase for antiperovskite Na 3OCl via tilting of Na 6O octahedra. 2018 , 124, 164106	8
1400	Frustrated Structural Instability in Superconducting Quasi-One-Dimensional K_{2}Cr_{3}As_{3}. 2018 , 121, 187002	9
1399	PCl: A Unique Post-Phosphorene 2D Material with Superior Properties against Oxidation. 2018 , 9, 6568-6575	12
1398	Ultrafast disordering of vanadium dimers in photoexcited VO. 2018 , 362, 572-576	92
1397	Ab initio investigation on the experimental observation of metallic hydrogen. 2018 , 98,	6
1396	Temperature-dependent structural transformation and friction behavior of nanocomposite VCN-(Ag) coatings. 2018 , 160, 964-973	16
1395	First-Principles Study on the Thermoelectric Properties of FeAsS. 2018 , 3, 13630-13635	6
1394	Lattice relaxations in disordered Fe-based materials in the paramagnetic state from first principles. 2018 , 98,	10
1393	A first-principles study of the structural, elastic, electronic, vibrational, and optical properties of BaSe1&Tex. 2018 , 17, 1478-1491	
1392	Coupled Raman-Raman modes in the ionic Raman scattering process. 2018 , 113, 112903	1
1391	Phase stability, elastic, anisotropic and thermodynamic properties of GdT2Al20 (T = Ti, V, Cr) compounds: A first-principles study. 2018 , 157, 312-319	33
1390	Strong Topological States and High Charge Carrier Mobility in Tetraoxa[8]circulene Nanosheets. 2018 , 122, 22216-22222	17
1389	The low-temperature heat capacity of the SbTe Se solid solution from experiment and theory. 2018 , 30, 405702	2
1388	Effect of density functionals on the vibrational and thermodynamic properties of Fe2VAl and Fe2TiSn compounds. 2018 , 155, 282-287	6
1387	Theoretical studies of electronic transport in monolayer and bilayer phosphorene: A critical overview. 2018 , 98,	43
1386	Thermodynamic Evaluation of Trace-Amount Transition-Metal-Ion Doping in NiOOH Films. 2018 , 165, F907-F913	5

1385	Tuning thermal transport in graphene via combinations of molecular antiresonances. 2018 , 140, 603-609	2
1384	Lattice dynamics, transport and superconducting properties of Ba-substituted Sr3SnO. 2018 , 284-286, 14-19	2
1383	Thermal and Chemical Expansion in Proton Ceramic Electrolytes and Compatible Electrodes. 2018 , 8, 365	64
1382	Dramatically improving thermoelectric performance of topological half-Heusler compound LuPtSb via hydrostatic pressure. 2018 , 6, 20069-20075	17
1381	Old puzzle of incommensurate crystal structure of calaverite AuTe and predicted stability of novel AuTe compound. 2018 , 115, 9945-9950	8
1380	First-principles prediction of the physical properties of ThM2Al20 (M= Ti, V, Cr) intermetallics. 2018 , 284-286, 75-83	34
1379	TiH2 as a Dynamic Additive for Improving the De/Rehydrogenation Properties of MgH2: A Combined Experimental and Theoretical Mechanistic Investigation. 2018 , 122, 21248-21261	31
1378	Entropy contributions to phase stability in binary random solid solutions. 2018, 4,	33
1377	Atomically dispersed tungsten on metal halide monolayer as a ferromagnetic Chern insulator. 2018 , 98,	5
1376	Interplay of lattice, electronic, and spin degrees of freedom in detwinned BaFe2As2: A Raman scattering study. 2018 , 98,	8
1375	First-Principles Investigation of Structural Stability, Mechanical, Anisotropic, and Thermodynamic Properties of CeT2Al20 Intermetallics. 2018 , 73, 1157-1167	2
1374	Room-Temperature Bound Exciton with Long Lifetime in Monolayer GaN. 2018 , 5, 4081-4088	18
1373	Distinct spin-lattice and spin-phonon interactions in monolayer magnetic Crl. 2018 , 20, 23546-23555	54
1372	Two-dimensional stable transition metal carbides (MnC and NbC) with prediction and novel functionalizations. 2018 , 20, 25437-25445	12
1371	Lattice thermal conductivity and bandgap engineering of a three-dimensional sp2-hybridized Dirac carbon material: HS-C48. 2018 , 155, 293-297	6
1370	Structural, thermodynamic, electronic and magnetic properties of Sr3Sn1 \square YxO (Y = V, Fe) from first-principles study. 2018 , 11, 283-290	3
1369	Elastic properties of Mn-rich #Intermetallic phase in engineering aluminum alloys: An ab initio study. 2018 , 124, 085109	4
1368	Rapid fabrication of SnO2 nanoparticle photocatalyst: computational understanding and photocatalytic degradation of organic dye. 2018 , 5, 3005-3014	54

1367	Low lattice thermal conductivity and excellent thermoelectric behavior in LiSb and LiBi. 2018, 30, 425401	11
1366	A novel superhard tungsten nitride predicted by machine-learning accelerated crystal structure search. 2018 , 63, 817-824	58
1365	Performance of various density-functional approximations for cohesive properties of 64 bulk solids. 2018 , 20, 063020	110
1364	Sum-frequency ionic Raman scattering. 2018 , 97,	31
1363	Novel two-dimensional semiconductor SnP3: high stability, tunable bandgaps and high carrier mobility explored using first-principles calculations. 2018 , 6, 11890-11897	99
1362	High-Pressure Synthesis of a Nitrogen-Rich Inclusion Compound ReN ?x N with Conjugated Polymeric Nitrogen Chains. 2018 , 57, 9048-9053	46
1361	Electric control of the heat flux through electrophononic effects. 2018 , 97,	17
1360	First-Principles Investigation of Native Interstitial Diffusion in Cr2O3. 2018 , 122, 12984-12993	15
1359	Novel phases and superconductivity of tin sulfide compounds. 2018 , 148, 194701	13
1358	High-Pressure Synthesis of a Nitrogen-Rich Inclusion Compound ReN8?x N2 with Conjugated Polymeric Nitrogen Chains. 2018 , 130, 9186-9191	11
1357	Ferroelectric Sr3Zr2O7: Competition between Hybrid Improper Ferroelectric and Antiferroelectric Mechanisms. 2018 , 28, 1801856	57
1356	Temperature dependence of NiTi martensite structures: Density functional theory calculations. Scripta Materialia, 2018, 154, 134-138 5.6	8
1355	Density functional study of the phase stability and Raman spectra of YbO, YbSiO and YbSiO under pressure. 2018 , 20, 16518-16527	18
1354	Phonon Instability and Broken Long-Ranged p Bond in Ge-Sb-Te Phase-Change Materials from First Principles. 2018 , 9,	4
1353	New Tungsten Borides, Their Stability and Outstanding Mechanical Properties. 2018, 9, 3470-3477	40
1352	Photoexcitation Dynamics in Janus-MoSSe/WSe Heterobilayers: Ab Initio Time-Domain Study. 2018 , 9, 2797-2802	60
1351	Mechanisms of Formation of H, HO, and Water and of Water Desorption in the Early Stages of Cellulose Pyrolysis. 2018 , 122, 12168-12176	10
1350	Sustainable p-type copper selenide solar material with ultra-large absorption coefficient. 2018 , 9, 5405-5414	13

(2018-2018)

1349	Performance of exchange-correlation functionals in density functional theory calculations for liquid metal: A benchmark test for sodium. 2018 , 148, 144501	2
1348	Evaluation of the structure and properties for the high-temperature phase of zirconium from the atomistic simulations. 2018 , 152, 51-59	8
1347	Lattice dynamics and thermodynamic properties of alkaline earth metal nitrates M(NO3)2 (M = Sr, Ba): A first principles study. 2018 , 122, 268-277	3
1346	Time-resolved Raman spectroscopy for shock-driven intramolecular electron redistribution of cyclotrimethylene trinitramine (RDX). 2018 , 49, 1645-1651	2
1345	All-Optical Detection of Periodic Structure of Chalcogenide Superlattice Using Coherent Folded Acoustic Phonons. 2018 , 12, 1800246	
1344	Coupling between acoustic and soft transverse optical phonons leads to negative thermal expansion of GeTe near the ferroelectric phase transition. 2018 , 97,	14
1343	Electronic and mechanical properties of MgN compound: Prediction of stable half-metallic ferromagnet in NaCl and ZB phases. 2018 , 466, 28-37	5
1342	Initial stage of C60 cation formation in superacids. 2018 , 513, 13-16	
1341	First-principles study of elastic, electronic, thermodynamic, and thermoelectric transport properties of TaCoSn. 2018 , 10, 458-465	52
1340	Electronic and lattice dynamical properties of Ti 2 SiB MAX phase. 2018 , 5, 076303	25
1339	Three-dimensional hexagonal boron nitride foam containing both sp2 and sp3 hybridized bonds. 2018 , 217, 5-10	3
1338	Spin-phonon couplings in transition metal complexes with slow magnetic relaxation. 2018 , 9, 2572	58
1337	The Ideal Crystal Structure of Cristobalite X-I: A Bridge in SiO2 Densification. 2018 , 122, 17437-17446	3
1336	High-throughput functionalization of single-layer electride Ca2N. 2018 , 5, 076306	1
1335	Theoretical and experimental investigations on high temperature mechanical and thermal properties of BaZrO3. 2018 , 44, 16475-16482	27
1334	Structural, electronic, dynamical and thermodynamic properties of Ca10(PO4)6(OH)2 and Sr10(PO4)6(OH)2: First-principles study. 2018 , 43, 13639-13648	7
1333	Novel compounds of cerium binary alloys from high-throughput first-principles calculations. 2018 , 123, 235102	2
1332	Interplay between p □and d □orbitals yields multiple Dirac states in one- and two-dimensional CrB 4. 2018 , 5, 035041	12

1331	First-principles stability ranking of molecular crystal polymorphs with the DFT+MBD approach. 2018 , 211, 253-274	23
1330	Compositional Effects and Electron Lone-pair Distortions in Doped Bournonites. 2018 , 19, 2635-2644	5
1329	Water oxidation chemistry of oxynitrides and oxides: Comparing NaTaO3 and SrTaO2N. 2018 , 677, 258-263	10
1328	Distorted Janus Transition Metal Dichalcogenides: Stable Two-Dimensional Materials with Sizable Band Gap and Ultrahigh Carrier Mobility. 2018 , 122, 19153-19160	32
1327	Two dimensional monolayer rhombic silicene on the diamond (111) surface. 2018 , 20, 21699-21704	3
1326	Two-dimensional zigzag-shaped Cd2C monolayer with a desirable bandgap and high carrier mobility. 2018 , 6, 9175-9180	10
1325	Translational Inelasticity of NO and CO in Scattering from Ultrathin Metallic Films of Ag/Au(111). 2018 , 122, 18942-18948	3
1324	TinBelenium Compounds at Ambient and High Pressures. 2018, 122, 18274-18281	6
1323	Giant Electron-Phonon Coupling and Deep Conduction Band Resonance in Metal Halide Double Perovskite. 2018 , 12, 8081-8090	123
1322	Structure and properties of a novel boride: ThNiB. 2018 , 47, 12933-12943	
1322	Structure and properties of a novel boride: ThNiB. 2018, 47, 12933-12943 Penta-PtN: an ideal two-dimensional material for nanoelectronics. 2018, 10, 16169-16177	30
		30
1321	Penta-PtN: an ideal two-dimensional material for nanoelectronics. 2018 , 10, 16169-16177 Monte-Carlo study of electronic transport in non-fi-symmetric two-dimensional materials: Silicene	
1321	Penta-PtN: an ideal two-dimensional material for nanoelectronics. 2018 , 10, 16169-16177 Monte-Carlo study of electronic transport in non-B-symmetric two-dimensional materials: Silicene and germanene. 2018 , 124, 044306 A comparative first-principles study of tetragonal TiAl and Ti4Nb3Al9 intermetallic compounds.	15
1321 1320 1319	Penta-PtN: an ideal two-dimensional material for nanoelectronics. 2018, 10, 16169-16177 Monte-Carlo study of electronic transport in non-fl-symmetric two-dimensional materials: Silicene and germanene. 2018, 124, 044306 A comparative first-principles study of tetragonal TiAl and Ti4Nb3Al9 intermetallic compounds. 2018, 101, 72-80 Structural, vibrational, and electronic properties of single-layer hexagonal crystals of group IV and	15
1321 1320 1319 1318	Penta-PtN: an ideal two-dimensional material for nanoelectronics. 2018, 10, 16169-16177 Monte-Carlo study of electronic transport in non-B-symmetric two-dimensional materials: Silicene and germanene. 2018, 124, 044306 A comparative first-principles study of tetragonal TiAl and Ti4Nb3Al9 intermetallic compounds. 2018, 101, 72-80 Structural, vibrational, and electronic properties of single-layer hexagonal crystals of group IV and V elements. 2018, 98, Structural, Spectroscopic, and Computational Characterization of the Concomitant Polymorphs of	15 8 53
1321 1320 1319 1318	Penta-PtN: an ideal two-dimensional material for nanoelectronics. 2018, 10, 16169-16177 Monte-Carlo study of electronic transport in non-fi-symmetric two-dimensional materials: Silicene and germanene. 2018, 124, 044306 A comparative first-principles study of tetragonal TiAl and Ti4Nb3Al9 intermetallic compounds. 2018, 101, 72-80 Structural, vibrational, and electronic properties of single-layer hexagonal crystals of group IV and V elements. 2018, 98, Structural, Spectroscopic, and Computational Characterization of the Concomitant Polymorphs of the Natural Semiconductor Indigo. 2018, 122, 18422-18431 Screening Surface Structure of MXenes by High-Throughput Computation and Vibrational	15 8 53

1313	Stability and Reactions of CaCO3 Polymorphs in the Earth's Deep Mantle. 2018 , 123, 6491	10
1312	Raman spectrum of CrI3: An abinitio study. 2018 , 98,	31
1311	In-Plane Optical Anisotropy and Linear Dichroism in Low-Symmetry Layered TlSe. 2018 , 12, 8798-8807	43
1310	Thermodynamic optimization of Si-Zr-N system using Calphad approach coupled with ab initio methods. 2018 , 62, 148-153	2
1309	Temperature coefficient of redox potential of LixFePO4. 2018 , 8, 065021	5
1308	Effects of the Aqueous Environment on the Stability and Chemistry of ENiOOH Surfaces. 2018 , 30, 5205-5219	25
1307	Theoretical prediction electronic properties of Group-IV diamond nanothreads. 2018, 8, 075107	5
1306	First-principles study of the thermoelectric properties of quaternary tetradymite BiSbSeTe2. 2018 , 51, 315501	4
1305	Machine Learning Directed Search for Ultraincompressible, Superhard Materials. 2018, 140, 9844-9853	135
1304	Fe-N system at high pressure reveals a compound featuring polymeric nitrogen chains. 2018 , 9, 2756	103
1303	Electronic and mechanical properties of stiff rhenium carbide monolayers: A first-principles investigation. 2018 , 458, 762-768	4
1302	Structural, electronic and thermodynamic properties of bulk and surfaces of terbium dioxide (TbO2). 2018 , 5, 085901	5
1301	Electronic band structure of carbon honeycombs. 2018 , 5, 72-77	3
1300	Substrate-induced magnetism and topological phase transition in silicene. 2018 , 10, 14667-14677	9
1299	Determination of Dynamically Stable Electrenes toward Ultrafast Charging Battery Applications. 2018 , 9, 4267-4274	7
1298	Unusual Pressure-Induced Periodic Lattice Distortion in SnSe_{2}. 2018 , 121, 027003	15
1297	Favourable band edge alignment and increased visible light absorption in EMoO3/EMoO3 oxide heterojunction for enhanced photoelectrochemical performance. 2018 , 43, 15773-15783	12
1296	Electronic Origin of Optically-Induced Sub-Picosecond Lattice Dynamics in MoSe Monolayer. 2018 , 18, 4653-4658	14

1295	Nonlinear phononic control and emergent magnetism in Mott insulating titanates. 2018, 98,	17
1294	Toward a Reliable Description of the Lattice Vibrations in Organic Molecular Crystals: The Impact of van der Waals Interactions. 2018 , 14, 4380-4390	20
1293	Slow thermal equilibration in methylammonium lead iodide revealed by transient mid-infrared spectroscopy. 2018 , 9, 2792	21
1292	Enhanced superconductivity upon weakening of charge density wave transport in 2H-TaS2 in the two-dimensional limit. 2018 , 98,	46
1291	Influence of interfaces on the phonon density of states of nanoscale metallic multilayers: Phonon confinement and localization. 2018 , 98,	9
1290	Raman Signatures of Broken Inversion Symmetry and In-Plane Anisotropy in Type-II Weyl Semimetal Candidate TaIrTe. 2018 , 30, e1706402	37
1289	Stability, structure, and suppression of the martensitic transition temperature by B19? compound twins in NiTi: ab initio and classical simulations. 2018 , 154, 182-189	15
1288	Anharmonic lattice dynamics of bcc sodium under high pressures. 2018 , 20, 14647-14651	3
1287	Thermodynamic consideration and ground-state search of icosahedral boron subselenide B12(B1\(\text{BSex} \))2 from a first-principles cluster expansion. 2018 , 97,	2
1286	First Full Structural Characterization of Chloro Formamidinium Salts. 2018 , 644, 1485-1491	1
1285	First principles calculations on the effect of interstitial oxygen on phase stability and 2 martensitic transformation in Ti N b alloys. 2018 , 53, 11473-11487	13
1284	Phase-transition temperature suppression to achieve cubic GeTe and high thermoelectric performance by Bi and Mn codoping. 2018 , 115, 5332-5337	130
1283	Spin valley and giant quantum spin Hall gap of hydrofluorinated bismuth nanosheet. 2018 , 8, 7436	4
1282	Diffusion of helium, hydrogen and deuterium in diamond: Experiment, theory and geochemical applications. 2018 , 232, 206-224	9
1281	Efficient Automatized Density-Functional Tight-Binding Parametrizations: Application to Group IV Elements. 2018 , 14, 2947-2954	13
1280	Giant Phonon Tuning Effect via Pressure-Manipulated Polar Rotation in Perovskite MAPbl. 2018 , 9, 3029-3034	· 13
1279	Vibration analysis of hydrogen, deuterium and tritium in metals: consequences on the isotope effect. 2018 , 30, 335402	10
1278	Description of phase transitions through accumulation of point defects: UN, UO2 and UC. 2018 , 510, 373-381	8

1277	Two-dimensional sheet of germanium selenide as an anode material for sodium and potassium ion batteries: First-principles simulation study. 2018 , 154, 204-211	50
1276	Ferromagnetism in a semiconducting Janus NbSe hydride monolayer. 2018 , 6, 9675-9681	9
1275	Theoretical discovery of novel two-dimensional V-N binary compounds with auxiticity. 2018 , 20, 22027-22037	35
1274	Bulk nanocrystalline gamma magnesium hydride with low dehydrogenation temperature stabilized by plastic straining via high-pressure torsion. <i>Scripta Materialia</i> , 2018 , 157, 54-57	19
1273	Study on Radial Temperature Distribution of Aluminum Dispersed Nuclear Fuels: U3O8-Al, U3Si2-Al, and UN-Al. 2018 , 4,	5
1272	Non-monotonic thickness dependence of Curie temperature and ferroelectricity in two-dimensional SnTe film. 2018 , 113, 082905	6
1271	Ab initio lattice thermal conductivity of bulk and thin-film ₽AI2O3. 2018 , 8, 1119-1123	10
1270	Possible doping of single-layer MoS2 with Pt: A DFT study. 2018 , 462, 409-416	13
1269	High-pressure Raman scattering in bulk HfS: comparison of density functional theory methods in layered MS compounds (M = Hf, Mo) under compression. 2018 , 8, 12757	12
1268	Summary report of CALPHAD XLVI - Saint-Malo, France, 2017. 2018 , 63, 229-290	
1267	Fully spin-polarized current in gated bilayer silicene. 2018 , 98,	10
1266		
1200	Stress-controlled carbon diffusion channeling in bct-iron: A mean-field theory. 2018 , 769, 1121-1131	15
1265	Stress-controlled carbon diffusion channeling in bct-iron: A mean-field theory. 2018 , 769, 1121-1131 Electronic structure and thermophysical properties of U3Si2: A systematic first principle study. 2018 , 510, 360-365	15
	Electronic structure and thermophysical properties of U3Si2: A systematic first principle study. 2018 , 510, 360-365	
1265	Electronic structure and thermophysical properties of U3Si2: A systematic first principle study. 2018 , 510, 360-365	11
1265	Electronic structure and thermophysical properties of U3Si2: A systematic first principle study. 2018, 510, 360-365 Ground-state structures, physical properties and phase diagram of carbon-rich nitride CN. 2018, 30, 385402 Commensurate lattice constant dependent thermal conductivity of misoriented bilayer graphene.	7
1265 1264 1263	Electronic structure and thermophysical properties of U3Si2: A systematic first principle study. 2018, 510, 360-365 Ground-state structures, physical properties and phase diagram of carbon-rich nitride CN. 2018, 30, 385402 Commensurate lattice constant dependent thermal conductivity of misoriented bilayer graphene. 2018, 138, 451-457	11 7 21

1259	Stability of U5Si4 phase in U-Si system: Crystal structure prediction and phonon properties using first-principles calculations. 2018 , 510, 331-336	15
1258	Toward Intrinsic Room-Temperature Ferromagnetism in Two-Dimensional Semiconductors. 2018 , 140, 11519-11525	170
1257	Heterometallic perovskite-type metal-organic framework with an ammonium cation: structure, phonons, and optical response of [NH]NaCrAl(HCOO) ($x = 0, 0.025$ and 0.5). 2018 , 20, 22284-22295	15
1256	High throughput screening for two-dimensional topological insulators. 2018 , 5, 045023	21
1255	Computational Predictions and Microwave Plasma Synthesis of Superhard Boron-Carbon Materials. 2018 , 11,	6
1254	Structures and Stability of Iron Halides at the Earth Mantle and Core Pressures: Implications for the Missing Halogen Paradox. 2018 , 2, 711-719	4
1253	Ab initio identification of the Li-rich phase in LiFePO. 2018 , 20, 17497-17503	7
1252	Intrinsic and anisotropic Rashba spin splitting in Janus transition-metal dichalcogenide monolayers. 2018 , 97,	124
1251	Design and exploration of semiconductors from first principles: A review of recent advances. 2018 , 11, 060101	70
1250	Finite temperature stability of single-layer black and blue phosphorus adsorbed on Au(1 1 1): a first-principles study. 2018 , 5, 035044	11
1249	Two-Dimensional Manganese Nitride Monolayer with Room Temperature Rigid Ferromagnetism under Strain. 2018 , 122, 14918-14927	30
1248	Diffusion of One-Dimensional Crystals in Channels of Single-Walled Carbon Nanotubes. 2018 , 63, 476-479	
1247	The effect of conformational freedom of side chain on low-frequency motions of amino acids in solid-state. 2018 , 1171, 87-93	2
1246	Structural, elastic, electronic and thermodynamic properties of ZrB2 under high-pressure: First-principle study. 2018 , 32, 1850200	1
1245	Lattice thermal conductivities of two SiO2 polymorphs by first-principles calculations and the phonon Boltzmann transport equation. 2018 , 97,	38
1244	A possible family of Ni-based high temperature superconductors. 2018 , 63, 957-963	9
1243	First-principles description of oxygen self-diffusion in rutile TiO: assessment of uncertainties due to enthalpy and entropy contributions. 2018 , 20, 17448-17457	10
1242	Two-Dimensional Deep-Ultraviolet Beryllium-Free KBeBOF Family Nonlinear-Optical Monolayer. 2018 , 57, 7503-7506	19

1241	Highly sensitive detection of polarized light using a new group IV № 2D orthorhombic SiP. 2018 , 6, 7219-7225	36
1240	Two-dimensional pentagonal CrX ($X = S$, Se or Te) monolayers: antiferromagnetic semiconductors for spintronics and photocatalysts. 2018 , 20, 18348-18354	20
1239	Double transition metal MXenes with wide band gaps and novel magnetic properties. 2018, 10, 11962-11968	51
1238	Lattice dynamics and metastability of fcc metals in the hcp structure and the crucial role of spin-orbit coupling in platinum. 2018 , 97,	11
1237	Designing and Discovering a New Family of Semiconducting Quaternary Heusler Compounds Based on the 18-Electron Rule. 2018 , 30, 4978-4985	26
1236	High-Performance Solid-State Thermionic Energy Conversion Based on 2D van der Waals Heterostructures: A First-Principles Study. 2018 , 8, 9303	13
1235	Phase Coexistence and Strain-Induced Topological Insulator in Two-Dimensional BiAs. 2018 , 122, 15047-15054	124
1234	Topological Dirac semimetal phase in GexSny alloys. 2018 , 112, 251601	6
1233	Two-Dimensional Tetragonal Titanium Carbide: a High-Capacity and High-Rate Battery Material. 2018 , 122, 15118-15124	31
1232	Prediction and Characterization of NaGaS, A High Thermal Conductivity Mid-Infrared Nonlinear Optical Material for High-Power Laser Frequency Conversion. 2019 , 58, 93-98	19
1231	A computational search for the zeta phase in the tantalum carbides. 2019 , 102, 1454-1462	10
1230	First principles investigation of topological phase in XMR material TmSb under hydrostatic pressure. 2019 , 31, 335401	3
1229	Arsenene monolayer as an outstanding anode material for (Li/Na/Mg)-ion batteries: density functional theory. 2019 , 21, 19951-19962	31
1228	Monitoring the electronic, thermal and optical properties of two-dimensional MoO under strain via vibrational spectroscopies: a first-principles investigation. 2019 , 21, 19904-19914	14
1227	Charge-Carrier Enrichment at BaZrO3/SrTiO3 Interfaces. 2019 , 123, 20808-20816	7
1226	Perspective on ab initio phonon thermal transport. 2019 , 126, 050902	42
1225	Structure-property correlation studies of alkaline-earth metal-azides M(N) (M = Sr, Ba). 2019 , 31, 475402	1
1224	Structural and topological phase transitions induced by strain in two-dimensional bismuth. 2019 , 31, 475001	2

1223	Symmetry-Protected Ideal Type-II Weyl Phonons in CdTe. 2019 , 123, 065501	31
1222	Frustrated Dipole Order Induces Noncollinear Proper Ferrielectricity in Two Dimensions. 2019 , 123, 067601	30
1221	Enhanced Electron-Phonon Interaction in Multivalley Materials. 2019 , 9,	25
1220	Mechanical and transport properties of BixSb2-xTe3 single quintuple layers. 2019 , 170, 109182	2
1219	pH-Dependent Distribution of Functional Groups on Titanium-Based MXenes. 2019 , 13, 9171-9181	45
1218	Effect of surface termination on the lattice thermal conductivity of monolayer Ti3C2Tz MXenes. 2019 , 126, 065101	27
1217	Prediction of C7N6 and C9N4: stable and strong porous carbon-nitride nanosheets with attractive electronic and optical properties. 2019 , 7, 10908-10917	37
1216	Tuning the Crystal Structure of A2CoPO4F (A = Li, Na) Fluoride-Phosphates: A New Layered Polymorph of LiNaCoPO4F. 2019 , 2019, 4365-4372	5
1215	Novel two-dimensional tetragonal vanadium carbides and nitrides as promising materials for Li-ion batteries. 2019 , 21, 19513-19520	14
1214	Phonon transport across crystal-phase interfaces and twin boundaries in semiconducting nanowires. 2019 , 11, 16007-16016	7
1213	Evolution of the free energy of the GaN(0001) surface based on first-principles phonon calculations. 2019 , 100,	19
1212	Ballistic thermoelectric properties of monolayer semiconducting transition metal dichalcogenides and oxides. 2019 , 100,	26
1211	Neutron Spectroscopic and Thermochemical Characterization of Lithium Aluminum-Layered Double Hydroxide Chloride: Implications for Lithium Recovery. 2019 , 123, 20723-20729	8
1210	On the Origin of the Negative Thermal Expansion Behavior of YCu. 2019 , 58, 11819-11827	
1209	Carrier Lifetimes and Recombination Pathways in Metal-Organic Frameworks. 2019, 10, 5041-5046	12
1208	Seismic velocities of CaSiO perovskite can explain LLSVPs in Earth's lower mantle. 2019 , 572, 643-647	26
1207	Improved thermoelectric performance of bilayer Bi2O2Se by the band convergence approach. 2019 , 7, 11029-11039	25
1206	Crystal Structure and Mechanical Properties of ThBC2. 2019 , 9, 389	О

1205	Sulfur-functionalized vanadium carbide MXene (VCS) as a promising anchoring material for lithium-sulfur batteries. 2019 , 21, 18559-18568	56
1204	Varying topological properties of two-dimensional honeycomb lattices composed of endohedral fullerenes. 2019 , 100,	1
1203	Tunable visible-light excitonic absorption and high photoconversion efficiency in two-dimensional group-VI monolayer materials. 2019 , 100,	10
1202	Data-Driven Discovery of Full-Visible-Spectrum Phosphor. 2019 , 31, 6286-6294	54
1201	Computationally Driven Discovery of a Family of Layered LiNiB Polymorphs. 2019 , 131, 16002-16009	3
1200	Hydrocarbons under Pressure: Phase Diagrams and Surprising New Compounds in the Cℍ System. 2019 , 123, 20497-20501	10
1199	Computer Modeling of Extended PnX3n + 2 Chains (X = F, Cl). 2019 , 64, 780-785	
1198	Monoclinic angle, shear response, and minimum energy pathways of NiTiCu martensite phases from ab initio calculations. 2019 , 178, 59-67	3
1197	Insights on Anisotropic Dissipative Quantum Transport in n-Type Phosphorene MOSFET. 2019,	1
1196	First-Principles Calculations of the Structural, Magnetic, and Electronic Properties of (hbox {Fe}_{2}hbox {MgB}) Full-Heusler Alloy. 2019 , 48, 7258-7262	3
1195	Phonon Anharmonicity in Few-Layer Black Phosphorus. 2019 , 13, 10456-10468	18
1194	Cohesive properties of the crystalline phases of twenty proteinogenic laminoacids from first-principles calculations. 2019 , 21, 18501-18515	11
1193	Phonons and anisotropic thermal expansion behavior of NiX (X = S, Se, Te). 2019 , 125, 205106	1
1192	Phase diagrams and mechanical properties of TiC-SiC solid solutions from first-principles. 2019 , 66, 101643	3
1191	Diffusivity of hydrogen and properties of point defects in beryllium investigated by DFT. 2019 , 524, 323-329	4
1190	Group theoretical approach to computing phonons and their interactions. 2019 , 100,	4
1189	Order-disorder transition in the prototypical antiferroelectric PbZrO3. 2019 , 100,	14
1188	Phonon Mean Free Path - Thermal Conductivity Relation in AlN. 2019,	O

1187	Lattice dynamics and lattice thermal conductivity of CrSi 2 calculated from first principles and the phonon Boltzmann transport equation. 2019 , 126, 025105	5
1186	Strain-Induced Room-Temperature Ferromagnetic Semiconductors with Large Anomalous Hall Conductivity in Two-Dimensional Cr2Ge2Se6. 2019 , 12,	35
1185	High-throughput Computational Study of Halide Double Perovskite Inorganic Compounds. 2019 , 31, 5392-5401	46
1184	Electronic, Optical, Mechanical and Lattice Dynamical Properties of MgBi2O6: A First-Principles Study. 2019 , 9, 1267	6
1183	Superatomic anion Al6O2D and the prospect for cluster assembled crystals. 2019 , 525, 110413	
1182	Two-dimensional ferroelastic topological insulator with tunable topological edge states in single-layer ZrAsX (X = Br and Cl). 2019 , 7, 9743-9747	6
1181	Evidence for the formation of metallic In after laser irradiation of InP. 2019 , 126, 025902	2
1180	Quantum chemical methods in charge density studies from X-ray diffraction data. 2019 , 88, 677-716	15
1179	Ferromagnetic nodal-line metal in monolayer h-InC. 2019 , 100,	8
1178	Fast anharmonic free energy method with an application to vacancies in ZrC. 2019, 100,	7
1177	Theoretical Investigation of V3C2 MXene as Prospective High-Capacity Anode Material for Metal-Ion (Li, Na, K, and Ca) Batteries. 2019 , 123, 18207-18214	46
1176	The control of the co	
,	Thermodynamic stability of hexagonal and rhombohedral boron nitride under chemical vapor deposition conditions from van der Waals corrected first principles calculations. 2019 , 37, 040603	6
1175		8
	deposition conditions from van der Waals corrected first principles calculations. 2019 , 37, 040603 Investigation of the on-site Coulomb correction and temperature dependence of the stability of	
1175	deposition conditions from van der Waals corrected first principles calculations. 2019 , 37, 040603 Investigation of the on-site Coulomb correction and temperature dependence of the stability of UBi phases using DFT+U. 2019 , 524, 157-163	8
1175 1174	deposition conditions from van der Waals corrected first principles calculations. 2019 , 37, 040603 Investigation of the on-site Coulomb correction and temperature dependence of the stability of UBi phases using DFT+U. 2019 , 524, 157-163 Vibrational properties of uranium fluorides. 2019 , 570, 194-205	8
1175 1174 1173	Investigation of the on-site Coulomb correction and temperature dependence of the stability of UBi phases using DFT+U. 2019, 524, 157-163 Vibrational properties of uranium fluorides. 2019, 570, 194-205 Density functional theory studies of the SrC and SrN compounds. 2019, 237, 121875	8 5 5

1169	Two-dimensional nanoporous metal chalcogenophosphates MP2X6 with high electron mobilities. 2019 , 493, 1334-1339	2
1168	Al2O3/FeAl interfacial behaviors by yttrium doping in high temperature oxidation. 2019 , 45, 22273-22280	6
1167	Electronic Properties, Phase Transformation, and Anionic Redox of Monoclinic Na2MnO3 Cathode Material for Sodium-Ion Batteries: First-Principle Calculations. 2019 , 6, 3987-3993	6
1166	Computational Design of One-Dimensional Ferromagnetic Semiconductors in Transition Metal Embedded Stannaspherene Nanowires. 2019 , 37, 1021-1024	3
1165	Microscopic theory of ultrafast out-of-equilibrium magnon-phonon dynamics in insulators. 2019 , 100,	7
1164	Structural engineering of bilayer PtSe thin films: a first-principles study. 2019 , 31, 455001	10
1163	Effect of substitutional impurities on vibrational properties of zircon: a first-principles study. 2019 , 31, 455402	1
1162	Analysis of Water Coupling in Inelastic Neutron Spectra of Uranyl Fluoride. 2019 , 9, 10476	4
1161	Density functional study of structural, electronic and magnetic properties of new half-metallic ferromagnetic double perovskite SrMnVO. 2019 , 31, 475501	2
1160	Electronic and Optical Properties of Two-Dimensional Tellurene: From First-Principles Calculations. 2019 , 9,	25
1159	Strain dependent electronic structure and optical properties tuning of InN/PtX2 (X=S, Se) van der waals heterostructures. 2019 , 168, 108805	9
1159 1158		9
	waals heterostructures. 2019 , 168, 108805 Single-Layer Ptl: A Multifunctional Material with Promising Photocatalysis toward the Oxygen	
1158	waals heterostructures. 2019, 168, 108805 Single-Layer Ptl: A Multifunctional Material with Promising Photocatalysis toward the Oxygen Evolution Reaction and Negative Poisson's Ratio. 2019, 11, 31793-31798 A comparative study on modeling of the ferromagnetic and paramagnetic states of uranium	10
1158	waals heterostructures. 2019, 168, 108805 Single-Layer Ptl: A Multifunctional Material with Promising Photocatalysis toward the Oxygen Evolution Reaction and Negative Poisson's Ratio. 2019, 11, 31793-31798 A comparative study on modeling of the ferromagnetic and paramagnetic states of uranium hydride using a DFT+U method. 2019, 21, 17628-17639 Intrinsically low thermal conductivity of bismuth oxychalcogenides originating from interlayer	10
1158 1157 1156	Single-Layer PtI: A Multifunctional Material with Promising Photocatalysis toward the Oxygen Evolution Reaction and Negative Poisson's Ratio. 2019, 11, 31793-31798 A comparative study on modeling of the ferromagnetic and paramagnetic states of uranium hydride using a DFT+U method. 2019, 21, 17628-17639 Intrinsically low thermal conductivity of bismuth oxychalcogenides originating from interlayer coupling. 2019, 21, 18259-18264	10 3 9
1158 1157 1156 1155	Single-Layer Ptl: A Multifunctional Material with Promising Photocatalysis toward the Oxygen Evolution Reaction and Negative Poisson's Ratio. 2019, 11, 31793-31798 A comparative study on modeling of the ferromagnetic and paramagnetic states of uranium hydride using a DFT+U method. 2019, 21, 17628-17639 Intrinsically low thermal conductivity of bismuth oxychalcogenides originating from interlayer coupling. 2019, 21, 18259-18264 Computationally Driven Discovery of a Family of Layered LiNiB Polymorphs. 2019, 58, 15855-15862	10 3 9 13

1151	Coupling the High-Throughput Property Map to Machine Learning for Predicting Lattice Thermal Conductivity. 2019 , 31, 5145-5151	35
1150	Melting Behavior of Alkaline-Earth Metal Carbodiimides and Their Thermochemistry from First-Principles. 2019 , 58, 8938-8942	7
1149	Transport and topological properties of ThOCh(Ch: S, Se and Te) in bulk and monolayer: a first principles study. 2019 , 31, 435504	
1148	Three dimensional metallic porous SiC4 allotropes: Stability and battery applications. 2019 , 63, 103862	7
1147	Structure and Dynamic and Nonlinear Optical Properties of Hg2F2 Crystals. 2019 , 128, 727-738	1
1146	Tailoring phononic, electronic, and thermoelectric properties of orthorhombic GeSe through hydrostatic pressure. 2019 , 9, 9490	6
1145	Improve the performance of machine-learning potentials by optimizing descriptors. 2019, 150, 244110	9
1144	PdH and NiH phase diagrams using cluster variation method and Monte Carlo simulation. 2019 , 99, 2376-2392	3
1143	Towards a simplified description of thermoelectric materials: accuracy of approximate density functional theory for phonon dispersions. 2019 , 31, 395901	4
1142	Phonon and electron transport in Janus monolayers based on InSe. 2019 , 31, 435501	15
1141	Lone-Pair Electron-Driven Thermoelectrics at Room Temperature. 2019 , 10, 4117-4122	10
1140	Pressure-induced novel metallic phase in non-stoichiometric cadmium selenides: A first-principles study. 2019 , 167, 191-197	1
1139	Stability, electronic and mechanical properties of superhard materials formed by 4+6+8 membered rings of carbon. 2019 , 277, 454-465	4
1138	Multiple superionic states in heliumWater compounds. 2019 , 15, 1065-1070	28
1137	High-pressure synthesis of ultraincompressible hard rhenium nitride pernitride Re(N)(N) stable at ambient conditions. 2019 , 10, 2994	40
1136	Strain to alter the covalency and superconductivity in transition metal diborides. 2019 , 7, 10700-10707	6
1135	Lattice thermal conductivity of TiS2, ZrS2, and HfS2: Periodic trends studied by dispersion-corrected hybrid density functional methods. 2019 , 100,	5
1134	Nature of the structural symmetries associated with hybrid improper ferroelectricity in Ca3X2O7(X=Mnand Ti). 2019 , 99,	4

Large-Scale Phonon Calculations Using the Real-Space Multigrid Method. 2019 , 15, 6859-6864	3
Electronic, mechanical and lattice dynamical properties of YXB4 (X = Cr, Mn, Fe, and Co) compounds. 2019 , 94, 125710	O
Structural and electronic properties of transition-metal chalcogenides Mo 5 S 4 nanowires. 2019 , 28, 106103	1
Intrinsically Low Lattice Thermal Conductivity Derived from Rattler Cations in an AMM?Q3 Family of Chalcogenides. 2019 , 31, 8734-8741	15
Superior Mechanical and Electronic Properties of Novel 2D Allotropes of As and Sb Monolayers. 2019 , 123, 27214-27221	5
1128 Machine-learning interatomic potential for radiation damage and defects in tungsten. 2019 , 100,	39
1127 Graphene Functionalization Strategies. 2019 ,	2
1126 First-Principle Calculation of High Absorption-TlGaTe for Photovoltaic Application. 2019 , 12,	1
Phase stability and thermoelectric properties of semiconductor-like tetragonal FeAl. 2019 , 20, 937-96	48 5
Nonstoichiometric Phases of Two-Dimensional Transition-Metal Dichalcogenides: From Chalcogen 1124 Vacancies to Pure Metal Membranes. 2019 , 10, 6492-6498	12
Supercompliant and Soft (CH_{3}NH_{3})_{3}Bi_{2}I_{9} Crystal with Ultralow Thermal Conductivity. 2019 , 123, 155901	20
1122 Lattice dynamics and thermoelectric properties of YCuSe2. 2019 , 21, 100617	2
Thermal conductivity modeling using machine learning potentials: application to crystalline and amorphous silicon. 2019 , 10, 100140	23
1120 Orthorhombic to monoclinic phase transition in NbNiTe2. 2019 , 100,	1
Lattice and magnetic dynamics in the polar, chiral, and incommensurate antiferromagnet Ni2InSbO6. 2019 , 100,	2
Blue phosphorene/graphene heterostructure as a promising anode for lithium-ion batteries: a first-principles study with vibrational analysis techniques. 2019 , 7, 611-620	56
Near Optimal Timing and Frequency Offset Estimation for 5G Integrated LEO Satellite Communication System. 2019 , 7, 113298-113310	28
1116 Strain Effect on Thermoelectric Performance of InSe Monolayer. 2019 , 14, 287	17

1115 First-principles study of thermoel	ectric properties of Li-based Nowotony-Juza phases. 2019 , 31, 505504	3
Phonon anomalies near the magn ¹¹¹⁴ density functional theory studies.	etostructural transition in Li2RuO3: Raman spectroscopy and 2019 , 100,	4
	electronic and optical properties of a new two-dimensional agonal graphene. 2019 , 21, 24758-24767	14
First principles calculations of into Ta2SnO6. 2019 , 126, 185701	rinsic mobilities in tin-based oxide semiconductors SnO, SnO2, and	24
First-principles DFT insights into t EZnP: implications for photovoltai	the structural, elastic, and optoelectronic properties of ⊞and c applications. 2019 , 31, 265501	1
Calculating the Lattice Dynamics 2019 , 61, 2019-2025	in the RFe3(BO3)4 Crystals in the Quasi-Harmonic Approximation.	2
The system thorium-palladium-bo 2019, 811, 151578	oron: A DFT study on the stability and properties of Th2Pd15B5.	
1108 Novel Metallic Crystalline Phase c	of Li2S3. 2019 , 123, 28027-28034	3
1107 Dark matter phonon coupling. 20	19 , 100,	11
1106 Pressure-Induced Structural Trans	sition to the Polar Phase in GdFe3(BO3)4. 2019 , 19, 6935-6944	2
Phase Stability and Ordering in Rowith PbX and SnX (X = S, Se, Te). 2	ock Salt-Based Thermoelectrics: NaSbX2, AgSbX2, and Their Alloys 2019, 31, 9445-9452	6
1104 Mysterious SiB: Identifying the Re	elation between ∃and &iB. 2019 , 4, 18741-18759	5
Theoretical prediction of a highly FeNiB2 system. 2019 , 115, 18260	responsive material: Spin fluctuations and superconductivity in 1	2
1102 Rigorous statistical thermodynam	nical model for lattice dynamics in alloys. 2019 , 100,	3
1101 Giant Electrophononic Response	in PbTiO_{3} by Strain Engineering. 2019 , 123, 185901	5
	tortion, and Symmetry-Driven Optical Band Gap Bowing in Mixed ouble Perovskites. 2019 , 31, 9430-9444	32
1099 Weyl semimetal phase in the non-	centrosymmetric superlattice W2XY(X,Y=S,Se,Te,XIY). 2019 , 100,	2

1097	Dual topological insulator and insulator-semimetal transition in mirror-symmetric honeycomb materials. 2019 , 100,	1
1096	Crystal Engineering of Bi2WO6 to Polar Aurivillius-Phase Oxyhalides. 2019 , 123, 29155-29161	9
1095	A new single-layer structure of MBene family: TiB. 2019 , 31, 505401	11
1094	Phase diagram of uranium from ab initio calculations and machine learning. 2019 , 100,	8
1093	Equilibrium hydrogen pressures in the VH system from first principles. 2019 , 44, 28909-28918	5
1092	Low-Energy Phases of Bi Monolayer Predicted by Structure Search in Two Dimensions. 2019 , 10, 7324-7332	8
1091	Electron-phonon coupling and Kohn anomaly due to floating two-dimensional electronic bands on the surface of ZrSiS. 2019 , 100,	2
1090	Simulating lattice thermal conductivity in semiconducting materials using high-dimensional neural network potential. 2019 , 12, 095001	20
1089	Spectroscopic Studies of the Magnetic Excitation and Spin-Phonon Couplings in a Single-Molecule Magnet. 2019 , 25, 15846-15857	11
1088	Structural, Electronic and Vibrational Properties of Al4C3. 2019 , 256, 1900037	3
1087	First-principles prediction of the quaternary half-metallic ferromagnets TiZrIrZ (Z = Al, Ga or In) for spintronics applications. 2019 , 690, 137564	10
1086	Ferroelectric switching in bilayer 3R MoS via interlayer shear mode driven by nonlinear phononics. 2019 , 9, 14919	7
1085	First-principles study of interfacial energy between alpha-zirconium and zirconium hydride. 2019 , 126, 135105	6
1084	Phonon dynamics in the layered negative thermal expansion compounds CuxNi2⊠(CN)4. 2019 , 100,	3
1083	Lattice dynamical properties of antiferromagnetic MnO, CoO, and NiO, and the lattice thermal conductivity of NiO. 2019 , 100,	6
1082	Configuration entropy effect on temperature coefficient of redox potential of P2-Na x CoO2. 2019 , 58, 065501	3
1081	Optimized Substrates and Measurement Approaches for Raman Spectroscopy of Graphene Nanoribbons. 2019 , 256, 1900343	13
1080	Phonon-induced electronic relaxation in a strongly correlated system: The Sn/Si(111) (3B) adlayer revisited. 2019 , 100,	1

1079 LiNiO2 as a high-entropy charge- and bond-disproportionated glass. 2019 , 100,	4
Rattling-Induced Ultralow Thermal Conductivity Leading to Exceptional Thermoelectric Performance in AgInS. 2019 , 11, 33894-33900	11
1077 Unusually strong heteroatomic bonding in the complex polyanion of intermetallic BaPtAl. 2019 , 48, 1410	03-141 <u>1</u> 4
Materials Compatibility in Rechargeable Aluminum Batteries: Chemical and Electrochemical Properties between Vanadium Pentoxide and Chloroaluminate Ionic Liquids. 2019 , 31, 7238-7247	22
1075 Cohesive Properties of Ionic Liquids Calculated from First Principles. 2019 , 15, 5563-5578	13
Diractweyl semimetal phase in noncentrosymmetric transition metal monochalcogenides MoTe and WTe. 2019 , 7, 12151-12159	8
A General Atomic Surface Modification Strategy for Improving Anchoring and Electrocatalysis Behavior of TiCT MXene in Lithium-Sulfur Batteries. 2019 , 13, 11078-11086	129
Two-dimensional VDW crystal SnP3 with high carrier mobility and extraordinary sunlight absorbance. 2019 , 32, 327-332	1
1071 Near-field infrared spectroscopy of monolayer MnPS3. 2019 , 100,	10
Improving Predicted Nuclear Magnetic Resonance Chemical Shifts Using the Quasi-Harmonic Approximation. 2019 , 15, 5259-5274	9
Monolayer Etellurene: a promising p-type thermoelectric material via first-principles calculations. 2019 , 11, 18116-18123	20
SymTopo: An automatic tool for calculating topological properties of nonmagnetic crystalline materials. 2019 , 28, 087102	9
Personalized employment recommendation method based on semantic matching of requirements. 2019 , 1213, 052014	1
1066 o-C8 carbon: A new allotrope of superhard carbon. 2019 , 32, 357-364	5
1065 Momentum-resolved lattice dynamics of parent and electron-doped Sr2IrO4. 2019 , 100,	3
1064 Photoinduced Phase Transitions in Ferroelectrics. 2019 , 123, 087601	17
1063 Theoretical analysis of spectral lineshapes from molecular dynamics. 2019 , 5,	5
1062 Two-dimensional metal carbide comrade for tracing CO and CO2. 2019 , 496, 143685	18

1061	Prediction of thermal conductivity in dielectrics using fast, spectrally-resolved phonon transport simulations. 2019 , 144, 118595	7
1060	Comparative First-Principles Study of Antiperovskite Oxides and Nitrides as Thermoelectric Material: Multiple Dirac Cones, Low-Dimensional Band Dispersion, and High Valley Degeneracy. 2019 , 12,	6
1059	Computer Design of Two-Dimensional Monolayers with Octahedral 1,6-Carborane Units. 2019 , 64, 1031-1034	3
1058	First-principles study of structural, mechanical, dynamical stability, electronic and optical properties of orthorhombic CH3NH3SnI3 under pressure. 2019 , 92, 1	1
1057	Two-Dimensional Room-Temperature Ferromagnetic Semiconductors with Quantum Anomalous Hall Effect. 2019 , 12,	25
1056	Unusual lattice thermal conductivity in the simple crystalline compounds TlXTe2(X=Ga,In). 2019 , 100,	9
1055	Highly Anisotropic Thermal Transport in LiCoO. 2019 , 10, 5552-5556	12
1054	Assessing negative thermal expansion in mesoporous metal@rganic frameworks by molecular simulation. 2019 , 7, 24019-24026	16
1053	First principles study of g-MgN as an anode material for Na-, K-, Mg-, Ca- and Al-ion storage 2019 , 9, 27378-27385	11
1052	Critical Sublattice Symmetry Breaking: A Universal Criterion for Dirac Cone Splitting. 2019 , 123, 23082-23088	0
1051	Ab initio molecular dynamics simulation of vibrational energy redistribution of selective excitation of C-H stretching vibrations for solid nitromethane. 2019 , 21, 20822-20828	2
1050	Structural, mechanical, and thermodynamic properties of R-3m ReB4 under high pressure. 2019 , 92, 1	1
1049	Unconventional inner-TL electric polarization in TL-LaOBiS with ultrahigh carrier mobility. 2019 , 11, 18436-184	43
1048	Predicting two-dimensional topological phases in Janus materials by substitutional doping in transition metal dichalcogenide monolayers. 2019 , 3,	25
1047	Temperature dependence of vacancy concentration and void growth mechanism in Al with constant hydrogen concentration: A first-principles study. 2019 , 216, 106508	3
1046	Deformed octagon-hexagon-square structure of group-IV and group-V elements and III-V compounds. 2019 , 100,	3
1045	Structural, stability and thermoelectric properties for the monoclinic phase of NaSbS2 and NaSbSe2: A theoretical investigation. 2019 , 92, 1	3
1044	Topological insulator nanoribbons IA new paradigm for high thermoelectric performance. 2019 , 66, 104092	2

Synergistically Optimizing Carrier Concentration and Decreasing Sound Velocity in n-type AgInSe2 Thermoelectrics. 2019 , 31, 8182-8190	13
First-principles thermal compatibility between Ru-based Re-substitute alloys and Ir coatings. 2019 , 170, 109199	2
1041 Si-Cmma: A silicon thin film with excellent stability and Dirac nodal loop. 2019 , 100,	22
Odd E ven Layer Effect of Bismuth Oxychalcogenide Nanosurfaces: A First-Principles Study. 2019 , 123, 24024-24030	4
Gaussian approximation potential for studying the thermal conductivity of silicene. 2019 , 126, 105103	13
Experimental Evidence for Vibrational Entropy as Driving Parameter of Flexibility in the Metal D rganic Framework ZIF-4(Zn). 2019 , 31, 8366-8372	18
Electronic Properties of a New Family of Layered Materials from Groups 14 and 15: First-Principles Simulations. 2019 , 123, 25470-25476	6
Synthesis of clathrate cerium superhydride CeH at 80-100 GPa with atomic hydrogen sublattice. 2019 , 10, 4453	64
1035 A First-Principles Exploration of NaxSy Binary Phases at 1 atm and Under Pressure. 2019 , 9, 441	3
Large-Gap Quantum Spin Hall States in the Bilayer Hexagonal Structure of Rhenium and Technetium Dinitrides: A First-Principles Study. 2019 , 123, 25524-25530	3
1033 Predictions on High-Power Trivalent Metal Pentazolate Salts. 2019 , 10, 6166-6173	30
Volcano Trend in Electrocatalytic CO2 Reduction Activity over Atomically Dispersed Metal Sites on Nitrogen-Doped Carbon. 2019 , 9, 10426-10439	96
1031 A High-Pressure Compound of Argon and Nickel: Noble Gas in the Earth Core?. 2019 , 3, 2517-2524	8
1030 A Universal Length-Dependent Vibrational Mode in Graphene Nanoribbons. 2019 , 13, 13083-13091	15
Precipitate/vanadium interface and its strengthening on the vanadium alloys: A first-principles study. 2019 , 527, 151821	7
1028 Pressure controllable phase transition in MoTe2 by the interlayer band occupancy. 2019 , 383, 126016	3
Negative thermal expansion behavior in orthorhombic Sc2(MoO4)3 and Sc2(WO4)3. 2019 , 126, 125114	8
An ab initio study on the transition path of carbon dioxide at high pressure: Evidence for a new intermediate P4?m2 phase. 2019 , 21, e00429	1

1025	Strong phonon localization in PbTe with dislocations and large deviation to Matthiessen rule. 2019 , 5,	19
1024	Vibrational spectroscopy at atomic resolution with electron impact scattering. 2019 , 15, 1237-1241	50
1023	Phonon limited anisotropic quantum transport in phosphorene field effect transistors. 2019 , 126, 114502	3
1022	Prediction of improved magnetization and stability in Fe16N2 through alloying. 2019 , 126, 093903	10
1021	Surface Induced Phenytoin Polymorph. 2. Structure Validation by Comparing Experimental and Density Functional Theory Raman Spectra. 2019 , 19, 6067-6073	1
1020	Assessing exchange-correlation functional performance in the chalcogenide lacunar spinels GaM4Q8 (M=Mo, V, Nb, Ta; Q=S,Se). 2019 , 100,	15
1019	The impact of humic acid on metaldehyde adsorption onto powdered activated carbon in aqueous solution 2018 , 9, 11-22	8
1018	A new metallic Econjugated carbon sheet used for the cathode of Li-S batteries 2018, 9, 92-98	4
1017	Unique Schrdinger semimetal state in ternary Be2P3N honeycomb lattice. 2019, 7, 4118-4123	7
1016	Suppression of magnetic ordering in XXZ-type antiferromagnetic monolayer NiPS. 2019 , 10, 345	136
1015	Accuracy and reproducibility in crystal structure prediction: the curious case of ROY. 2019 , 21, 2080-2088	37
1014	2D planar penta-MN (M = Pd, Pt) sheets identified through structure search. 2018 , 21, 246-251	21
1013	VC and VMnC nanosheets with robust mechanical and thermal properties as promising materials for Li-ion batteries. 2019 , 21, 1606-1613	6
1012	Effects of the number of layers on the vibrational, electronic and optical properties of alpha lead oxide. 2019 , 21, 3868-3876	14
1011	Atomically thin NiB monolayer: a robust Dirac material. 2019 , 21, 617-622	17
1010	Shell model extension to the valence force field: application to single-layer black phosphorus. 2018 , 21, 322-328	5
1009	Mixed phononic and non-phononic transport in hybrid lead halide perovskites: glass-crystal duality, dynamical disorder, and anharmonicity. 2019 , 12, 216-229	31
1008	Strong interfacial interactions induced a large reduction in lateral thermal conductivity of transition-metal dichalcogenide superlattices 2019 , 9, 1387-1393	5

1007	An experimental and theoretical study into NaSbS2 as an emerging solar absorber. 2019 , 7, 2059-2067	13
1006	Theoretical investigations on structural, elastic, thermodynamic and electronic properties of Al3Ti and Al3V compounds in L12 structure under high pressure. 2019 , 6, 056536	4
1005	Fokker-Planck equation for lattice vibration: Stochastic dynamics and thermal conductivity. 2019 , 99,	1
1004	Lattice dynamics and negative thermal expansion in the framework compound ZnNi(CN)4 with two-dimensional and three-dimensional local environments. 2019 , 99,	12
1003	New high-pressure phases of FeN and FeC stable at Earth's core conditions: evidences for carbon-nitrogen isomorphism in Fe-compounds 2019 , 9, 3577-3581	13
1002	Room Temperature Commensurate Charge Density Wave in Epitaxial Strained TiTe2 Multilayer Films. 2019 , 6, 1801850	23
1001	Two-Dimensional Anti-Van't Hoff/Le Bel Array AlB with High Stability, Unique Motif, Triple Dirac Cones, and Superconductivity. 2019 , 141, 3630-3640	109
1000	Magnesium based materials for hydrogen based energy storage: Past, present and future. 2019 , 44, 7809-785	9264
999	Insight into the Discharge Products and Mechanism of Room-Temperature SodiumBulfur Batteries: A First-Principles Study. 2019 , 123, 3988-3995	18
998	PCF-Graphene: A 2D sp2-Hybridized Carbon Allotrope with a Direct Band Gap. 2019 , 123, 4567-4573	13
997	Phonon Scattering by Dislocations in GaN. 2019 , 11, 8175-8181	18
996	Crystal structures, dielectric properties, and phase transition in hybrid improper ferroelectric Sr3Sn2O7-based ceramics. 2019 , 125, 044101	15
995	Janus Chromium Dichalcogenide Monolayers with Low Carrier Recombination for Photocatalytic Overall Water-Splitting under Infrared Light. 2019 , 123, 4186-4192	28
994	Electronic structure, optical properties, and phonon transport in Janus monolayer PtSSe via first-principles study. 2019 , 99, 1025-1040	37
993	Density Functional Theory Calculations of Structural, Electronic, and Magnetic Properties of the 3d Metal Trifluorides MF (M = Ti-Ni) in the Solid State. 2019 , 40, 1190-1197	6
992	Machine learning coarse grained models for water. 2019 , 10, 379	55
991	Strong phonon anharmonicity and low thermal conductivity of monolayer tin oxides driven by lone-pair electrons. 2019 , 114, 031901	11
990	Single-layer ferromagnetic and piezoelectric CoAsS with pentagonal structure. 2019 , 7, 011101	6

989	Infrared-pump electronic-probe of methylammonium lead iodide reveals electronically decoupled organic and inorganic sublattices. 2019 , 10, 482	13
988	Stabilities and novel electronic structures of three carbon nitride bilayers. 2019 , 9, 1025	8
987	Low lattice thermal conductivity and high thermoelectric figure of merit in Na2MgSn. 2019, 99,	6
986	Raman spectroscopy of the low-dimensional antiferromagnet SrRu2O6 with large NBl temperature. 2019 , 99,	6
985	Discovery of a ferroelastic topological insulator in a two-dimensional tetragonal lattice. 2019 , 21, 5165-5169	4
984	The role of decomposition reactions in assessing first-principles predictions of solid stability. 2019 , 5,	32
983	Direct probe of the nuclear modes limiting charge mobility in molecular semiconductors. 2019 , 6, 182-191	37
982	Surface phonons of lithium ion battery active materials. 2019 , 3, 508-513	13
981	Extremely high tensile strength and superior thermal conductivity of an sp3-hybridized superhard C24 fullerene crystal. 2019 , 7, 3426-3431	6
980	Proposal of a stable B3S nanosheet as an efficient hydrogen evolution catalyst. 2019 , 7, 3752-3756	22
979	A new 2D high-pressure phase of PdSe2 with high-mobility transport anisotropy for photovoltaic applications. 2019 , 7, 2096-2105	43
978	A novel hydrogenated boron-carbon monolayer with high stability and promising carrier mobility. 2019 , 21, 2572-2577	6
977	Effects of tensile strain and finite size on thermal conductivity in monolayer WSe. 2018, 21, 468-477	36
976	Density functional theory calculations and thermodynamic analysis of bridgmanite surface structure. 2019 , 21, 1009-1013	3
975	Two-dimensional antiferromagnetic boron form first principles. 2019 , 9, 055211	2
974	Exploration of crystal structure and the origin of unexpected intrinsic ductility of £107Ta2. 2019 , 797, 1198-1204	1
973	Observation of 🛮 AlSm reveals motif-aware structural evolution in Al-Sm alloys. 2019 , 9, 6692	3
972	Electronic structure and high-temperature thermochemistry of BaZrO perovskite from first-principles calculations. 2019 , 21, 12468-12476	3

971	Energy storage properties of a two-dimensional TiB monolayer. 2019 , 21, 13151-13156	7
970	Predicting three-dimensional icosahedron-based boron B60. 2019 , 99,	15
969	Lattice dynamics of thermoelectric palladium sulfide. 2019 , 798, 484-492	7
968	Reliable thermodynamic estimators for screening caloric materials. 2019 , 802, 712-722	18
967	Diversities of stoichiometry and electrical conductivity in sodium sulfides. 2019 , 7, 16472-16478	6
966	Quantum dynamics of hydrogen in the iron-based superconductor LaFeAsO0.9D0.1 measured with inelastic neutron spectroscopy. 2019 , 99,	1
965	Stable, one-dimensional suspended and supported monatomic chains of pnictogens: a metal-insulator framework. 2019 , 21, 14832-14845	4
964	Computational polymorph screening reveals late-appearing and poorly-soluble form of rotigotine. 2019 , 2,	24
963	Band vs. polaron: vibrational motion and chemical expansion of hydride ions as signatures for the electronic character in oxyhydride barium titanate. 2019 , 7, 16211-16221	13
962	Anisotropic Thermal Boundary Resistance across 2D Black Phosphorus: Experiment and Atomistic Modeling of Interfacial Energy Transport. 2019 , 31, e1901021	19
961	Stability predictions of magnetic MAX compounds. 2019 , 31, 405902	11
960	Reliable electrochemical phase diagrams of magnetic transition metals and related compounds from high-throughput ab initio calculations. 2019 , 3,	18
959	Tunable valley splitting and an anomalous valley Hall effect in hole-doped WS by proximity coupling with a ferromagnetic MnO monolayer. 2019 , 11, 13567-13575	23
958	Importance of zero-point energy for crystalline ice phases: A comparison of force fields and density functional theory. 2019 , 150, 234504	4
957	Carboneyane: A nodal line topological carbon with splp2 lp3 chemical bonds. 2019 , 152, 909-914	10
956	Temperature-dependent properties of magnetic CuFeS2 from first-principles calculations: Structure, mechanics, and thermodynamics. 2019 , 9, 065021	7
955	Ultralow thermal conductivity of BaAg2SnSe4 and the effect of doping by Ga and In. 2019 , 9, 100098	14
954	A comparative study of the thermoelectric performance of graphene-like BX ($X = P$, As, Sb) monolayers. 2019 , 31, 385701	8

953	High thermal conductivity of high-quality monolayer boron nitride and its thermal expansion. 2019 , 5, eaav0129	143
952	Vibrational spectra of PbBiTe, PbBiTe, and PbBiTe topological insulators: temperature-dependent Raman and theoretical insights from DFT simulations. 2019 , 21, 15030-15039	12
951	Reststrahlen Band Studies of RuCrX (X = Si, Ge, Sn) Half Heusler Alloys. 2019 , 48, 5323-5327	5
950	First-principles prediction of magnetically ordered half-metals above room temperature. 2019 , 5, 404-412	9
949	Transition-Metal Diboride: A New Family of Two-Dimensional Materials Designed for Selective CO2 Electroreduction. 2019 , 123, 16294-16299	25
948	Hematene: a 2D magnetic material in van der Waals or non-van der Waals heterostructures. 2019 , 6, 045002	12
947	Sampling-dependent systematic errors in effective harmonic models. 2019 , 99,	3
946	First-principles calculation study of Mg2XH6 (X=Fe, Ru) on thermoelectric properties. 2019 , 6, 085536	Ο
945	Room-Temperature Quantum Anomalous Hall Effect in Single-Layer CrP2S6. 2019 , 123, 14707-14711	5
944	How is Honeycomb Borophene Stabilized on Al(111)?. 2019 , 123, 14858-14864	26
944	How is Honeycomb Borophene Stabilized on Al(111)?. 2019 , 123, 14858-14864 Effect of Ta addition on the structural, thermodynamic and mechanical properties of CoCrFeNi high entropy alloys. 2019 , 9, 16447-16454	26 5
	Effect of Ta addition on the structural, thermodynamic and mechanical properties of CoCrFeNi high	
943	Effect of Ta addition on the structural, thermodynamic and mechanical properties of CoCrFeNi high entropy alloys. 2019 , 9, 16447-16454 Novel Metallic Clathrates of Group-IV Elements and Their Compounds in a Dense Hexagonal	5
943	Effect of Ta addition on the structural, thermodynamic and mechanical properties of CoCrFeNi high entropy alloys. 2019 , 9, 16447-16454 Novel Metallic Clathrates of Group-IV Elements and Their Compounds in a Dense Hexagonal Lattice. 2019 , 123, 15330-15338 The n- and p-type thermoelectric response of a semiconducting Co-based quaternary Heusler alloy:	5
943 942 941	Effect of Ta addition on the structural, thermodynamic and mechanical properties of CoCrFeNi high entropy alloys. 2019, 9, 16447-16454 Novel Metallic Clathrates of Group-IV Elements and Their Compounds in a Dense Hexagonal Lattice. 2019, 123, 15330-15338 The n- and p-type thermoelectric response of a semiconducting Co-based quaternary Heusler alloy: a density functional approach. 2019, 7, 7664-7671 A New sp28p3-Hybridized Metallic Carbon Network for Lithium-Ion Battery Anode with Enhanced	5 3 12
943 942 941 940	Effect of Ta addition on the structural, thermodynamic and mechanical properties of CoCrFeNi high entropy alloys. 2019, 9, 16447-16454 Novel Metallic Clathrates of Group-IV Elements and Their Compounds in a Dense Hexagonal Lattice. 2019, 123, 15330-15338 The n- and p-type thermoelectric response of a semiconducting Co-based quaternary Heusler alloy: a density functional approach. 2019, 7, 7664-7671 A New sp28p3-Hybridized Metallic Carbon Network for Lithium-Ion Battery Anode with Enhanced Safety and Lithium-Ion Diffusion Rate. 2019, 123, 15412-15418 Syntheses and Characterization of Diammine-Nickel/Cobalt(II)-Bisdicyanamide M(NH)[N(CN)] with	5 3 12
943 942 941 940 939	Effect of Ta addition on the structural, thermodynamic and mechanical properties of CoCrFeNi high entropy alloys. 2019, 9, 16447-16454 Novel Metallic Clathrates of Group-IV Elements and Their Compounds in a Dense Hexagonal Lattice. 2019, 123, 15330-15338 The n- and p-type thermoelectric response of a semiconducting Co-based quaternary Heusler alloy: a density functional approach. 2019, 7, 7664-7671 A New sp28p3-Hybridized Metallic Carbon Network for Lithium-Ion Battery Anode with Enhanced Safety and Lithium-Ion Diffusion Rate. 2019, 123, 15412-15418 Syntheses and Characterization of Diammine-Nickel/Cobalt(II)-Bisdicyanamide M(NH)[N(CN)] with M = Ni and Co. 2019, 58, 7803-7811	5 3 12 10

935	Lithium diffusion in Li2X (X=O, S, and Se): Ab initio simulations and inelastic neutron scattering measurements. 2019 , 99,	6
934	Quantum anomalous Hall effect and gate-controllable topological phase transition in layered EuCd2As2. 2019 , 99,	8
933	Competing Polar and Antipolar Structures in the Ruddlesden P opper Layered Perovskite Li2SrNb2O7. 2019 , 31, 4418-4425	15
932	Theoretical and Experimental Investigation of 2D Hematite. 2019 , 123, 16359-16365	9
931	Topological phase transition induced by magnetic proximity effect in two dimensions. 2019 , 31, 395502	1
930	On-Surface Synthesis and Characterization of Acene-Based Nanoribbons Incorporating Four-Membered Rings. 2019 , 25, 12074-12082	18
929	Perfect planar tetra-coordinated MC monolayer: superior anode material for Li-ion battery. 2019 , 21, 15187-15194	9
928	Optimizing the thermoelectric transport properties of BiOSe monolayer via biaxial strain. 2019 , 21, 15097-15	510 5
927	Absorption edge, urbach tail, and electron-phonon interactions in topological insulator Bi2Se3 and band insulator (Bi0.89In0.11)2Se3. 2019 , 114, 162105	1
926	Ab Initio Search of Polymer Crystals with High Thermal Conductivity. 2019 , 31, 4649-4656	4
925	Infrared and Raman spectra of BiOX and BiOX ($X = S$, Se, and Te) studied from first principles calculations 2019 , 9, 18042-18049	14
924	Stable group-IIB elements I n, Cd and Hg at terapascal pressures. 2019 , 126, 36001	1
923	Robust two-dimensional ferroelectricity in single-layer EbbP and EbbAs. 2019 , 11, 11864-11871	18
922	Improved thermodynamic properties of doped LiBH4 for hydrogen storage: First-principal calculation. 2019 , 44, 16793-16802	13
921	Indications of Phonon Hydrodynamics in Telescopic Silicon Nanowires. 2019 , 11,	5
920	Neutron diffraction study of temperature-dependent elasticity of B19? NiTiElinvar effect and elastic softening. 2019 , 173, 281-291	13
919	Discovery of hexagonal ternary phase TilnB and its evolution to layered boride TiB. 2019 , 10, 2284	72
918	A scattering rate model for accelerated evaluation of lattice thermal conductivity bypassing anharmonic force constants. 2019 , 125, 205104	3

917	Effect of point defects on electronic and magnetic properties of single-layer SiO. 2019, 99, 2340-2353	2
916	Lead-free double perovskites CsInCuCl and (CHNH)InCuCl: electronic, optical, and electrical properties. 2019 , 11, 11173-11182	18
915	Strain-induced N-N bonding and magnetic changes in monolayer intrinsic ferromagnetic TmN (Tm = Tc and Nb). 2019 , 31, 335801	3
914	Computational prediction and characterization of two-dimensional pentagonal arsenopyrite FeAsS. 2019 , 166, 105-110	5
913	Thermal conductivity and diffusion mechanisms of noble gases in uranium dioxide: A DFT+U study. 2019 , 521, 137-145	18
912	Double Half-Heuslers. 2019 , 3, 1226-1238	46
911	Coupling of Spinons with Defects and Phonons in the Spin Chain Compound $Ca_{2}CuO_{3}$. 2019 , 122, 185901	4
910	New Paradigm for Gas Sensing by Two-Dimensional Materials. 2019 ,	13
909	Ferroelectricity and Large Piezoelectric Response of AlN/ScN Superlattice. 2019, 11, 20482-20490	22
908	Thermodynamic modeling of the Si-Y system aided by first-principles and phonon calculations. 2019 , 65, 282-290	4
907	Characterization of two-dimensional Ga1Al N ordered alloys with varying chemical composition. 2019 , 167, 13-18	2
906	Atomic structure and enhanced thermostability of a new structure MgYZn4 formed by ordered substitution of Y for Mg in MgZn2 in a Mg-Zn-Y alloy. 2019 , 35, 2058-2063	6
905	Computational Dissection of 2D SiC7 Monolayer: A Direct Band Gap Semiconductor and High Power Conversion Efficiency. 2019 , 2, 1900058	8
904	Predicted dynamically stable new phase for CrO2 compound: DFT´+ U calculations. 2019 , 21, e00400	3
903	Structural instability and magnetism of superconducting KCr3As3. 2019 , 99,	6
902	New horizons in thermoelectric materials: Correlated electrons, organic transport, machine learning, and more. 2019 , 125, 180902	31
901	Ultrahigh-pressure induced decomposition of silicon disulfide into silicon-sulfur compounds with high coordination numbers. 2019 , 99,	7
900	Novel high/ultrahigh pressure structures of TiO2 with low band gaps. 2019 , 166, 303-310	4

899	Shock induced phase transition in SiC polytypes. 2019 , 125, 185903	5
898	Drastic enhancement of the Raman intensity in few-layer InSe by uniaxial strain. 2019 , 99,	18
897	Magnetic borophenes from an evolutionary search. 2019 , 99,	15
896	Computational Discovery of Transparent Conducting In-Plane Ordered MXene (i-MXene) Alloys. 2019 , 31, 4124-4132	5
895	First-principles study of structural stability, electronic properties and lattice thermal conductivity of KAgX (X = S, Se, Te). 2019 , 92, 1	6
894	Ab initio exploration and prediction of AE-containing nitrido(litho/magneso)tetrelates (AE = Ca, Sr; Tt = Si, Ge) with [SiN] or [GeN] units. 2019 , 48, 8671-8677	O
893	Evidence of ferromagnetic ground state and strong spin phonon coupling in Zr2TiAl with bi-axial strain: first principles study. 2019 , 3, 055010	
892	Super-stretchability in two-dimensional RuCl3 and RuBr3 confirmed by first-principles simulations. 2019 , 113, 79-85	4
891	Structural prediction of stabilized atomically thin tin layers. 2019 , 3,	11
890	High bond difference parameter-induced low thermal transmission in carbon allotropes with sp and sp hybridization. 2019 , 21, 12611-12619	3
889	Oxygenation-Induced Two-Dimensional Topological Insulators in Antimony Arsenide. 2019 , 13, 1900146	0
888	Covalent bonding versus total energy: On the attainability of certain predicted low-energy carbon allotropes. 2019 , 148, 151-158	6
887	Atomistic and experimental study on thermal conductivity of bulk and porous cerium dioxide. 2019 , 9, 6326	11
886	Phase stability, elastic, anisotropic and thermodynamic properties of HoT2Al20 (T = Ti, V, Cr) intermetallic cage compounds. 2019 , 45, 833-840	9
885	Theoretical study of M⊞ (M=Ti, V, Zr or Nb) structure phase diagram at high pressures. 2019 , 44, 13592-13605	2
884	Thermal Conductivity Enhancement in MoS_{2} under Extreme Strain. 2019 , 122, 155901	37
883	First-principles analysis of structural stability, electronic and phonon transport properties of lateral MoS2-WX2 heterostructures. 2019 , 19, e00389	2
882	Thermal Expansion and Other Thermodynamic Properties of -TiAl and -TiAl Intermetallic Phases from First Principles Methods. 2019 , 12,	9

881	A Metastable Fo-III Wedge in Cold Slabs Subducted to the Lower Part of the Mantle Transition Zone: A Hypothesis Based on First-Principles Simulations. 2019 , 9, 186	2
880	First-principles investigation of the concentration effect on equilibrium fractionation of Ca isotopes in forsterite. 2019 , 38, 497-507	3
879	Thermodynamics, Electronic Structure, and Vibrational Properties of Sn (S Se) Solid Solutions for Energy Applications. 2019 , 31, 3672-3685	6
878	Investigation of structural, electronic and lattice dynamical properties of XNiH (X´=´Li, Na and K) perovskite type hydrides and their hydrogen storage applications. 2019 , 44, 15173-15182	18
877	Anharmonic Vibrational States of Solids from DFT Calculations. Part I: Description of the Potential Energy Surface. 2019 , 15, 3755-3765	17
876	Anharmonic Vibrational States of Solids from DFT Calculations. Part II: Implementation of the VSCF and VCI Methods. 2019 , 15, 3766-3777	23
875	Improvement of Visible-Light Photocatalytic Efficiency in a Novel InSe/Zr2CO2 Heterostructure for Overall Water Splitting. 2019 ,	40
874	Natural sulvanite Cu3MX4 (M = Nb, Ta; $X = S$, Se): Promising visible-light photocatalysts for water splitting. 2019 , 165, 137-143	4
873	Simulation of a collimator and sapphire filter for PGAA facility of the Moroccan TRIGA MARK II research reactor. 2019 , 150, 14-18	4
872	Lattice and spin dynamics in multiferroic BiFeO and MnO. 2019 , 6, 642-652	6
871	Tandem Conversion of CO2 to Valuable Hydrocarbons in Highly Concentrated Potassium Iron Catalysts. 2019 , 11, 2879-2886	37
870	Tunable gap in stable arsenene nanoribbons opens the door to electronic applications 2019 , 9, 11818-11823	2
869	DFT based study on structural stability and transport properties of Sr3AsN: A potential thermoelectric material. 2019 , 34, 2635-2642	3
868	Energy, Phonon, and Dynamic Stability Criteria of Two-Dimensional Materials. 2019 , 11, 24876-24884	33
867	A Li2CuPS4 superionic conductor: a new sulfide-based solid-state electrolyte. 2019 , 7, 12645-12653	22
866	Thermoelectric Properties of Hexagonal MIIIM = As, Sb, and Bi) Monolayers from First-Principles Calculations. 2019 , 9,	16
865	Structural and electronic properties of predicting two-dimensional BC2P and BC3P3 monolayers by the global optimization method. 2019 , 726, 69-76	5
864	Development of interatomic potentials for the complex binary compound Sb2Te3 and the prediction of thermal conductivity. 2019 , 99,	2

863	Exploring planar and nonplanar siligraphene: a first-principles study 2019 , 9, 12276-12281	4
862	A Large Family of Synthetic Two-Dimensional Metal Hydrides. 2019 , 141, 7899-7905	16
861	Outstanding strength, optical characteristics and thermal conductivity of graphene-like BC3 and BC6N semiconductors. 2019 , 149, 733-742	93
860	StrainBpintronics: Modulating Electronic and Magnetic Properties of Hf2MnC2O2 MXene by Uniaxial Strain. 2019 , 123, 12451-12459	19
859	Prediction of Superconductivity in Porous, Covalent Triazine Frameworks. 2019 , 1, 30-36	10
858	First-Principles Study of Chemical Driving Force for Face Centered Cubic to Hexagonal Close Packed Martensitic Transformation in Hydrogen-Charged Iron. 2019 , 50, 3019-3023	3
857	First-principles study on the two-dimensional siligene (2D SiGe) as an anode material of an alkali metal ion battery. 2019 , 165, 121-128	31
856	B3S monolayer: prediction of a high-performance anode material for lithium-ion batteries. 2019 , 7, 12706-12	71239
855	Computational screening of MX (M = Ga, Ge, Sn, In; $X = As$, Se) van der Waals heterostructures as suitable candidates for solar cells. 2019 , 52, 335303	3
854	Predicting Accurate Phonon Spectra: An Improved Description of Lattice Dynamics in Thermoelectric Clathrates Based on the SCAN Meta-GGA Functional. 2019 , 31, 2571-2576	4
853	DHQ-graphene: a novel two-dimensional defective graphene for corrosion-resistant coating. 2019 , 7, 8967-8974	14
852	Hybrid improper ferroelectricity and possible ferroelectric switching paths in Sr3Hf2O7. 2019 , 125, 114105	10
851	A 2D nonsymmorphic Dirac semimetal in a chemically modified group-VA monolayer with a black phosphorene structure. 2019 , 11, 7256-7262	7
850	Structural prediction and multilayer Li+ storage in two-dimensional VC2 carbide studied by first-principles calculations. 2019 , 7, 8873-8881	20
849	General method for atomistic spin-lattice dynamics with first-principles accuracy. 2019 , 99,	13
848	Ammonothermal Synthesis, X-Ray and Time-of-Flight Neutron Crystal-Structure Determination, and Vibrational Properties of Barium Guanidinate, Ba(CNH). 2019 , 8, 327-332	6
847	A New Family of Two-Dimensional Crystals: Open-Framework T X ($T = C$, Si, Ge, Sn; X = O, S, Se, Te) Compounds with Tetrahedral Bonding. 2019 , 19, 2694-2699	7
846	Machine-Learning-Assisted Development and Theoretical Consideration for the AlFeSi Thermoelectric Material. 2019 , 11, 11545-11554	43

845	Catalytic de-chlorination of products from PVC degradation by magnetite (Fe3O4). 2019 , 480, 792-801		9
844	Phase equilibria of the Zn-Ti system: Experiments, first-principles calculations and Calphad assessment. 2019 , 64, 213-224		4
843	Perfect mechanical and robust electronic properties of new carbon nanothreads: A first principles study. 2019 , 111, 37-43		7
842	Understanding the molar volume of alkali-alkaline earth-silicate glasses via Voronoi polyhedra analysis. <i>Scripta Materialia</i> , 2019 , 166, 1-5	5.6	7
841	Rational synthesis and electrochemical performance of LiVOPO4 polymorphs. 2019 , 7, 8423-8432		16
840	Electronic, and thermoelectric properties of half-heusler compounds MCoSb (M = Ti, Zr, Hf): a first principles study. 2019 , 6, 066307		15
839	Origin of anisotropy and compositional dependence of phonon and electron transport in ZnO based natural superlattices and role of atomic layer interfaces. 2019 , 59, 651-666		3
838	Determination of the scattering cross section of calcium using the VESUVIO spectrometer. 2019 , 927, 443-450		6
837	Neural network force fields for simple metals and semiconductors: construction and application to the calculation of phonons and melting temperatures. 2019 , 21, 6506-6516		16
836	Tunable 2D-gallium arsenide and graphene bandgaps in a graphene/GaAs heterostructure: an ab initio study. 2019 , 31, 265502		5
835	Thermal conductivity and phonon hydrodynamics in transition metal dichalcogenides from first-principles. 2019 , 6, 035002		25
834	Self-consistent site-dependent DFT+U study of stoichiometric and defective SrMnO3. 2019 , 99,		21
833	Intrinsic Flexibility of the EMT Zeolite Framework under Pressure. 2019, 24,		6
832	Theoretical study on the mechanical and thermal properties of uranium dioxide doped with lanthanide fission products. 2019 , 519, 128-136		6
831	Design Strategy for High-Performance Thermoelectric Materials: The Prediction of Electron-Doped KZrCuSe3. 2019 , 31, 3018-3024		11
830	Atomic-scale design of friction and energy dissipation. 2019 , 99,		17
829	Thermochemical analysis of Mo-C-H system for synthesis of molybdenum carbides. 2019 , 676, 27-32		2
828	Low Lattice Thermal Conductivity of a Two-Dimensional Phosphorene Oxide. 2019 , 9, 5149		10

827	BX1 B X2 (X1, X2 = P, As, Sb) lateral heterostructure: novel and efficient two-dimensional photovoltaic materials with ultra-high carrier mobilities. 2019 , 7, 10684-10695	21
826	Ground-state structure of semiconducting and superconducting phases in xenon carbides at high pressure. 2019 , 9, 2459	13
825	The influence of lattice vibrations and electronic free energy on phase stability of titanium silicides and Si solubility in hcp titanium: A DFT study. 2019 , 65, 194-203	3
824	Accelerated Discovery of New 8-Electron Half-Heusler Compounds as Promising Energy and Topological Quantum Materials. 2019 , 123, 7074-7080	21
823	Growth and Thermo-driven Crystalline Phase Transition of Metastable Monolayer 1T'-WSe Thin Film. 2019 , 9, 2685	13
822	Intrinsic ferromagnetism and topological properties in two-dimensional rhenium halides. 2019 , 11, 6101-6107	15
821	Comprehensive analysis of thermodynamic properties of calcium nitrate. 2019 , 134, 187-194	7
820	Understanding the elastic and thermal response in TiC-based ceramic-metal composite systems: First-principles and mechanical studies. 2019 , 789, 712-719	8
819	Axion Insulator State in a Ferromagnet/Topological Insulator/Antiferromagnet Heterostructure. 2019 , 19, 2472-2477	12
818	Two-Dimensional Anisotropic C Carbon Allotrope with Mechanically Tunable Band Gap. 2019 , 4, 5002-5011	4
817	Thermodynamic evidence of fractionalized excitations in R uCl3. 2019 , 99,	25
816	Differential anharmonicity and thermal expansion coefficient in 3C-SiC nanowires. 2019, 99,	5
815	Materials Design of Solar Cell Absorbers Beyond Perovskites and Conventional Semiconductors via Combining Tetrahedral and Octahedral Coordination. 2019 , 31, e1806593	29
814	Challenges and Opportunities in Modeling Oxides for Energy and Information Devices. 2019 , 1-13	
813	Single-layer Ag6S2: First principles investigation of a new two-dimensional direct bandgap semiconductor. 2019 , 163, 278-281	7
812	The Effect of Pressure on Elastic Anisotropy, Vibration and Optical Properties of a AgScSi Compound. 2019 , 48, 4050-4056	4
811	Thermodynamic modelling of Al-B-N system. 2019 , 65, 291-298	3
810	Significant THz absorption in CHNH molecular defect-incorporated organic-inorganic hybrid perovskite thin film. 2019 , 9, 5811	12

(2019-2019)

809	scrain- and carrier-tunable magnetic properties or a two-dimensional intrinsically refromagnetic semiconductor: CoBr2 monolayer. 2019 , 99,	16
808	Structural and electronic properties of T graphene nanotubes: a first-principles study. 2019 , 21, 053015	6
807	Promoted high temperature carrier mobility and thermoelectric performance of InTe enabled by altering scattering mechanism. 2019 , 7, 11690-11698	16
806	⊞MnO2 under pressure: Possible route to ⊕MnO2. 2019 , 6, 076108	2
805	Stability of 2D Alkaline-Earth Metal Silicides, Germanides and Stannides. 2019 , 18, 1940013	1
804	DFT calculations of the synergistic effect of EMnO/graphene composites for electrochemical adsorption of lithium ions. 2019 , 21, 8133-8140	16
803	Pressure-Stabilized High-Energy-Density Alkaline-Earth-Metal Pentazolate Salts. 2019 , 123, 10205-10211	37
802	First-Principles Prediction of Room-Temperature Ferromagnetic Semiconductor MnS2 via Isovalent Alloying. 2019 , 123, 10114-10119	19
801	First-principles prediction of phonon-mediated superconductivity in XBC (X = Mg, Ca, Sr, Ba). 2019 , 21, 8767-8773	5
800	Two-dimensional Blue-AsP monolayers with tunable direct band gap and ultrahigh carrier mobility show promising high-performance photovoltaic properties. 2019 , 11, 8260-8269	38
799	Electric-Field-Controlled Thermal Switch in Ferroelectric Materials Using First-Principles Calculations and Domain-Wall Engineering. 2019 , 11,	17
798	Thermodynamic and physical properties of Zr3Fe and ZrFe2 intermetallic compounds. 2019 , 109, 189-196	9
797	Dynamical stability and vibrational properties of Pt clusters. 2019 , 131, 131-138	4
796	MnB nanosheet and nanotube: stability, electronic structures, novel functionalization and application for Li-ion batteries. 2019 , 11, 7857-7865	13
795	Predicting two-dimensional pentagonal transition metal monophosphides for efficient electrocatalytic nitrogen reduction. 2019 , 7, 11444-11451	35
794	First principles study on the structural, electronic and phonon properties of monolayer B2Si. 2019 , 59, 21-27	2
793	Rare-earth magnetic nitride perovskites. 2019 , 2, 025003	14
79 ²	Stabilizing the isolated Sn2Bi nanosheet and tailoring its electronic structure by chemical functionalization: A computational study. 2019 , 114, 073103	8

791	2D selenium allotropes from first principles and swarm intelligence. 2019 , 31, 235702	11
790	Advances in Density-Functional Calculations for Materials Modeling. 2019 , 49, 1-30	56
789	First-principles study of square phase MX2 and Janus MXY (M=Mo, W; X, Y=S, Se, Te) transition metal dichalcogenide monolayers under biaxial strain. 2019 , 110, 134-139	27
788	Synthesis, crystallographic structure and thermodynamic properties of T2-Al2MgC2. 2019 , 273, 150-157	6
787	Equilibrium Mg isotope fractionation among aqueous Mg2+, carbonates, brucite and lizardite: Insights from first-principles molecular dynamics simulations. 2019 , 250, 117-129	24
786	Tunable Topological State, High Hole-Carrier Mobility, and Prominent Sunlight Absorbance in Monolayered Calcium Triarsenide. 2019 , 10, 761-767	12
785	A first-principles theoretical study on the potential thermoelectric properties of MgH2 and CaH2. 2019 , 6, 055510	1
7 ⁸ 4	sp3 bonded 2-dimensional allotrope of carbon: A first-principles prediction. 2019 , 146, 430-437	16
783	Design of pentagonal NbX monolayers for electronics and electrocatalysis. 2019 , 479, 595-600	11
782	T4,4,4-graphyne: A 2D carbon allotrope with an intrinsic direct bandgap. 2019 , 293, 23-27	9
781	Thermodynamic and Mechanical Stability of Crystalline Phases of Li2S2. 2019 , 123, 4674-4681	10
7 ⁸ 0	Machine Learning-Aided Design of Materials with Target Elastic Properties. 2019 , 123, 5042-5047	13
779	Phonon thermal conductance across GaN-AlN interfaces from first principles. 2019 , 99,	28
778	Phase stabilities and vibrational analysis of hydrogenated diamondized bilayer graphenes: A first principles investigation. 2019 , 146, 468-475	21
777	Simulation of Inelastic Neutron Scattering Spectra Using OCLIMAX. 2019 , 15, 1974-1982	48
776	Tetragonal C24: a topological nodal-surface semimetal with potential as an anode material for sodium ion batteries. 2019 , 7, 5733-5739	40
775	Using nanotubes to study the phonon spectrum of two-dimensional materials. 2019 , 21, 5215-5223	2
774	Stability and flexibility of heterometallic formate perovskites with the dimethylammonium cation: pressure-induced phase transitions. 2019 , 21, 4200-4208	9

773	Thermal Resistance by Transition Between Collective and Non-Collective Phonon Flows in Graphitic Materials. 2019 , 23, 247-258	6
772	Thermal transport in MoS2 from molecular dynamics using different empirical potentials. 2019 , 99,	31
771	High thermoelectric performance in the hexagonal bilayer structure consisting of light boron and phosphorus elements. 2019 , 99,	15
770	Isolation of Single-Wired Transition-Metal Monochalcogenides by Carbon Nanotubes. 2019 , 19, 4845-4851	31
769	From DFT to machine learning: recent approaches to materials science review. 2019 , 2, 032001	206
768	One-dimensionally extended oxygen vacancy states in perovskite oxides. 2019 , 99,	4
767	Catalogue of topological electronic materials. 2019 , 566, 475-479	354
766	Origin of Ultralow Thermal Conductivity in n-Type Cubic Bulk AgBiS2: Soft Ag Vibrations and Local Structural Distortion Induced by the Bi 6s2 Lone Pair. 2019 , 31, 2106-2113	44
765	Using Green-Kubo modal analysis (GKMA) and interface conductance modal analysis (ICMA) to study phonon transport with molecular dynamics. 2019 , 125, 081101	14
764	Electronic and phonon structure of nickel hydroxide: first-principles calculation study. 2019 , 92, 1	
763	Investigation of two-dimensional hf-based MXenes as the anode materials for li/na-ion batteries: A DFT study. 2019 , 40, 1352-1359	16
762	First-principles study of elastic, thermal and optical properties of a metal-shrouded two-dimensional semiconductor Tl2O. 2019 , 293, 40-47	4
761	Edge Segregated Polymorphism in 2D Molybdenum Carbide. 2019 , 31, e1808343	40
760	Thermodynamic properties of tin: Part I Experimental investigation, ab-initio modelling of ∃ Ephase and a thermodynamic description for pure metal in solid and liquid state from 0 K. 2019 , 65, 50-72	17
759	Composition change-driven texturing and doping in solution-processed SnSe thermoelectric thin films. 2019 , 10, 864	39
75 ⁸	Modified embedded-atom method potential of niobium for studies on mechanical properties. 2019 , 161, 351-363	11
757	A comparative evaluation of the activities of thiol group and hydroxyl group in low-frequency vibrations using terahertz spectroscopy and DFT calculations. 2019 , 214, 246-251	6
756	Kondo-like phonon scattering in thermoelectric clathrates. 2019 , 10, 887	23

755	Phonon spectrum attributes for the negative thermal expansion of MZrF6 (M = Ca, Mn \mathbb{N} i, Zn). 2019 , 6, 1022-1028	0
754	First-principles study of VPOO as a cathode material for rechargeable Mg batteries. 2019 , 21, 4947-4952	4
753	Phonons in deformable microporous crystalline solids. 2019 , 234, 513-527	3
752	Intrinsic Half-Metallicity in 2D Ternary Chalcogenides with High Critical Temperature and Controllable Magnetization Direction. 2019 , 29, 1808380	34
751	The Hiphive Package for the Extraction of High-Order Force Constants by Machine Learning. 2019 , 2, 1800184	75
75°	Phonon transport and thermoelectric properties of semiconducting BiTeX (X = S, Se, Te) monolayers. 2019 , 21, 5679-5688	34
749	The role of strontium deficiency and pressure on electron-phonon superconductivity in Sr3SnO. 2019 , 559, 42-49	
748	Structure and Stability of the Stoichiometric Al3Fe Phase. 2019 , 9, 1322	4
747	Two functionals approach in DFT for the prediction of thermoelectric properties of FeScX ($X = P$, As, Sb) full-Heusler compounds. 2019 , 31, 435701	7
746	Thermomechanical, electronic and thermodynamic properties of ZnS cubic polymorphs: an ab initio investigation on the zinc-blende-rock-salt phase transition. 2019 , 75, 1042-1059	10
745	First-principles investigation of elastic, mechanical, electronic and thermodynamic properties of Al3Li compound under pressure. 2019 , 6, 1265g6	1
744	Relaxation of electrons in quantum-confined states in Pb/Si(111) thin films from master equation with first-principles-derived rates. 2019 , 21, 123023	O
743	Parametrically constrained geometry relaxations for high-throughput materials science. 2019 , 5,	8
742	Evolution of the Structural, Mechanical, and Phonon Properties of GeSe Polymorphs in a Pressure-Induced Second-Order Phase Transition. 2019 , 12,	2
741	How carbon vacancies can affect the properties of group IV color centers in diamond: A study of thermodynamics and kinetics. 2019 , 126, 195103	5
740	Compressive sensing lattice dynamics. II. Efficient phonon calculations and long-range interactions. 2019 , 100,	14
739	First-Principles Prediction of a New Family of Layered Topological Insulators. 2019 , 2, 1900033	3
738	Analysis of Dihydrogen Bonding in Ammonium Borohydride. 2019 , 123, 28631-28639	14

737	The thermoelectric properties of monolayer SiP and GeP from first-principles calculations. 2019 , 126, 185106	8
736	Super-resolution energy spectra from neutron direct-geometry spectrometers. 2019 , 90, 105109	9
735	Hybrid neural network potential for multilayer graphene. 2019 , 100,	24
734	First Principles Investigation of Anomalous Pressure-Dependent Thermal Conductivity of Chalcopyrites. 2019 , 12,	5
733	Characterization and Stability of Janus TiXY ($X/Y = S$, Se, and Te) Monolayers. 2019 , 123, 29922-29931	19
732	Hydrostatic pressure induced structural phase transition and mechanical properties of fluoroperovskite. 2019 , 31, 505406	2
731	A new tool for validating theoretically derived anisotropic displacement parameters with experiment: directionality of prolate displacement ellipsoids. 2019 , 21, 6396-6404	3
730	Robust Second-Order Topological Insulators with Giant Valley Polarization in Two-Dimensional Honeycomb Ferromagnets.	O
729	Atomic-Scale Pentagraphene Ribbons Stabilized with Alkali Metals under Moderate Pressures.	О
728	Multifunctional PbS2 Monolayer with an In-Plane Negative Poisson Ratio and Photocatalytic Water Splitting Properties. 10494-10499	O
727	Raman spectroscopy of lithium niobite (LiNbO2). 2022 , 807, 140111	О
726	Native point defects and polaron transport in zirconium pyrovanadate. 2022 , 386, 116033	O
725	Interlayer Coupling Induced Phonon-GlassElectron-Crystal Behavior in van der Waals Heterostructure PtSe2/EGeSe.	0
724	Strong band renormalization and emergent ferromagnetism induced by electron-antiferromagnetic-magnon coupling. 2022 , 13,	O
723	First principle studies of TiO2-ZnO alloys under high pressure.	О
722	Charge order landscape and competition with superconductivity in kagome metals.	O
721	Temperature-dependent impact of antiphase boundaries on properties of Fe3Al. 2022, 151, 107746	О
720	Exploring high pressure structural transformations, electronic properties and superconducting properties of MH2 (M´=´Nb, Ta). 2022 , 15, 104347	O

719	Non-trivial band topology in Bi doped Lanthanum monopnictides (LaX; X = As and Sb). 2022 , 358, 114976	О
718	First-principles investigation of TiB3 under high pressure. 2022 , 358, 114989	O
717	Zeolite framework silicon allotropes with direct band gap. 2022 , 15, 104377	0
716	First-principles study of elastic and thermodynamic properties of UO2, LUO3 and LU3O8. 2022 , 572, 154084	O
715	Thermodynamic properties and hydration behavior of ye'elimite. 2022, 162, 106995	0
714	Role of vibrational entropy in impurity segregation at grain boundaries in bcc iron. 2023 , 216, 111858	O
713	First principle studies on electronic and thermoelectric properties of Fe2TiSn based multinary Heusler alloys. 2023 , 216, 111856	0
712	Ab initio study of two-dimensional MgAl2Se4 and MgIn2Se4 with high stability, high electron mobility, and high thermoelectric figure of merit. 2023 , 931, 167586	2
711	The N-body interatomic potentials for molecular dynamics simulations of diffusion in C15 Cr2Ta Laves phase. 2023 , 216, 111841	О
710	Grain boundaries induce significant decrease in lattice thermal conductivity of CdTe. 2023 , 11, 100210	O
709	Structural, elastic, electronic and optical properties of double perovskites Ba2NaXO6 (X = Cl, Br, I): First-principles study. 2023 , 153, 107165	0
708	Diverse electronic structures governed by N-substitution in stable two-dimensional dumbbell carbonitrides. 2023 , 609, 155463	O
707	Roles of hydrogen in structural stability and electronic property of bulk hydrogenated amorphous silicon. 2023 , 216, 111846	1
706	Hydrogen production from H2S on metal-doped FeS Mackinawite monolayer via DFT calculations. 2023 , 609, 155322	Ο
705	The electronic, mechanical properties and in-plane negative Poisson® ratio in novel pentagonal NiX2 (X´=´S, Se, Te) monolayers with strong anisotropy: A first-principles prediction. 2023 , 216, 111873	О
704	Tuning of Thermoelectric performance of CrSe2 material using dimension engineering. 2023, 172, 111083	O
703	PHP-graphene nanoribbon-assembled porous metallic carbon for sodium-ion battery anode with high specific capacity. 2023 , 202, 112-118	О
702	First-principles calculations of the temperature dependence of stacking fault energies in Mg. 2023 , 224, 115075	Ο

701	Thermoelectric performance in disordered Cu2ZnSnSe4 nanostructures driven by ultra-low thermal conductivity. 2023 , 933, 167756	1
700	First-principles study of electronic, piezoelectric, optical, and strain-dependent carrier mobility of Janus TiXY (XIY, X/Y=Cl, Br, I) monolayers.	O
699	Storage of Na in 2D SnS for Na ion batteries: A DFT Prediction.	О
698	Revealing the anisotropic phonon behaviours of layered SnS by angle/temperature-dependent Raman spectroscopy. 2022 , 12, 32262-32269	Ο
697	Trends in opto-electronic properties of MgxZn1-xSnN2 using first principles methods. 2023 , 294, 126995	0
696	Structural, optoelectronic and thermal response of new stable MgBe2X2 (X´=´As, P) Zintl phases: First-principles calculation. 2023 , 287, 116136	O
695	Grileisen parameters of Weyl semimetal CoSi. 2023 , 287, 116133	О
694	First-principles predictions of stable structure of AuAl2 under high pressure. 2023 , 359, 115009	O
693	Signatures of anharmonic phonon transport in ultrahigh thermal conductance across atomically sharp metal/semiconductor interface. 2023 , 201, 123628	О
692	High-performance thermoelectric monolayer EGeSe and its group-IV monochalcogenide isostructural family. 2023 , 454, 140242	О
691	The structural, mechanical, and optoelectronic properties of Cu2-II-Sn-VI4 (II = Mg, Zn, Cd; VI = S, Se): A DFT study. 2023 , 154, 107207	O
690	Ab initio Methods for Electronic Transport in Semiconductors and Nanostructures. 2023, 1515-1558	O
689	Janus V2AsP monolayer: a ferromagnetic semiconductor with a narrow band gap, a high Curie temperature and controllable magnetic anisotropy.	O
688	Cr3GeN: A Nitride with Orthorhombic Antiperovskite Structure.	Ο
687	Single pair of multi-Weyl points in nonmagnetic crystals. 2022 , 106,	О
686	Heat-conserving three-temperature model for ultrafast demagnetization in nickel. 2022, 106,	Ο
685	Electronic structures and magnetic properties of two-dimensional honeycomb-kagome structured V2O3 monolayer and V. 2022 , 170161	О
684	Anisotropic mechanical response of a 2D covalently bound fullerene lattice. 2022,	1

683	Prediction of electronic structure and magnetic anisotropy of two- dimensional MSi2N4 (M=3d transition-metal) monolayers. 2022 , 155693	0
682	Tunable electronic properties and negative differential resistance effect of the intrinsic type-III ZrS2/WTe2 van der Waals heterostructure. 2022 , 155644	O
681	Anti-Jahn-Teller effect induced ultrafast insulator to metal transition in perovskite BaBiO3. 2022, 8,	0
680	Iron-rich Fe-O compounds at Earth's core pressures. 2022 , 100354	1
679	General invariance and equilibrium conditions for lattice dynamics in 1D, 2D, and 3D materials. 2022 , 8,	0
678	Pressure-Tailored Self-Driven and Broadband Photoresponse in PbI 2. 2201044	2
677	Ground-state structures, electronic structure, transport properties and optical properties of Ca-based anti-Ruddlesden-Popper phase oxide perovskites. 2022 , 6,	0
676	Two-dimensional half Chern-Weyl semimetal with multiple screw axes. 2022, 106,	O
675	Photoinduced Rippling of Two-Dimensional Hexagonal Nitride Monolayers.	0
674	Predicted superconductivity and superionic state in the electride Li5N under high pressure. 2022 , 24, 113012	O
673	Improving thermoelectric performance of asymmetrical Janus 1T-SnSSe monolayer by the synergistic effect of band convergence and crystal lattice softening under strain engineering. 2022 , 100923	1
672	Iron and silicon isotope fractionation in silicate melts using first-principles molecular dynamics. 2022 ,	O
671	Enhanced Curie temperature and skyrmion stability by strain in room temperature ferromagnetic semiconductor CrISe monolayer. 2022 , 121, 202402	0
670	Thermal conductivity of group-III phosphides: The special case of GaP. 2022 , 106,	O
669	Scandium wetting of tungsten surfaces in Bcandatelthermionic cathodes. 2022 , 102476	O
668	Prediction of 2D ferromagnetic metal VNI monolayer with tunable topological properties. 2022 , 132, 183913	1
667	Topological nodal-link phonons, three-fold, Dirac and six-fold nodal-point phonons in the insulator SiO\$_2\$.	0
666	Investigation of Polymeric CO Synthesized at High Pressure and Its Stability under Ambient Conditions: A First-Principles Study.	O

665	Hole-doping induced ferromagnetism in 2D materials. 2022 , 8,	О
664	A Novel Membrane-like 2D AEMoS2 as Anode for Lithium- and Sodium-Ion Batteries. 2022 , 12, 1156	O
663	Internal Electric Fields in Asymmetric Single-layer Lattices for Enhancing Photocatalytic Solar-to-Hydrogen Efficiency.	0
662	Thermal expansion of plasma-exposed tungsten. 2022 , 132, 185102	O
661	Bandgap tuning and thermoelectric characteristics of Sc-based double halide perovskites K2ScAgZ6 (Z = Cl, Br, I) for solar cells applications. 2022 , 111115	0
660	Vibrationally resolved optical excitations of the nitrogen-vacancy center in diamond. 2022 , 8,	1
659	2D WSe2/MoSi2N4 type-II heterojunction with improved carrier separation and recombination for photocatalytic water splitting. 2022 , 155674	1
658	Transport characteristics and lattice dynamics with phonon topology accentuation in layered CuTlX (X: S, Se). 2022 , 97, 125820	O
657	Experimental X-ray Charge-Density Studies-A Suitable Probe for Superconductivity? A Case Study on MgB2. 2022 , 126, 8494-8507	1
656	Boronflitrogen co-terminated diamond (110) surface for nitrogen-vacancy quantum sensors from first-principles calculations. 2023 , 51, 025001	Ο
655	Two-Dimensional Penta-NiPS Sheets: Two Stable Polymorphs. 2022 , 126, 19455-19461	1
654	Theoretical Prediction of Spinel Na 2 In x Sc 0.666lk Cl 4 and Rock-Salt Na 3 In 1lk Sc x . 2200569	O
653	Li2NiSe2: a new type intrinsic two dimensional ferromagnetic semiconductor above 200 K.	0
652	Large Gap Topological Insulating Phase and Anisotropic Rashba and Chiral Spin Textures in Monolayer Zintl A2MX2.	O
651	Ab initio investigation of elastic properties of dilute Cu alloys for high-gradient accelerating structures. 2022 , 132, 175112	0
650	Topological nodal line phonons: Recent advances in materials realization. 2022 , 9, 041304	1
649	First-principles study on bilayer SnP3 as a promising thermoelectric material.	O
648	Experimental Absence of the Non-Perovskite Ground State Phases of MaPbI3 Explained by a Funnel Hopping Monte Carlo Study Based on a Neural Network Potential.	Ο

647	Transferable Potential Function for Flexible H2O Molecules Based on the Single-Center Multipole Expansion.	2
646	Electronic properties and storage capability of two-dimensional nitridosilicate MnSi2N4 from first-principles. 2022 , 12, 115127	Ο
645	Anomalous thermal response of bulk diamond to uniaxial (100) strain: A first-principles prediction. 2022 , 106,	Ο
644	Tuning of the Electronic and Vibrational Properties of Epitaxial MoS2 through He-Ion Beam Modification.	O
643	Phononic Stiefel-Whitney topology with corner vibrational modes in two-dimensional Xenes and ligand-functionalized derivatives. 2022 , 106,	Ο
642	Two-dimensional hourglass Weyl nodal loop in monolayer Pb(ClO2)2 and Sr(ClO2)2.	O
641	2D transitional-metal nickel compounds monolayer: Highly efficient multifunctional electrocatalysts for the HER, OER and ORR. 2022 ,	Ο
640	Fine-tuned local coordination environment of Pt single atoms on ceria controls catalytic reactivity. 2022 , 13,	3
639	Synergistic Approach Toward a Reproducible High zT in n-Type and p-Type Superionic Thermoelectric Ag2Te.	1
638	Thermal properties of the metallic delafossite PdCoO2 : A combined experimental and first-principles study. 2022 , 6,	O
637	First-principles calculations to investigate structural stability, half-metallic behavior, thermophysical and thermoelectric properties of Co2YAl (Y= Mo, Tc) Full Heusler compounds. 2022 , 113943	Ο
636	Boron-doped g-CN monolayer as a promising anode for Na/K-ion batteries. 2022 , 102479	Ο
635	On the Stability of Potential Photovoltaic Absorber In5S4.	Ο
634	First principles prediction of the Al-Li phase diagram including configurational and vibrational entropic contributions. 2023 , 217, 111898	Ο
633	An insight into the structural, electronic, magnetic and optical properties of Cs doped and Cs-X (X=Mn, Fe) co-doped CdS for optoelectronic applications. 2023 , 135, 107079	Ο
632	First-principles Phonon Calculations with Phonopy and Phono3py. 2023 , 92,	O
631	Alleviation of Self-Heating Effect in Top-Gated Ultrathin In\$_{text{2}}\$O\$_{text{3}}\$ FETs Using a Thermal Adhesion Layer. 2022 , 1-8	0
630	New family of layered N-based cathode materials for sodium-ion batteries. 2022 , 12, 34200-34207	1

629	Soft Anharmonic Coupled Vibrations of Li and SiO4 Enable Li-ion Diffusion in Amorphous Li2Si2O5.	О
628	Stability and electronic structures of Cmmm-Pt3M alloys. 2023 , 457, 128540	O
627	Stacking pattern induced high ZTs in monolayer SnSSe and bilayer SnXY (X/Y´=´S, Se) materials with strong anharmonic phonon scattering. 2023 , 455, 140832	1
626	Theoretical design of two-dimensional AMInP2X3Y3 (AM = Li, Na, K; $X/Y = S$, Se, Te) monolayers for highly efficient excitonic solar cells.	O
625	Study of lead-free double perovskites X2AgBiI6 (X = K, Rb, Cs) for solar cells and thermoelectric applications. 2023 , 22, 913-922	О
624	High thermoelectric performance of a Sc2Si2Te6 monolayer at medium temperatures: an ab initio study.	O
623	Na2Mn(CO3)2: A carbonate based prototype cathode material for Na-ion batteries with high rate capability An ab-initio study. 2023 , 439, 141687	О
622	CASM IA software package for first-principles based study of multicomponent crystalline solids. 2023 , 217, 111897	O
621	Diamond-XII: A New Type of Exotic Cubic Carbon Allotrope.	0
620	Metastable properties of a garnet type Li5La3Bi2O12 solid electrolyte towards low temperature pressure driven densification. 2022 , 11, 364-373	O
619	Raman Spectra of 2D Titanium Carbide MXene from Machine-Learning Force Field Molecular Dynamics.	0
618	Two-dimensional Cs3Sb2I9/C2N van der Waals type-II heterostructure: a promising photocatalyst for high efficiency water splitting. 2022 , 25, 486-493	1
617	Mixed mismatch model in predicting the interfacial thermal conductance of metal/semiconductor interface. 2023 , 0	0
616	Ultralow lattice thermal conductivity and promising thermoelectric properties of a new 2D MoW3Te8 membrane. 2023 , 44, 106136	o
615	Electron density and thermal motion of diamond at elevated temperatures. 2023, 79, 41-50	O
614	Ab initio thermo-elasticity of ⊡MHx (M=Zr, Ti). 2023 , 218, 111953	O
613	Dynamical, mechanical, anisotropic, and thermodynamic properties of Mg-XL-Y (XL = Zn, Al) alloys with long-period stacking ordered structures: A first-principles calculation. 2023 , 208, 111723	O
612	Negative Poisson's ratio and thickness-dependent optoelectronic response in two-dimensional thermoelectric TlCuSe. 2023 , 295, 127155	o

611	Effect of transition metals on the crystal field in CeCo0.4Fe0.6Ge3. 2023 , 153, 107776	O
610	High-pressure stability and superconductivity of vanadium hydrides*. 2023 , 651, 414603	О
609	Accurate Fe⊞e machine learning potential for studying He effects in BCC-Fe. 2023 , 574, 154183	0
608	First-principles calculations to investigate third-order elastic constant, anharmonicity and temperature dependent second elastic constant of thermoelectric materials Cu3MSe4(M´=V and Nb). 2023 , 812, 140254	O
607	Role of lattice thermal conductivity in thermoelectric properties of chalcopyrite-type antimonides XSiSb2 (X = Mg, Be): A DFT insight. 2023 , 295, 127190	O
606	Reconstruction of interfacial thermal transport mediated by hotspot in silicon-based nano-transistors. 2023 , 202, 123676	O
605	Simulations of martensitic transformations in AuCd shape memory alloys. 2023 , 34, 105096	0
604	⊞n2O3 monolayer: A promising material as field-effect phototransistor and out-of-plane piezoelectric device. 2023 , 614, 156198	O
603	Density functional theory study of the structural, electronic, mechanical, and thermal properties of Hf6Ta2O17. 2023 , 34, 105065	0
602	First-principles investigation of the structural, mechanical, electronic and thermoelectric properties of ZnFeNbAl Heusler compound. 2023 , 34, 105046	O
601	Optimising 1T-NiS2 monolayer thermoelectric performance via valley engineering. 2023, 34, 105169	О
600	Pristine and metal decorated biphenylene monolayer for enhanced adsorption of nitrobenzene: A DFT approach. 2023 , 613, 155995	O
599	PtSe2/SnS2 heterostructure as a direct Z-scheme photocatalyst for water decomposition. 2023 , 155, 107225	O
598	Two novel phases of germa-graphene: Prediction, electronic and transport applications. 2023 , 614, 156107	O
597	First-principles investigation on the novel half-Heusler VXTe (X=Cr, Mn, Fe, and Co) alloys for spintronic and thermoelectric applications. 2023 , 155, 107233	1
596	Buckling in novel graphene-like thoriumene and uraniumene monolayers: Electronic, mechanical, and optical properties from first-principles calculations. 2023 , 34, 105075	O
595	Augmented thermoelectric performance of LiCaX (X = As, Sb) Half Heusler compounds via carrier concentration optimization. 2023 , 174, 111182	0
594	Mechanism of the low thermal conductivity in novel two-dimensional NaCuSe. 2023 , 613, 156064	O

593	Thermodynamic assessment of RuO4 oxide. 2023 , 80, 102508	О
592	Heat capacity and thermal conductivity of CdCr2Se4 ferromagnet: Magnetic field dependence, experiment and calculations. 2023 , 174, 111139	O
591	Variable thermal transport in black, blue, and violet phosphorene from extensive atomistic simulations with a neuroevolution potential. 2023 , 202, 123681	О
590	Experimental determination of the HHf phase diagram using in situ neutron diffraction. 2023 , 937, 168353	O
589	First-principles calculations of local structure and electronic properties of Er³⁺-doped TiO₂. 2022 , 71, 246102	O
588	Strain and thickness effects on the electronic structures of low-energy two-dimensional CdxTey phases. 2022 , 24, 29772-29780	O
587	A mechanism for aragonite to post-aragonite transition in MCO3 (M = Ca, Sr and Ba) carbonates: evidence of a hidden metastable polymorph. 2022 , 24, 29205-29213	O
586	Ab-initio techniques, VASP and CASTEP, are used to investigate the electronic properties of B2 compounds formed between Ti and group VIII elements - a comparative study. 2022 , 370, 02005	O
585	Polarization-resolved and helicity-resolved Raman spectra of monolayer XP3 (X=Ge and In).	O
584	Reliable force field potential for modelling thermal transport in AlN. 2022,	O
583	HfSe2/GaSe Heterostructure as a Promising Near-Room-Temperature Thermoelectric Material. 2022 , 126, 20326-20331	0
582	Elemental excitations in MoI3 one-dimensional van der Waals nanowires. 2022 , 121, 221901	3
581	A universal graph deep learning interatomic potential for the periodic table. 2022 , 2, 718-728	О
580	Instability of the magnetic state of MPX3(M=Mn,Ni;X=S,Se). 2022 , 106,	O
579	Ab initio construction of full phase diagram of MgO-CaO eutectic system using neural network interatomic potentials. 2022 , 6,	O
578	Uncovering 0D and 1D Electrides with Low Work Function in a Sc P System. 2022 , 126, 20710-20716	O
577	High thermal conductivity in wafer-scale cubic silicon carbide crystals. 2022, 13,	О
576	Topological charge-2 Dirac phonons in three dimensions: Theory and realization. 2022 , 106,	O

575	Classical and machine learning interatomic potentials for BCC vanadium. 2022, 6,	O
574	Axion insulators protected by C2T symmetry, their K -theory invariants, and material realizations. 2022 , 106,	O
573	Strain-induced antipolar phase in hafnia stabilizes robust thin-film ferroelectricity. 2022, 8,	2
572	DFT insights into the origin of d0 ferromagnetism, mechanical stability, elastic, and acoustic anisotropy in AZrO3 (A= K, rb, Cs) cubic perovskites. 2022 , 414521	O
571	Metastable Phase Cu with Optimized Local Electronic State for Efficient Electrocatalytic Production of Ammonia from Nitrate. 2212236	1
570	Emergent charge order in pressurized kagome superconductor CsV3Sb5. 2022 , 611, 682-687	O
569	Phonon structure engineering for intrinsically spectrally selective emitters by anion groups.	0
568	Sifting for substitutional elements that decrease thermal conductivity of a thermal barrier material. 2022 , 137,	O
567	Low Lattice Thermal Conductivity in a Wider Temperature Range for Biphasic-Quaternary (Ti,V)CoSb Half-Heusler Alloys. 2022 , 14, 54736-54747	0
566	Multiferroic nitride perovskites with giant polarizations and large magnetic moments. 2022, 106,	1
565	Comprehensive investigation of the extremely low lattice thermal conductivity and thermoelectric properties of BaIn2Te4. 2022 , 106,	1
564	Enhanced Electron Correlation and Significantly Suppressed Thermal Conductivity in Dirac Nodal-Line Metal Nanowires by Chemical Doping. 2204424	O
563	An Efficient Strategy for Searching High Lattice Thermal Conductivity Materials. 2022, 5, 15356-15364	0
562	The structural, mechanical, electronic, and optical properties of Janus Hf2CXY (X, Y = O, S, Se or Te, X \Box Y) MXenes. 2022 , 19, 771-784	O
561	The thermoelectric properties of XTe (X = Ge, Sn and Pb) monolayers from first-principles calculations. 2022 , 97, 125709	O
560	Piezo- and Pyroelectricity in Zirconia: A Study with Machine-Learned Force Fields. 2022 , 18,	0
559	Bonding Heterogeneity Leads to Hierarchical and Ultralow Lattice Thermal Conductivity in Sodium Metavanadate. 2022 , 13, 11160-11168	О
558	Sulfur-Vacancy Passivation via Selenium Doping in Sb2S3 Solar Cells: Density Functional Theory Analysis. 2022 , 126, 20786-20792	1

557	Tunable thermal properties of the biphenylene and the lateral heterostructure formed with graphene: A molecular dynamics investigation. 10,	0
556	Origin of Near-Zero Thermal Expansion in A2O(PO4)2 Oxides over an Ultrawide Temperature Range.	O
555	First-principles study of energy transport in tin oxynitride lattice.	0
554	Euphonic: inelastic neutron scattering simulations from force constants and visualization tools for phonon properties. 2022 , 55, 1689-1703	O
553	Atomic-size dependence of the cohesive energy, bandgap, Young's modulus, and Raman frequency in different MA2Z4: A bond relaxation investigation. 2022 , 121, 244105	2
552	Hourglass charge-three Weyl phonons. 2022 , 106,	0
551	Thermodynamical and topological properties of metastable Fe3Sn. 2022, 8,	0
550	Low lattice thermal conductivity in alkali metal based Heusler alloys. 2022, 6,	0
549	Effects of structural ordering on infrared active vibrations within Bi2(Te(1☑)Sex)3. 2022, 106,	0
548	Designing two-dimensional ferroelectric materials from phosphorus-analogue structures.	0
547	Stress effect on lattice thermal conductivity of anode material NiNb2O6 for lithium-ion batteries.	O
546	Comprehensive investigation on lattice dynamics of neutron multiplier beryllides: vibrational spectra and thermal performances.	O
545	Pressure Stabilized Lithium-Aluminum Compounds with Both Superconducting and Superionic Behaviors. 2022 , 129,	1
544	First-principles prediction of 1H-Na2Se monolayer: Elects of external strain and point defects associated with constituent atoms.	O
543	Identification of the Kirkendall effect as a mechanism responsible for thermal decomposition of the InGaN/GaN MQWs system. 2022 , 24, 123007	0
542	Triple hourglass Weyl phonons. 2022 , 106,	O
541	Symmetry-enforced planar nodal chain phonons in non-symmorphic materials. 2022 , 132, 224401	1
540	Density Functional Theory Analysis Identifying the Mechanism for Ignition Sensitivity of Ammonium Perchlorate.	0

539	Layer-stacking of chalcogenide-terminated MXenes Ti2CT2(T = O, S, Se, Te) and their applications in metal-ion batteries. 2023 , 34, 105704	O
538	Computational discovery of two-dimensional rare-earth iodides: promising ferrovalley materials for valleytronics. 2023 , 10, 015021	O
537	Isotope doping-induced crossover shift in the thermal conductivity of thin silicon nanowires. 2023 , 35, 085702	O
536	Growth mechanism of carbon nanotubes from Co-W-C alloy catalyst revealed by atmospheric environmental transmission electron microscopy. 2022 , 8,	1
535	Theoretical study of Cr2X3S3 ($X = Br$, I) monolayers for thermoelectric and spin caloritronics properties. 2023 , 34, 095704	O
534	In Situ Raman Spectroscopy and DFT Studies of the Phase Transition from Zircon to Reidite at High PII Conditions. 2022 , 12, 1618	1
533	In2Se3, In2Te3, and In2(Se,Te)3 Alloys as Photovoltaic Materials. 12026-12031	O
532	First-principles calculations to investigate structural, elastic, electronic and thermodynamic properties of NbCoSn and VRhSn Half-Heusler compounds. 2022 , 43, 106132	O
531	First-principle prediction of one-dimensional silicon allotropes: Promising new candidate for chemical and electrochemical hydrogen storage. 2022 ,	0
530	Multiple Open and Closed Nodal-Line Phonons in Solids with a 1 Space Group. 2200085	O
529	Unlocking the hidden chemical space in cubic-phase garnet solid electrolyte for efficient quasi-all-solid-state lithium batteries. 2022 , 13,	1
528	An embedded interfacial network stabilizes inorganic CsPbI3 perovskite thin films. 2022, 13,	O
527	Ab Initio Study of High-Capacity Hydrogen Storage in Lithium-Shrouded Honeycomb Borophene Oxide Nanosheet. 2022 , 126, 20762-20772	0
526	All hourglass bosonic excitations in the 1651 magnetic space groups and 528 magnetic layer groups. 2022 , 6,	O
525	Machine learning guided discovery of ternary compounds involving La and immiscible Co and Pb elements. 2022 , 8,	O
524	Stability, Electronic Structures, and Thermoelectric Properties of 2D Janus LiZnX (X = N, P, As). 2022 , 5, 14815-14824	O
523	Origin of negative electrocaloric effect in Pnma -type antiferroelectric perovskites. 2022, 106,	O
522	A scheme to fabricate magnetic graphene-like cobalt nitride CoN4 monolayer proposed by first-principles calculations. 2023 , 16, 015505	O

521	Thermal Transport Properties of Sulfur-Loaded Carbon-Based Nanotubes and Composite Sulfur Cathodes in LithiumBulfur Batteries.	O
520	Chiral magnetism, lattice dynamics, and anomalous Hall conductivity in V3AuN antiferromagnetic antiperovskite. 2022 , 6,	O
519	Cation ordering induced two-dimensional vertical ferroelectricity in tungsten and molybdenum trioxides. 2022 , 106,	0
518	Structure, Stability, and Electronic Properties of Hydrogenated Monolayer 2D Silicon Allotropes by First-Principles Calculation. 2200426	O
517	Effects of Selenium Doping in Zinc Telluride from First Principles. 2022 , 126, 21348-21355	О
516	Vacancy-Ordered Double Perovskites Cs2BI6 (B = Pt, Pd, Te, Sn): An Emerging Class of Thermoelectric Materials. 2022 , 13, 11655-11662	O
515	Mean-field approach for Anderson-type off-diagonal disorder. 2022 , 106,	О
514	Electrical and magnetic properties of antiferromagnetic semiconductor MnSi2N4 monolayer. 10,	O
513	Collective Atomic Motion in Crystals Under Shear Stress by First Principles Phonon Calculations. 2022 , 61, 841-843	О
512	Structural defects in a Janus MoSSe monolayer: A density functional theory study. 2022 , 106,	O
511	Ab initio study of magnetic structure transitions of FePS3 under high pressure. 2022 , 106,	0
510	WI3 Monolayer: Electronic Band Structure and Magnetic Anisotropy Under an External Electric Field.	Ο
509	Effects of lattice strain on hydrogen diffusion, trapping and escape in bcc iron from ab-initio calculations. 2022 ,	0
508	New Two-Dimensional WS2/ZrSi2N4 Heterostructure as photocatalyst for Water Splitting into Hydrogen. 2022 , 2390, 012029	O
507	Hardness increases due to (Fe, Cr)2C carbide precipitated during natural aging in high chromium cast iron. 2022 , 111766	0
506	Two-dimensional binary transition metal nitride MN4 ($M = V$, Cr, Mn, Fe, Co) with a graphenelike structure and strong magnetic properties. 2022 , 106,	O
505	Modeling polar order in compressively strained SrTiO3. 2022 , 106,	0
504	Anisotropic phonon and magnon vibration and gate-tunable optoelectronic properties of nickel thiophosphite.	Ο

503	Periodic Density Functional Theory Calculations of Uranyl Tetrachloride Compounds Engaged in UranylCation and UranylHydrogen Interactions: Electronic Structure, Vibrational, and Thermodynamic Analyses.	O
502	Spin direction tunable topological transition in two-dimensional frustrate antiferromagnetic triangular lattice T-FeO2 monolayer. 2022 , 121, 232405	O
501	Accurate prediction on the lattice thermal conductivities of monolayer systems by a high-throughput descriptor. 2023 , 56, 045304	O
500	Thermoelectric Figure of Merit of a Superatomic Crystal Re6Se8I2 Monolayer. 2022 , 18,	O
499	Strong strain-dependent phonon hydrodynamic window in bilayer graphene. 2022 , 121, 252202	2
498	Facile Low-Energy and Open-Air Synthesis of Mixed-Cation Perovskite Quantum Dots for High-Performance Solar Cells. 2022 , 141107	O
497	Simultaneous capturing phonon and electron dynamics in MXenes. 2022, 13,	1
496	Exploring strong and weak topological states on isostructural substitutions in TlBiSe\$\$_2\$\$. 2022 , 12,	O
495	New Insights into the Volume Isotope Effect of Ice Ih from Polarizable Many-Body Potentials. 2022 , 13, 11831-11836	О
494	The quantum dynamics of H2 on Cu(111) at a surface temperature of 925 K: comparing state-of-the-art theory to state-of-the-art experiments 2.	О
493	Effect of oxygen defects on microstructure, optical and vibrational properties of ScN films deposited on MgO substrate from experiment and first principles. 2022 , 156203	О
492	Theoretical Study of Dynamical and Electronic Properties of Noncentrosymmetric Superconductor NbReSi. 2023 , 16, 78	O
491	Correlated Rattling of Sodium-Chains Suppressing Thermal Conduction in Thermoelectric Stannides. 2207646	О
490	Conductive C3NS Monolayer with Superior Properties for K Ion Batteries. 12055-12060	O
489	Temperature-dependent mechanical properties of TaC and HfC.	О
488	High-Throughput Computational Screening of Two-Dimensional Semiconductors. 2022 , 13, 11581-11594	1
487	Impact of magnetic and antisite disorder on the vibrational densities of states in Ni2MnSn Heusler alloys. 2022 , 106,	1
486	Structural, Electronic and Optical Properties of Titanium Based Fluoro-Perovskites MTiF3 (M = Rb and Cs) via Density Functional Theory Computation. 2022 , 7, 47662-47670	Ο

485	Magnetic proximity controlled Rashba and valley splittings in monolayer Janus ZrNX/VTe2 (X = Br, I) heterostructure. 2022 , 115616	О
484	CRYSTAL23: A Program for Computational Solid State Physics and Chemistry.	1
483	Microscopic origin of the abnormal elastic behavior accompanying the superconducting transition in Nb3Sn crystals: an extended ab initio study. 2023 , 168891	0
482	Spin-polarized linear dispersions, lattice dynamics and transport properties of quaternary Heusler alloys (LiMgXSb). 2023 , 127373	0
481	Novel Janus 2D structures of XMoY (X, Y = O, S, Se, Te) composition for solar hydrogen production. 2023 ,	0
480	Electronic and optical properties of Janus-like hexagonal monolayer materials of group IV-VI. 2023 , 7,	0
479	High-accuracy thermodynamic properties to the melting point from ab initio calculations aided by machine-learning potentials. 2023 , 9,	0
478	Mn2P2S3Se3: two-dimensional Janus room-temperature antiferromagnetic semiconductor with a large out-of-plane piezoelectricity.	O
477	Machine learning-driven synthesis of TiZrNbHfTaC5 high-entropy carbide. 2023 , 9,	1
476	Towards an efficient f-in-core/f-in-valence switchable description for DFTB calculations of Ce 4f states in ceria.	Ο
475	The pressure and temperature evolution of the Ca3V2O8 crystal structure using powder X-ray diffraction.	Ο
474	Ab Initio Theoretical Study of DyScO3 at High Pressure. 2023 , 13, 165	Ο
473	Orientation and size effects on phonon thermal conductivity in silicon/germanium multilayer structures. 2023 , 62, SD0804	Ο
472	Unexpected Enhanced Thermal Conductivity of GaxIn1⊠Sb Ternary Alloys.	Ο
471	Tuning of band gap by anions (Cl, Br, I) of double perovskites Rb2AgAsX6 (Cl, Br, I) for solar cells and thermoelectric applications. 2023 , 98, 025811	1
470	Details of structure transformations in pure uranium and U-Mo alloys: insights from classical atomistic simulation. 2023 , 154265	Ο
469	Machine learning interatomic potential for molecular dynamics simulation of the ferroelectric KNbO3 perovskite. 2023 , 107,	0
468	Electron magnetic moment of transient chiral phonons in KTaO3. 2023 , 107,	0

467	Prediction of Novel Ultrahard Phases in the BCN System from First Principles: Progress and Problems. 2023 , 16, 886	O
466	Halogen-Doped Chevrel Phase Janus Monolayers for Photocatalytic Water Splitting. 2023, 13, 368	1
465	Topological phonons in Cs-Te binary systems. 2023 , 107,	1
464	Probing how Ti- and Nb-substitution affect the stability and improve the electrochemical performance of <code>Band</code> <code>Livopo4</code> .	O
463	Electronic and topological properties of kagome lattice LaV3Si2.	О
462	Vibrational properties of TiVC-based Mxenes by first-principles calculation and experiments. 2023 , 105396	О
461	Discovery of Clustered-P1 Borophene and Its Application as the Lightest High-Performance Transistor. 2023 , 15, 3182-3191	0
460	Superconductivity in the Li-B-C system at 100 GPa. 2023 , 107,	O
459	Evolution of static charge density wave order, amplitude mode dynamics, and suppression of Kohn anomalies at the hysteretic transition in EuTe4. 2023 , 107,	0
458	Highly Efficient Hydrogen Storage of Sc Decorated Biphenylene Monolayer near Ambient-temperature: An Ab-initio Simulations.	О
457	Effect of osmium substitution on structural, electronic, mechanical, and thermodynamic properties of WDs alloys: A first-principles study.	O
456	First-principles calculations of monolayered Al2Te5: a promising 2D donor semiconductor with ultrahigh visible light harvesting.	1
455	Theoretical prediction of type-II BP/SiH heterostructure for high-efficient electronic devices.	О
454	Defect physics in 2D monolayer I-VII semiconductor AgI. 2023 , 100304	O
453	First-principles investigation of equilibrium magnesium isotope fractionation among mantle minerals: Review and new data. 2023 , 104315	0
452	High-pressure hP3 yttrium allotrope with CaHg2 -type structure as a prototype of the hP3. 2023 , 107,	O
451	First-Principles Prediction of Structure and Properties of the Cu2TeO6 Monolayer. 2023, 13, 815	0
450	Theoretical Prediction of Thermoelectric Performance for Layered LaAgOX (X = S, Se) Materials in Consideration of the Four-Phonon and Multiple Carrier Scattering Processes. 2201368	O

449	A First-principles investigation of the structural and electronic properties of Two-dimensional Hf2CSe2. 2023 ,	О
448	Preparation of AgBe2O3-Based black and electrically insulating coatings by magnetron sputtering from metal targets. 2023 , 111839	O
447	Doping-induced magnetism and magnetoelectric coupling in one-dimensional NbOCl3 and NbOBr3.	О
446	Correlation between orbital hybridizations, phonon spectra, and thermal properties of graphene, germanene, and plumbene.	О
445	Computational Exploration of Ultralow Lattice Thermal Conductivity and High Figure of Merit in p-Type Bulk RbX2Sb ($X = K$, Na).	1
444	Monolayer group-V binary compounds BiP and SbP with ultrahigh piezoelectricity and stability. 2023 , 7,	o
443	Enhancement in photocatalytic water splitting using van der Waals heterostructure materials based on penta-layers.	О
442	Experimental evidence for the significance of optical phonons in thermal transport of tin monosulfide.	O
441	Superconducting and structural properties of the phosphorus-rich Nb2P5 superconductor under high pressure.	0
440	Tutorial: Systematic development of polynomial machine learning potentials for elemental and alloy systems. 2023 , 133, 011101	О
439	A BC2N/blue phosphorene heterostructure as an anode material for high-performance sodium-ion batteries: first principles insights.	0
438	Tunable anomalous valley Hall effect and magnetic phase transition in MHfN2Cl2 (M = V, Cr) bimetallic nitrogen halide monolayers. 2023 , 122, 022404	О
437	Anisotropic phonon dispersion and optoelectronic properties of a few layers HfS2.	0
436	Understanding the ultra-low lattice thermal conductivity of monoclinic RETaO 4 from acoustic-optical phonon anti-crossing property and a comparison with ZrO 2.	O
435	S-functionalized 2D V2B as a promising anode material for rechargeable lithium ion batteries.	О
434	Structural and electronic properties of cubic BiFeO3 from first-principles calculations. 2023, 115065	О
433	Theoretical determination of superior high-temperature thermoelectricity in the n-type doped 2H-ZrI2 monolayer.	О
432	Critical role of magnetic moments in the lattice dynamics of YBa2Cu3O6. 2023 , 107,	0

431	Mechanochemical Synthesis of Sustainable Ternary and Quaternary Nanostructured Cu2SnS3, Cu2ZnSnS4, and Cu2ZnSnSe4 Chalcogenides for Thermoelectric Applications. 2023 , 13, 366	2
430	Predicted THz-wave absorption properties observed in all-inorganic perovskite CsPbI3 thin films: Integrity at the grain boundary. 2023 , 30, 100960	Ο
429	Theoretical proposal and material realization of ferromagnetic negative charge-transfer energy insulator. 2023 , 107,	О
428	Predicting and Accessing Metastable Phases.	O
427	Valley physics and anomalous valley Hall effect in single-layer hMNX (M=Ti, Zr, Hf; X. 2023, 107,	О
426	Improved Thermoelectric Performance of NbCoSb with Intrinsic Nb Vacancies and Ni-Doping-Induced Band Degeneracy.	O
425	First principles study of layered scandium disulfide for use as Li-ion and beyond-Li-ion batteries. 2023 , 25, 2167-2178	О
424	Calculated magnetic exchange interactions in the van der Waals layered magnet CrSBr.	O
423	Irida-graphene: A new 2D carbon allotrope. 2023 , 37, 100469	О
422	Finite Temperature Properties of Uranium Mononitride. 2023 , 154241	O
421	Conventional High-Temperature Superconductivity in Metallic, Covalently Bonded, Binary-Guest CB Clathrates.	O
420	Machine learning-based discovery of vibrationally stable materials. 2023 , 9,	O
419	High-Throughput Screening Assisted Discovery of a Stable Layered Anti-Ferromagnetic Semiconductor: CdFeP 2 Se 6. 2210965	O
418	Stability and Strength of Monolayer Polymeric C60.	Ο
417	First-principles calculations for comparative band structure study of SrTiO3 perovskite on bulk and layered phases for efficient optoelectronic conversion. 2023 , 1220, 114006	O
416	Construction of two-dimensional lateral heterostructures by graphenelike ZnO and GaN monolayers for potential optoelectronic applications. 2023 , 36, 102635	Ο
415	Enhancing topological Weyl Semimetals by Janus transition-metal dichalcogenides structures. 2023 , 218, 112004	0
414	Calculation of tunable electronic and optical properties of AlSb/CdSe heterojunction based on first principles. 2023 , 614, 156261	O

413	Modeling of ultrafast polarization switching in PbTiO3. 2023, 27, 101681	O
412	First-principles study on physical properties of actinide-based ternary (UC)mAl3C2 (m = 1, 2, 3) carbides. 2023 , 209, 111810	O
411	Theoretical study on spintronic and optical property prediction of doped magnetic Borophene. 2023 , 34, e00783	0
410	Electronic, mechanical, and optical properties of BP nanotubes: A first-principles study. 2023 , 34, e00785	O
409	Cmc21-CdO: Emerging direct band gap semiconductor with ultrahigh mobility and enhanced visible-light optical absorptions. 2023 , 652, 414645	0
408	First-principle studies of monolayer and bulk InSe1⊠Sx. 2023 , 615, 156389	O
407	Excellent high temperature elasticity and thermodynamic properties of W-Cr alloys: A first-principles study. 2023 , 34, 101367	О
406	Transport behavior and thermoelectric properties of AMg2Sb2-based Zintl phases: The first-principles study. 2023 , 34, 105367	О
405	Structural, phonon, thermodynamic, and electronic properties of MgFeH3 at different pressures: DFT study. 2023 , 1221, 114030	О
404	Bulk substitution of F-terminations from Ti3C2Tx MXene by cation pillaring and gas hydrolysation. 2023 , 38, 100470	О
403	Hexagonal and tetragonal ScX (X´= \hat{P} , As, Sb) nanosheets for optoelectronics and straintronics. 2023 , 615, 156306	О
402	Experimental and computational studies on the formation of mixed amide-hydride solid solutions for CsNH2tsH system. 2023 , 17, 100895	O
401	Giant band gap bowing in two dimensional Pb1\(\mathbb{B}\)SnxO alloys and Janus PbSnO monolayers. 2023 , 175, 111203	1
400	Computational screening of two-dimensional substrates for stabilizing honeycomb borophene. 2023 , 615, 156388	O
399	Novel ternary compound transition metal dichalcogenide TiNbS4 as promising anodes materials for Li-ion batteries: A DFT study. 2023 , 615, 156322	О
398	Superconductivity and topological properties in the kagome metals CsM3Te5 (M =Ti, Zr, Hf): A first-principles investigation. 2022 , 106,	Ο
397	High-Pressure X-ray Diffraction and DFT Studies on Spinel FeV2O4. 2023 , 13, 53	О
396	Prediction of novel tetravalent metal pentazolate salts with anharmonic effect. 2022 ,	О

395	High-temperature ferromagnetism and strong Etonjugation feature in two-dimensional manganese tetranitride.	0
394	Switchable large-gap quantum spin Hall state in the two-dimensional MSi2Z4 class of materials. 2022 , 106,	1
393	Calculating electron-phonon coupling matrix: Theory introduction, code development and preliminary application. 2023 , 66, 204-214	0
392	First-Principle Study of Ca3Y2Ge3O12 Garnet: Dynamical, Elastic Properties and Stability under Pressure. 2023 , 13, 29	Ο
391	Hybrid-Density Functional Calculations of Structural, Electronic, Magnetic, and Thermodynamic Properties of ⊞u2P2O7. 2023 , 13, 498	0
390	Electronic properties of 3 d transition metal dihalide monolayers predicted by DFT methods: Is there a pattern or are the results random?.	Ο
389	Activation of metal-free porous basal plane of biphenylene through defects engineering for hydrogen evolution reaction. 2022 ,	Ο
388	Pseudo-structural Transition and Thermal Stress-Induced Microcracking in the NdCu Intermetallic.	Ο
387	Nanolaminated Fe2AB2 and Mn2AB. 2022 , 6,	Ο
386	Dirac phonons in two-dimensional materials. 2022 , 106,	Ο
386 385	Dirac phonons in two-dimensional materials. 2022, 106, Enhanced Intrinsic Anomalous Valley Hall Effect Induced by SpinDrbit Coupling in MXene Monolayer M3N2O2 (M = Y, La). 2023, 14, 132-138	0
J	Enhanced Intrinsic Anomalous Valley Hall Effect Induced by SpinDrbit Coupling in MXene	
385	Enhanced Intrinsic Anomalous Valley Hall Effect Induced by SpinDrbit Coupling in MXene Monolayer M3N2O2 (M = Y, La). 2023 , 14, 132-138 Large kagome family candidates with topological superconductivity and charge density waves.	0
385	Enhanced Intrinsic Anomalous Valley Hall Effect Induced by SpinDrbit Coupling in MXene Monolayer M3N2O2 (M = Y, La). 2023, 14, 132-138 Large kagome family candidates with topological superconductivity and charge density waves. 2022, 106, Orbital contribution to the regulation of the spin-valley coupling in antiferromagnetic monolayer	0
385 384 383	Enhanced Intrinsic Anomalous Valley Hall Effect Induced by Spin Drbit Coupling in MXene Monolayer M3N2O2 (M = Y, La). 2023, 14, 132-138 Large kagome family candidates with topological superconductivity and charge density waves. 2022, 106, Orbital contribution to the regulation of the spin-valley coupling in antiferromagnetic monolayer MnPTe3. 2023, 107, A New 3D Carbon Allotrope Composed of Penta-graphene Nanotubes with Low Lattice Thermal	0 0
385 384 383 382	Enhanced Intrinsic Anomalous Valley Hall Effect Induced by Spin Drbit Coupling in MXene Monolayer M3N2O2 (M = Y, La). 2023, 14, 132-138 Large kagome family candidates with topological superconductivity and charge density waves. 2022, 106, Orbital contribution to the regulation of the spin-valley coupling in antiferromagnetic monolayer MnPTe3. 2023, 107, A New 3D Carbon Allotrope Composed of Penta-graphene Nanotubes with Low Lattice Thermal Conductivity. 2023, 14, 1082-1087 Atomic mean square displacement study of the bond breaking mechanism of energetic materials	o o o
385 384 383 382 381	Enhanced Intrinsic Anomalous Valley Hall Effect Induced by SpinDrbit Coupling in MXene Monolayer M3N2O2 (M = Y, La). 2023, 14, 132-138 Large kagome family candidates with topological superconductivity and charge density waves. 2022, 106, Orbital contribution to the regulation of the spin-valley coupling in antiferromagnetic monolayer MnPTe3. 2023, 107, A New 3D Carbon Allotrope Composed of Penta-graphene Nanotubes with Low Lattice Thermal Conductivity. 2023, 14, 1082-1087 Atomic mean square displacement study of the bond breaking mechanism of energetic materials before explosive initiation.	0 0 0

377	The Evolution of Band Topology in Two-Dimensional Weyl Half-Metals. 2023, 14, 825-831	О
376	Monolayer Beryllene as an anode material for magnesium-ion batteries with high capacity and low diffusion energy barrier.	О
375	Phase Competition and Strong SHG Responses of the Li2MIIMIVSe4 Family: Atom Response Theory Predictions versus Experimental Results.	0
374	Resolving Diverse Oxygen Transport Pathways Across Sr-Doped Lanthanum Ferrite and Metal-Perovskite Heterostructures. 2202276	o
373	Prediction of hot zone-center optical phonons in laser-irradiated molybdenum disulfide with a semiconductor multitemperature model. 2023 , 107,	0
372	Prediction of a Cyclic Hydrogenated Boron Molecule as a Promising Building Block for Borophane. 2023 , 28, 1225	О
371	Exploring the Dirac nature of RbBi2. 2023 , 107,	0
370	Antiferromagnetic metal phase in an electron-doped rare-earth nickelate.	1
369	Enhancement of Perpendicular Magnetic Anisotropy and Curie Temperature in V-Doped Two-Dimensional CrSI Janus Semiconductor Monolayer. 2023 , 127, 2003-2011	0
368	Large gap two-dimensional topological insulators with the coexistence of a significant Rashba effect and piezoelectricity in functionalized PbGe monolayers.	О
367	First Theoretical Realization of a Stable Two-Dimensional Boron Fullerene Network. 2023 , 13, 1672	0
366	Hardness and Mechanical Properties of Wurtzite BCN Compounds. 2023, 127, 2581-2588	О
365	Excitonic luminescence of iodine-intercalated HfS2. 2023 , 122, 042102	1
364	Two-Dimensional Ordered Double-Transition Metal Carbides for the Electrochemical Nitrogen Reduction Reaction. 2023 , 15, 6797-6806	O
363	First-Principles Study of Lattice Thermal Conductivity in Janus MoSSe Bilayers with Different Stacking Modes.	O
362	Anisotropic Rashba effect in two-dimensional non-Janus transition-metal dichalcogenide, MSSe´(M=Mo,W) alloys. 2023 , 107,	0
361	A database of synthetic inelastic neutron scattering spectra from molecules and crystals. 2023, 10,	0
360	Spin-Phonon Interactions Induced Anomalous Thermal Conductivity in Nickel (Ii) Oxide.	o

359	Predicting the Lattice Thermal Conductivity in Nitride Perovskite LaWN 3 from ab initio Lattice Dynamics. 2205934	Ο
358	Abnormal behavior of preferred formation of the cationic vacancies from the interior in a EGeSe monolayer with the stereo-chemical antibonding lone-pair state.	Ο
357	Investigation of thermal control in phase-changing ABO3 perovskites via first-principles predictions: General mechanism of emittance.	Ο
356	Phonon transport in Janus monolayer siblings: a comparison of 1T and 2H-ISbTe. 2023 , 13, 4202-4210	O
355	Searching for Simple FAIMIIIO2-type Intrinsic Ferroelectric Semiconductors with Simultaneous Robust Built-in Electric Field and Full-Spectrum Absorption for Superior Photocatalyst.	0
354	Novel Ultrahard Extended Hexagonal C10, C14 and C18 Allotropes with Mixed sp2/sp3 Hybridizations: Crystal Chemistry and Ab Initio Investigations. 2023 , 9, 11	O
353	Modeling phonons in nanomaterials. 2023 , 125-149	Ο
352	Non-centrosymmetric Weyl semimetal state and strain effect in the twisted-brick phase transition metal monochalcogenides. 2023 , 15, 2882-2890	O
351	Prediction and Characterization of Two-Dimensional Zn2VN3. 2023 , 14, 1148-1155	1
350	Sliding ferroelectricity in bilayer honeycomb structures: A first-principles study. 2023 , 107,	O
349	Molecular-Dynamics Analysis of the Mechanical Behavior of Plasma-Facing Tungsten.	Ο
348	Valley Hall effect in graphene-like SnX (X=Si , Ge) buckled monolayers with high charge carrier mobility and low lattice thermal conductivity. 2023 , 107,	O
347	Raman Spectroscopy Signatures of Boron-Rich Superhard Materials from Density Functional Theory. 2023 , 127, 2104-2115	О
346	Excitonic quenching of the oxygen-chain phonon in the photoinduced metal-to-insulator transition of photoexcited Sr0.95NbO3.37 studied by ultraviolet-resonance Raman scattering. 2023 , 107,	Ο
345	Ordered vacancy compounds: the case of the Mangli phases of TiO2. 2023 , 533-565	Ο
344	Theoretical prediction of two-dimensional II-V compounds. 2023 , 7,	O
343	Catching the Killer: Dynamic Disorder Design Rules for Small-Molecule Organic Semiconductors. 2213370	Ο
342	Effect of vacancy defects on the electronic and mechanical properties of two-dimensional MoSi2N4. 2023 , 13, 5307-5316	O

341	Exploration of thermal conductivity and optical properties of <code>BandEnitrogene</code> .	O
340	Theoretical investigation of the physical properties of cubic perovskite oxides SrXO3 (X=. 2023 , 158, 107340	O
339	SrCuP and SrCuSb Zintl phases as potential thermoelectric materials. 2023 , 942, 169123	O
338	Comparison of thermal expansion path of the Fe2Mo Laves phase calculated using the DFT-based phonon and Debye-Grfieisen approaches. 2023 , 35, 105550	O
337	Combined piezoelectricity, valley splitting and DzyaloshinskiiMoriya interaction in Janus GdXY (X, Y = Cl, Br, I) magnetic semiconductors. 2023 , 25, 8600-8607	O
336	Terahertz spectroscopic characterization and DFT calculations of vanillin cocrystals with nicotinamide and isonicotinamide. 2023 , 25, 2038-2051	O
335	Efficient photocatalytic hydrogen evolution and CO2 reduction by HfSe2/GaAs3 and ZrSe2/GaAs3 heterostructures with direct Z-schemes. 2023 , 25, 8861-8870	2
334	Janus EPdXY (X/Y = S, Se, Te) materials with high anisotropic thermoelectric performance. 2023 , 15, 5964-5975	O
333	Ternary pentagonal BXN (X = C, Si, Ge, and Sn) sheets with high piezoelectricity. 2023 , 13, 9636-9641	О
332	The effect of magnetic order on the thermal transport properties of the intrinsic two-dimensional magnet 2H-VSe2. 2023 , 25, 9817-9823	O
331	Electron-phonon coupling, bipolar effect, and thermoelectric performance of the CuSbS2 monolayer.	О
330	Nonharmonic contributions to the high-temperature phonon thermodynamics of Cr. 2023, 107,	O
329	Enabling the transition to ductile MAX phases and the exfoliation to MXenes via tuning the A element. 2023 , 106, 3765-3776	O
328	Structure and Optical Properties of Polymeric Carbon Nitrides from Atomistic Simulations. 2023 , 35, 1547-1559	O
327	Effect of hydrostatic strain on the thermal conductivity of EsiC: A combined molecular dynamics and lattice dynamics investigation. 2023 , 38, 1634-1643	О
326	Structures and properties of uraniumBiobium intermetallic compounds under high pressure: A first principles study. 2023 , 133, 095901	O
325	Ab initio Boltzmann approach to coupled magnon-phonon thermal transport in ferromagnetic crystals. 2023 , 107,	O
324	Anharmonic Terms of the Potential Energy Surface: A Group Theoretical Approach.	1

323	Type-II van der Waals heterostructures of GeC, ZnO and Al2SO monolayers for promising optoelectronic and photocatalytic applications. 2023 ,	0
322	Theoretical exploration of the structure and physical properties of YbZn2X2 (X = N, P, As, Sb). 2023 , 124057	O
321	Electroluminescence, UV sensing, and pressure-induced conductance of Li+/Al3+ modified NiO: theoretical/experimental insights.	0
320	Pressure-induced enhancement of thermoelectric performance of CoP3 by the structural phase transition. 2023 , 248, 118773	O
319	Spin and current transport in the robust half-metallic magnet \$c\$-CoFeGe.	O
318	Investigating the structural, electronic, and elastic properties of Li-based quaternary Heusler alloy semiconductors using hybrid functional [HSE06 bandgap recalculations. 2023 , 150, 110479	O
317	Promising high temperature thermoelectric performance of layered oxypnictide YZnAsO. 2023 , 657, 414811	0
316	Magnetic and transport properties of two-dimensional ferromagnet VSe2 with Se vacancies. 2023 , 574, 170683	O
315	Theoretical studies of sliding ferroelectricity, magnetoelectric couplings, and piezo-multiferroicity in two-dimensional magnetic materials. 2023 , 818, 140430	0
314	Dehydration kinetics and mechanism of the stable isonicotinamide hydrate revealed by terahertz spectroscopy and DFT calculation. 2023 , 638, 122893	O
313	Prediction of new stable crystal structures for ternary ErAgTe2 and YAgTe2 semiconductors: Ab initio study. 2023 , 139, 107160	0
312	Thermal resistance from non-equilibrium phonons at Siße interface. 2023 , 34, 101063	O
311	Dependence of predicted bulk properties of hexagonal hydroxyapatite on exchangellorrelation functional. 2023 , 224, 112153	0
310	Structural phase stability and thermodynamical properties of transition metal complex hydrides Na2MgTMH7 (TM=Sctu) for hydrogen storage applications. 2023 , 321, 123867	O
309	Intrinsic Rashba effect and anomalous valley Hall effect in one-dimensional magnetic nanoribbon. 2023 , 573, 170662	0
308	First-principles analysis of the physical properties of XAcTe2 (X´=´Li, Na) Heusler alloys for optoelectronic and thermoelectric devices. 2023 , 224, 112156	O
307	Equilibrium fractionation of REE isotopes in nature: Insights from NRIXS and DFT+U studies of Eu and Dy phonon density of states. 2023 , 348, 323-339	0
306	Intriguing optical and photocatalytic properties of pentagonal penta-PtPS, -PtPSe and -PtPTe monolayers: A first-principle study. 2023 , 177, 111280	O

305	Surface alloy with sulfur leading piezoelectricity from non-piezoelectricity of pentagonal-PdPSe. 2023 , 947, 169640	1
304	Theoretical insight on the electronic band structure, mechanical, vibrational and thermodynamic characteristic of antiperovskites RE3InN (RE=Y and La). 2023 , 35, 105618	1
303	2D Mg2M2X5 (M´=´B, Al, Ga, In, Tl; X´=´S, Se, Te) monolayers: Novel stable semiconductors for water splitting photocatalysts. 2023 , 621, 156892	O
302	Correlation between spontaneous polarization and thermal conductivity in ferroelectric HfO2 from first principles. 2023 , 207, 123971	O
301	Nitrogen-doped or boron-doped twin T-graphene as advanced and reversible hydrogen storage media. 2023 , 622, 156895	0
300	Structural, electronic, elastic and thermal properties of Cr-doped U3Si2: A DFT study. 2023 , 579, 154388	O
299	Calculation of tunable electronic and optical properties of AlP/InSe heterostructure based on first principles. 2023 , 160, 107443	O
298	Physical and optoelectronic properties of double halide perovskites A2CuSbX6 (A´=´Cs, Rb, K; X´=´Cl, Br, I) based on first principles calculations. 2023 , 570, 111897	O
297	Pressure induced bands convergence and strength enhancement in thermoelectric semiconductor EnSe. 2023 , 947, 169687	O
296	NaCuX (X´=´Se, Te): Novel 2D materials simultaneously with ultra-low thermal conductivity and high thermoelectric figure of merit. 2023 , 35, 105987	O
295	Strain tuning of the electronic structure and optical properties of novel Janus MgBrI monolayer: Insights from first-principles calculations. 2023 , 35, e00802	O
294	Theoretical study on mechanical and electronic properties of ternary diborides Sc0.5V0.5B2, Sc0.5Nb0.5B2 and Sc0.5Ta0.5B2. 2023 , 35, 105760	O
293	Ab initio prediction of temperature-dependent stability of heterogeneous B19? phase in TiNi alloy using atomistically informed Eshelby ellipsoidal inclusion. 2023 , 35, 105861	O
292	The stability, mechanical, electronic and thermoelectric properties of unexplored monolayer Ca4Sb2O and Ca4Bi2O. 2023 , 212, 112008	O
291	First-principles studies on the structural, electronic and thermal transport characteristics of half-Heusler compounds LiXN (X=Mg, Zn). 2023 , 366-367, 115156	O
290	Trends in mechanical, anisotropic, electronic, and thermal properties of MAX phases: a DFT study on M2SX phases. 2023 , 35, 105759	O
289	Architecture design of novel carbon family: Polyhedra as building blocks. 2023, 11, 100256	0
288	Thermodynamic re-modeling of the Yb-Sb system aided by first-principles calculations. 2023 , 81, 102541	O

287	First-principles investigations of the crystal and electronic structures, dynamical and mechanical stabilities, Born effective charges and dielectric permittivities of a novel tetragonal zirconia. 2023 , 659, 414862	О
286	Theoretical investigation of the V2BX2 (X $=$ $\%$, Se, and Te) monolayers as anode materials for Na-ion batteries. 2023 , 35, 105923	Ο
285	Cubic and tetragonal phases competition of magnetic RuVZ(Si;Ge) Heusler compounds: ab initio investigation. 2023 , 366-367, 115161	Ο
284	First-principles investigation of two-dimensional magnesium chloride: Environmental stability and fundamental properties. 2023 , 151, 115715	O
283	Chiral phonons in binary compounds ABi (A = K, Rb, Cs) with P21. 2023 , 35, 105888	Ο
282	Prediction of novel final phases in aged uranium-niobium alloys. 2023 , 579, 154394	Ο
281	Two-dimensional van der Waals layered VSi2N4 as anode materials for alkali metal (Li, Na and K) ion batteries. 2023 , 178, 111339	0
280	DFT study of superlight ambient temperature reversible H2 storage media based on Li decorated on new planar BCN. 2023 , 622, 156947	Ο
279	Multi-functional lead-free Ba2XSbO6 (X´=´Al, Ga) double perovskites with direct bandgaps for photocatalytic and thermoelectric applications: A first principles study. 2023 , 35, 105617	0
278	Tuned electronic band structure and intensified phonon scattering of Ge2Sb2Te5 by strain engineering for thermoelectric performance. 2023 , 35, 105839	O
277	Band modification towards high thermoelectric performance of SnSb2Te4 with strong anharmonicity driven by cation disorder. 2023 , 154, 140-148	0
276	New Janus structure photocatalyst having widely tunable electronic and optical properties with strain engineering. 2023 , 155, 142-147	O
275	Observation of low thermal expansion behavior and weak thermal anisotropy in M3A2C phases. 2023 , 154, 210-216	0
274	Atomic diffusion in bcc FelMn alloys: Theoretical analysis and experimental measurements across the Curie temperature. 2023 , 251, 118883	O
273	Efficacy of pyrostilpnite (Ag3SbS3) mineral as thermoelectric material: A first principles study. 2023 , 162, 107513	0
272	Chemical ordering effects on martensitic transformations in Mg-Sc alloys. 2023 , 249, 118854	O
271	Equilibrium hydrogen isotope fractionation between portlandite/brucite and water: Implication from the vibrational spectra at elevated temperature and pressure. 2023 , 627, 121470	0
270	Strain driven anomalous anisotropic enhancement in the thermoelectric performance of monolayer MoS2. 2023 , 626, 157139	O

269	Decreasing the W-Cr solid solution decomposition rate: Theory, modelling and experimental verification. 2023 , 576, 154288	О
268	Theory of Energy Dispersion of Chiral Phonons. 2023 , 92,	1
267	Reversible Transformation and Distribution Determination of Diverse Pt Single-Atom Species. 2023 , 145, 2523-2531	0
266	Two-dimensional dual topological insulator in hexagonal IrO. 2023 , 25, 023010	O
265	Atomistic mechanism of high ionic conductivity in lithium ytterbium-based halide solid electrolytes: A first-principles study. 2023 ,	O
264	Revealing the decisive factors of the lattice thermal conductivity reduction by electron-phonon interactions in half-Heusler semiconductors. 2023 , 31, 100993	O
263	Realizing spontaneous valley polarization and topological phase transitions in monolayer ScX2 (X´=´Cl, Br, I). 2023 , 246, 118731	О
262	Bill monolayer as a promising 2D anode material for Li, Na, and K-ion batteries. 2023 , 25, 4980-4986	Ο
261	Half-Heusler phase TmNiSb under pressure: intrinsic phase separation, thermoelectric performance and structural transition. 2023 , 13,	0
260	Superconducting state of the van der Waals layered PdH2 structure at high pressure. 2023,	O
259	Novel ultrahard sp2/sp3 hybrid carbon allotrope from crystal chemistry and first principles: Body-centered tetragonal C6 (Eeoglitter) 2023, 133, 109747	О
258	Novel Boron-rich Phosphides with High Hardness, Large Strain, and Magnetism. 2023 , 14, 1310-1317	Ο
257	Pressure and temperature effects on (TiZrTa)C medium-entropy carbide from first-principles. 2023 , 2288-2300	1
256	Probing the Local Environment of Al-Substitution into Ferrihydrite Using DFT + U Calculations. 2023 , 127, 3285-3294	O
255	A DFT study of new full Heusler compound Li2MgC insights into the structural, electronic and thermoelectric properties: A high efficiency performance thermoelectric material. 2023 , 814, 140352	О
254	Surface-Enhanced Raman Spectroscopy (SERS) Chemical Enhancement in the Vibronically Coupled Langmuir Layer of Mixed Dichalcogenide 1T-MoSSe with Adsorbed R6G. 2023 , 127, 3131-3141	O
253	Electric-field-tunable thermal conductivity in anti-ferroelectric materials. 2023, 32, 100998	О
252	Thermodynamics modeling of ZrCo-H systems with biaxial compressive strain during desorption. 2023 , 577, 154301	Ο

251	First-Principles Study of Structural and Electronic Properties of Monolayer PtX2 and Janus PtXY (X, $Y = S$, Se, and Te) via Strain Engineering. 2023 , 8, 5715-5721	0
250	X2Pd3Se4 (X´=´K, Rb, Cs): Unexplored 2D semiconductors with high n-type transport performance. 2023 , 38, 100482	O
249	Monolayer Kagome metals AV3Sb5. 2023 , 14,	О
248	DFT study of Mg decorated on the planar B2N as a novel hydrogen storage media. 2023 , 46, 106263	О
247	Coupled Spin-Valley, Rashba Effect, and Hidden Spin Polarization in WSi2N4 Family. 2023, 14, 1494-1503	1
246	Pressure tuning of structure, magnetic frustration, and carrier conduction in the Kitaev spin liquid candidate Cu2IrO3. 2023 , 107,	О
245	Giant Rashba effect and nonlinear anomalous Hall conductivity in a two-dimensional molybdenum-based Janus structure. 2023 , 107,	0
244	Million-scale data integrated deep neural network for phonon properties of heuslers spanning the periodic table. 2023 , 9,	О
243	Synthesis of technetium hydride TcH1.3 at 27 GPa. 2023 , 107,	О
242	New High-Pressure Structures of Transition Metal Carbonates with O3CIIO3 Orthooxalate Groups. 2023 , 15, 421	О
241	High-Pressure Synthesis and Thermal Conductivity of Semimetallic Tantalum Nitride. 2212957	О
240	Interfacial interaction of monolayer MX2 (M=Mo, W; X=S, Se, Te)/SiO2 interfaces for composite optical fibers. 2023 , 37, 102739	O
239	Delocalized Bi-tetrahedral cluster induced ultralow lattice thermal conductivity in Bi3Ir3O11. 2023 , 32, 101005	O
238	Ab initio study of water dissociation on a charged Pd(111) surface. 2023 , 158, 094707	О
237	Strain Tunable Thermoelectric Material: Janus ZrSSe Monolayer. 2023 , 39, 2719-2728	О
236	Effect of Hydrostatic Pressure on Lone Pair Activity and Phonon Transport in Bi2O2S. 2023 , 6, 2401-2411	О
235	Thermal transport properties of two-dimensional boron dichalcogenides from first-principles and machine learning approach.	0
234	High-throughput computation of Raman spectra from first principles. 2023 , 10,	О

233	Cooperative diffusion in body-centered cubic iron in Earth and super-Earths Inner core conditions. 2023 , 35, 154002	1
232	Ab Initio Study on Stability, Electronic and Optical Properties of Monolayer Mo1\(\mathbb{R}\)WxSe2 Alloys. 2022 ,	О
231	Magnetoelastic interactions in SrCu2(BO3)2 studied by Raman scattering experiments and first principles calculations. 2023 , 107,	О
230	First-principles calculations to investigate structure and fundamental physical properties of BaM2As2 (M´=´Mg, Zn, Cd) and their alloys. 2023 , 23, 3284-3293	О
229	Two-Dimensional Octuple-Atomic-Layer M2Si2N4 (M = Al, Ga and In) with Long Carrier Lifetime. 2023 , 14, 405	О
228	Universal ion-transport descriptors and classes of inorganic solid-state electrolytes.	O
227	Monolayer group IV monochalcogenides T-MX ($M = Sn$, Ge ; $X = S$, Se) with fine piezoelectric performance and stability. 2023 , 122, 062903	О
226	Theoretical study of phonon and electron transport in low band gap Janus MXene monolayer MoWCO2 for thermoelectric application. 2023 , 122, 063902	O
225	Multiple Weyl and double-Weyl points in the phonon dispersion of P4332 BaSi2. 11,	О
224	Structural dynamics of Schottky and Frenkel defects in CeO2: a density-functional theory study. 2023 , 5, 025004	O
223	Phonon, electron, and magnon excitations in antiferromagnetic L10 -type MnPt. 2023, 107,	О
222	Thermal conductivity switch via the reversible 2H-1Tlphase transition in monolayer MoTe2.	O
221	Decay processes of long-lived phonons in 6H-SiC. 2023 , 35, 175701	О
220	First-principles study of the structural and electronic properties of tetragonal ZrOX (X = S, Se, and Te) monolayers and their vdW heterostructures for applications in optoelectronics and photocatalysis. 2023 , 158, 094708	O
219	First-principles study of the physical properties of Ti2SnX (X: C, N) based 211-MAX phases. 2023 , 568, 111850	О
218	Electronic and Excitonic Properties of MSi 2 Z 4 Monolayers. 2206444	О
217	Ferroelectricity and High Curie Temperature in a 2D Janus Magnet.	О
216	Quantum Anomalous Hall Effects Controlled by Chiral Domain Walls. 2023 , 40, 037502	O

215	First-principles study on the thermoelectric properties of Sr2Si and Sr2Ge. 2023 , 32, 101015	О
214	Surface Tamm States of 2B nm Nanodiamond via Raman Spectroscopy. 2023 , 13, 696	О
213	Effects of hydrostatic pressure on the thermoelectric performance of BaZrS3. 2023, 138,	О
212	High Curie temperature Chern insulator and spin-gapless semiconducting ferromagnetic h-CrC monolayer: A first-principles study. 2023 , 220, 112070	O
211	Melting of MgSiO3 determined by machine learning potentials. 2023, 107,	O
2 10	Electrochemical Conversion of Cu Nanowire Arrays into Metal-Organic Frameworks HKUST-1. 2023 , 170, 022506	O
209	Phonons, magnons and lattice thermal transport in 2H-NbSe2: A first principles study. 2023 , 655, 414739	О
208	Triggering superconductivity, semiconducting states, and ternary valley structure in graphene via functionalization with Si-N layers. 2023 , 107,	O
207	Ab Initio Study of the Raman Spectra of Amorphous Oxides: Insights into the Boson Peak Nature in Glassy TeO 2. 2023 , 17,	О
206	An overview of 2D metal sulfides and carbides as Na host materials for Na-ion batteries. 2023 , 461, 141924	O
205	Double-perovskite van der Waals heterostructure Cs2NaInCl6-XS2 (X=Cr, Mo, W) as great potential material in photovoltaic devices. 2023 , 37, 102734	0
204	Correlation-Driven Topological Transition in Janus Two-Dimensional Vanadates. 2023 , 16, 1649	O
203	Computational insight into structural, electronic and thermal properties of novel two-dimensional NiXO (X´=´Cl, Br) monolayers: Ab initio perspective. 2023 ,	О
202	Emergence of Rashba-/Dresselhaus effects in Ruddlesden P opper halide perovskites with octahedral rotations. 2023 , 35, 174001	O
201	Surface-induced ferromagnetism and anomalous Hall transport at Zr2S(001). 2023, 7,	0
200	Effect of intrinsic point defects on the catalytic and electronic properties of Cu2WS4 single layer: Ab initio calculations. 2023 , 7,	O
199	High-Temperature Equilibrium of 3D and 2D Chalcogenide Perovskites. 2201078	О
198	Mechanical and electronic properties of transition metal hexa-nitrides in hexagonal structure from density functional theory calculations. 2023 , 221, 112084	О

197	Abnormal thermal expansion coefficients in (Nd 1 $\bar{l}k$ Dy x) 2Zr 2O 7 pyrochlore: The effect of low-lying optical phonons. 2023 , 1-14	0
196	Structural ordering governs stiffness and ductile-to-brittle transition in Alli alloys. 2023, 158, 104303	O
195	First-Principles Study of the Structural, Mechanical and Thermodynamic Properties of Al11RE3 in Aluminum Alloys. 2023 , 13, 347	1
194	Two-dimensional XY ferromagnetism above room temperature in Janus monolayer V2XN ($X = P$, As). 2023 , 25, 9311-9319	0
193	Effects of NH4+ doping on the hydrogen storage properties of metal hydrides. 2023,	0
192	Optical Effect Modulation in Polarized Raman Spectroscopy of Transparent Layered &MoO 3. 2206932	O
191	Stable Rb-B compounds under high pressure. 2023 , 5,	0
190	First-principles study of crystal structure search, stability and mechanical property of magnesium-lithium binary system. 2023 , 98, 045801	0
189	Isotope Effects on the Optical Phonons of Cubic Boron Phosphide. 2200585	0
188	Effects of Temperature Induced Phase Transition in Bulk CdS Structures. 2022,	Ο
187	Evidence of high-temperature exciton condensation in a two-dimensional semimetal. 2023, 14,	0
186	Comprehensive study on electronic structures of SiGe/Ga\$\$_{2}\$\$SeTe vdW heterobilayer. 2023 , 58, 4020-4030	Ο
185	The First-Principles Investigation of Structural Stability, Mechanical, Vibrational, Thermodynamic, and Optical Properties of CaHfS3 for Optoelectronic Application. 2023 , 2023, 1-13	0
184	Anharmonic lattice dynamics and the origin of intrinsic ultralow thermal conductivity in AgI materials. 2023 , 107,	O
183	Tunable magnetic interactions in mono-transition metal spinels MgCr2X4′(X=O,S,Se). 2023 , 7,	O
182	Strain-Induced Ferroelectric Phase Transition in Group-V Monolayer Black Phosphorus. 2023, 6,	O
181	Rattling-induced suppression of thermal transport in cubic In2O3 with Sn-Ga diatomic defect. 2023 , 35, 195701	0
180	Maximally charged single-pair multi-Weyl point phonons in P23 -type BeH2. 2023, 107,	O

179	Electronic, Optical, Mechanical, and Electronic Transport Properties of SrCu2O2: A First-Principles Study. 2023 , 16, 1829	0
178	Thermodynamic stability of Li B C compounds from first principles. 2023 , 25, 7344-7353	O
177	Rapid prediction of phonon structure and properties using the atomistic line graph neural network (ALIGNN). 2023 , 7,	0
176	Coupling between Charge Density Wave Ordering and Magnetism in Ho2Ir3Si5. 2023 , 35, 1980-1990	O
175	Hybrid nodal-chain semimetal with emergent flat band in MgCaN2. 2023, 25, 033005	O
174	High thermoelectric performance of layered LaAgXO (X=Se,Te) from electrical and thermal transport calculations. 2023 , 7,	O
173	Physical Insights on the Phonon Dispersion of TiS 2. 2200821	0
172	Phase formation of powders sputtered from X2BC targets and XC+XB powder mixtures $\{X = Nb, Ta, W\}$. 2023 , 458, 129379	O
171	Ab-initio study of C2/c, Cmca-12, Pbcn and P6122 phases of solid hydrogen. 2023 , 655, 414772	O
170	Understanding photoluminescence of bismuth-doped ternary alkaline earth d10 metal oxides via first-principles calculations. 2023 , 107,	O
169	First-Principles Investigation on Phonon Mode Conversion of Thermal Transport in Silicene Under Tensile Strain. 2023 , 44,	O
168	Strain effect on the high T c superconductor YBa2Cu3O7: an ab initio study comparing bulk and monolayer models. 2023 , 5, 015002	O
167	Phase diagram and thermoelastic property of iron oxyhydroxide across the spin crossover under extreme conditions. 2023 , 107,	1
166	Magnesium oxide-water compounds at megabar pressure and implications on planetary interiors. 2023 , 14,	O
165	First Principles Computation of New Topological B2X2Zn (X = Ir, Rh, Co) Compounds. 2023 , 6, 152-163	0
164	Revisiting the Storage Capacity Limit of Graphite Battery Anodes: Spontaneous Lithium Overintercalation at Ambient Pressure. 2023 , 2,	O
163	Anharmonic phonon renormalization and two-channel thermal transport in SrTiO3 using full temperature-dependent interatomic force constant. 2023 , 467, 128727	0
162	Structural-Stability Study of Antiperovskite Na 3 OCl for . 2023 , 19,	O

161	Significantly reinforced thermoelectric performance in the novel 1T-Au6Se2 monolayer. 2023, 11, 031103	O
160	Density functional theory study of Zn(1☑)FexSe: Electronic structure, phonon, and magnetic properties. 2023 , 13, 035102	O
159	Strain induced metal-semiconductor transition in two-dimensional topological half metals. 2023 , 26, 106312	Ο
158	How to validate machine-learned interatomic potentials. 2023 , 158, 121501	O
157	Study of optoelectronic and thermoelectric properties of double perovskites X2HfI6 (X = Ga, In, Tl) for renewable energy. 2023 , 98, 045814	О
156	Extremely promising monolayer materials with robust ferroelectricity and extraordinary piezoelectricity: PAsN, PSbN, and PBiN. 2023 , 15, 6363-6370	O
155	Two-Dimensional AMgB (A = Na, K; B = P, As, Sb, Bi) with Promising Optoelectronic and Thermoelectric Performances. 2023 , 5, 1405-1419	Ο
154	First-principles-based simulation of the electrocaloric effect. 2023 , 63-91	O
153	Exploring and machine learning structural instabilities in 2D materials. 2023 , 9,	0
152	Nanowires exfoliated from one-dimensional van der Waals transition metal trihalides and quadrihalides. 2023 , 5, 2096-2101	Ο
151	Mechanical properties and magnetic and electronic properties tuned via strain in two-dimensional non-van der Waals hematene. 2023 , 2, 100061	0
150	Ab-initio predictions of mechanical, electronic, magnetic, and transport properties of bulk and heterostructure of a novel Fe-Cr based full Heusler chalcogenide. 2023 , 178, 111307	Ο
149	Truncated atomic plane wave method for subband structure calculations of moir systems. 2023 , 107,	0
148	Uncertainty-aware molecular dynamics from Bayesian active learning for phase transformations and thermal transport in SiC. 2023 , 9,	O
147	Two-Dimensional Carbon Networks with a Negative Poisson Ratio. 2023, 13, 442	Ο
146	C3N2: the missing part of highly stable porous graphitic carbon nitride semiconductors.	Ο
145	The versatile characteristics of Ars/SGaInS van der Waals heterostructures.	Ο
144	Effect of hydrostatic strain on the mechanical properties and topological phase transition of bi-alkali pnictogen NaLi2Bi. 2023 , 98, 045905	O

143	Profiling the off-center atomic displacements in CuCl at finite temperatures with a deep-learning potential. 2023 , 7,	0
142	Tuning the mechanical anisotropy of biphenylene by boron and nitrogen doping. 2023 , 222, 112119	O
141	A general-purpose machine learning Pt interatomic potential for an accurate description of bulk, surfaces, and nanoparticles. 2023 , 158, 134704	0
140	Mismatched atomic bonds and ultralow thermal conductivity in Ag-based ternary chalcopyrites. 2023 , 107,	O
139	Intrinsic Instability of Rhombohedral (Hf, Zr)O2 Phases and Endurance Crisis of Hf-based Ferroelectric Devices.	0
138	Two-Dimensional Iron Silicide (FeSix) Alloys with Above-Room-Temperature Ferromagnetism. 2023 , 23, 2332-2338	Ο
137	Modulating the Combinatorial Target Power of MgSnN2 via RF Magnetron Sputtering for Enhanced Optoelectronic Performance: Mechanistic Insights from DFT Studies.	0
136	Depolarization induced IIIIV triatomic layers with tristable polarization states.	О
135	Controlled synthesis of monodispersed ZnSe microspheres for enhanced photo-catalytic application and its corroboration using density functional theory. 2023 , 25, 10567-10582	0
134	Systematic atomic structure datasets for machine learning potentials: Application to defects in magnesium. 2023 , 107,	O
133	Electron P honon Interaction Contribution to the Total Energy of Group IV Semiconductor Polymorphs: Evaluation and Implications. 2023 , 8, 11251-11260	0
132	Fluence dependent dynamics of excitons in monolayer MoSi2Z4 (Z = pnictogen). 2023 , 35, 235701	O
131	Anomalous interlayer exciton diffusion in WS2/WSe2 moir[heterostructure.	0
130	Tensile strain and finite size modulation of low lattice thermal conductivity in monolayer TMDCs (HfSe2 and ZrS2) from first-principles: a comparative study. 2023 , 25, 9225-9237	O
129	Indirect Exciton Phonon Dynamics in MoS 2 Revealed by Ultrafast Electron Diffraction. 2206395	0
128	Study of pnictides for photovoltaic applications. 2023 , 25, 9626-9635	O
127	First-Principles Study on Thermoelectric Properties of Bi\$\$_2\$\$O\$\$_2\$\$Se.	0
126	Investigating the role of phonons in the phase stability of uranium-based Laves phases. 2023, 13, 8646-8656	Ο

125	Theoretical design of a photodetector based on a two-dimensional SnSe2/GaP type-II heterostructure. 2023 , 25, 2326-2338	О
124	Heterogeneous intercalated metal-organic framework active materials for fast-charging non-aqueous Li-ion capacitors. 2023 , 14,	О
123	Ferroelectric and negative piezoelectric properties in oxyhydroxide monolayers $EXOOH$ (X = Al, Ga, and In).	О
122	Lattice dynamics and in-plane antiferromagnetism in MnxZn1NPS3 across the entire composition range. 2023 , 107,	О
121	Spin-phonon interaction and short-range order in Mn3Si2Te6. 2023 , 107,	0
120	Absorption Modulation and Anomalous Thermal Transport in Two-dimensional X-AlN(X=C,Si,TC) Semiconductor. 2023 , 0	О
119	Van der Waals Stacked 2D-Layered Co2Ge2Te6 with High Curie Temperature and Large Magnetic Crystal Anisotropy. 2023 , 127, 5991-6001	О
118	First-principles study of ferroelectricity, antiferroelectricity, and ferroelasticity in two-dimensional BAlOOH. 2023 , 107,	О
117	Enhanced Curie temperature in partially decorated CrSnSe3 monolayer with alkali metals (Li, Na, and K). 2023 , 25, 9437-9444	О
116	DFT characterization of a new possible two-dimensional BN allotrope with a biphenylene network structure.	О
115	Enhancement in the Thermoelectric Performance of SnS Monolayer by Strain Engineering. 2023, 6, 3944-3	952 o
114	Theoretical study on structural and mechanical properties of Si-containing ternary transition metal nitrides M0.5Si0.5N (M = Ti, Zr, Hf). 2023 , 13, 9109-9118	О
113	Oxygen isotope effect in VO2. 2023 , 107,	О
112	Hard-breakable Ohmic contact in 2D CrSi2N4-metal heterostructures: A DFT study. 2023 , 13, 035127	O
111	Investigating magnetic van der Waals materials using data-driven approaches.	О
110	Symmetry-Enforced 2D Hourglass Phononic Nodal Net.	O
109	Resonant exciton scattering reveals Raman forbidden phonon modes in layered GeS.	О
108	Ab Initio Study of the Electronic Structure and Lattice Dynamics of Scheelite Type AgTcO4.	O

107	Effect of Pressure on VTe2/NbTe2 Heterostructure in Photonic Applications: A First-Principles Study. 2023 ,	0
106	Experimental and theoretical thermodynamic studies in Ba2MgReO6the ground state in the context of Jahn-Teller effect. 2023 , 35, 245603	O
105	Enhanced Thermoelectric Performance of Nanostructured Cu2SnS3 (CTS) via Ag Doping. 2023 , 6, 6323-6333	О
104	Nanoscale thermal interface rectification in the quantum regime. 2023 , 122, 122204	О
103	Strong Scattering from Low-Frequency Rattling Modes Results in Low Thermal Conductivity in Antimonide Clathrate Compounds. 2023 , 35, 2918-2935	О
102	Thermoelectric response of 1T-ZrS2 monolayer: Ab-initio study. 2023 ,	О
101	PtTe2/Sb2S3 Nanoscale Heterostructures for the Photocatalytic Direct Z-Scheme with High Solar-to-Hydrogen Efficiency: A Theoretical Investigation. 2023 , 6, 5591-5601	О
100	Accelerated Perovskite Oxide Development for Thermochemical Energy Storage by a High-Throughput Combinatorial Approach. 2203833	O
99	First-principles study of the lattice thermal conductivity of the nitride perovskite LaWN3. 2023 , 107,	О
98	Automatic differentiation for orbital-free density functional theory. 2023 , 158, 124801	O
97	Abnormal phonon angular momentum due to off-diagonal elements in the density matrix induced by a temperature gradient. 2023 , 107,	0
96	lodine Vacancies do not Cause Nonradiative Recombination in Halide Perovskites. 2023 , 2,	O
95	Dynamics of photoinduced ferromagnetism in oxides with orbital degeneracy. 2023 , 5,	О
94	Spin P honon Interactions and Anharmonic Lattice Dynamics in Fe 3 GeTe 2. 2200089	Ο
93	First-principles study on the optoelectronic properties of the quasi-one-dimensional flexible semiconductor K2PdPS4I. 2023 , 47, 106396	O
92	Physics guided deep learning for generative design of crystal materials with symmetry constraints. 2023 , 9,	O
91	Lattice Thermal Transport of BAs, CdSe, CdTe, and GaAs: A First Principles Study. 2023 , 52, 3401-3412	0
90	Magnetism and charge density wave order in kagome FeGe.	О

89	Structural, mechanical and thermal properties of cubic bixbyite-structured high-entropy oxides. 2023 , 464, 142649	О
88	Ab Initio Prediction of Ultra-Wide Band Gap B x Al 1៤ N Materials.	Ο
87	Evaluating the harmonic approximation for the prediction of thermodynamic formation properties of solids. 2023 , 223, 112152	0
86	Intersite Coulomb Interactions in Charge-Ordered Systems. 2023 , 130,	Ο
85	Unraveling the role of Sm 4f electrons in the magnetism of SmFeO3. 2023 , 107,	0
84	Ferromagnetic vanadium disulfide VS2 monolayers with high Curie temperature and high spin polarization. 2023 , 25, 10143-10154	O
83	First-Principles Calculation of the Temperature-Dependent Transition Energies in Spin Defects. 2023 , 14, 3266-3273	0
82	Alloyed triple half-Heuslers: a route toward high-performance thermoelectrics with intrinsically low lattice thermal conductivity.	Ο
81	Photoinduced control of ferroelectricity in hybrid-improper ferroelectric superlattices. 2023, 107,	Ο
80	Radiation Resistance and Adsorption Behavior of Aluminum Hexacyanoferrate for Pd. 2023 , 11, 321	Ο
79	Straight and twisted open nodal-line phonon states in the CaI2 family of materials. 2023, 25, 10561-10566	0
78	Chemical Aspect of Displacive-Type Ferroaxial Phase Transition from Perspective of Second-Order Jahn Teller Effect: NASICON Systems as an Example. 2023 , 145, 8090-8098	Ο
77	On-the-fly machine learning potential accelerated accurate prediction of lattice thermal conductivity of metastable silicon crystals. 2023 , 7,	0
76	Magnetic iron-cobalt silicides discovered using machine-learning. 2023, 7,	Ο
75	Two-dimensional rare-earth Janus 2HthdXY′(X,Y=Cl,Br,I;´. 2023 , 107,	Ο
74	Pressure-Induced Structural Phase Transition and Enhanced Interlayer Coupling in Two-Dimensional Ferromagnet CrSiTe3. 2023 , 14, 3320-3328	Ο
73	First-principles investigation on the structural, vibrational, mechanical, electronic, and optical properties of MSi2Z4 (M : Pd and Pt, . 2023 , 7,	0
72	Influence of spin fluctuations on structural phase transitions of iron. 2023 , 107,	O

71	First-principles study of electronic, mechanical and piezoelectric properties of Janus MoSH. 1-15	O
70	Activating the paddle-wheel effect towards lower temperature in a new sodium-ion solid electrolyte, Na3.5Si0.5P0.5Se4.	o
69	Structural, Electronic Properties, and Relative Stability Studies of Low-Energy Indium Oxide Polytypes Using First-Principles Calculations. 2023 , 8, 12928-12943	0
68	Green Diamond: A Superhard Boron Carbonitride with Bandgap in Green-Light Region and Anisotropic High Carrier Mobilities. 2023 , 14, 3403-3412	O
67	Coherent Phonon-Induced Modulation of Charge Transfer in 2D Hybrid Perovskites.	0
66	A simulation study on the phase transition behavior of solid nitrogen under extreme conditions.	o
65	Promising anode materials for alkali metal ion batteries: a case study on cobalt anti-MXenes.	0
64	Giant Pressure-Induced Spectral Shift in Cyan-Emitting Eu 2+ -Activated Sr 8 Si 4 O 12 Cl 8 Microspheres for Ultrasensitive Visual Manometry.	O
63	Pressure-induced superconductivity in the photoelectric semiconductor BiSeI. 2023, 107,	O
62	Nonvolatile electrical control of spin polarization in the 2D bipolar magnetic semiconductor VSeF. 2023 , 9,	O
61	Theoretical Prediction of the Sublimation Behavior by Combining Ab Initio Calculations with Statistical Mechanics. 2023 , 16, 2826	0
60	Semiconducting nonperovskite ferroelectric oxynitride designed ab initio. 2023 , 122, 142902	O
59	Spontaneous spin and valley polarizations in a two-dimensional Cr2S3 monolayer. 2023 , 133, 134301	0
58	C4N4: A symmetry-protected semimetal. 2023 , 224, 112165	O
57	Relative Stability of Pyrazinamide Polymorphs Revisited: A Computational Study of Bending and Brittle Forms Phase Transitions in a Broad Temperature Range. 2023 , 13, 617	0
56	Machine-learning-assisted discovery of boron-doped graphene with high work function as an anode material for Li/Na/K-ion batteries.	o
55	Two-dimensional ferromagnetic semiconductors of rare-earth Janus 2H-GdIBr monolayers with large valley polarization.	0
54	The effects of intercalated environmental gas molecules on carrier dynamics in WSe2/WS2 heterostructures.	О

53	First-Principles Insights into the Relative Stability, Physical Properties, and Chemical Properties of MoSe2. 2023 , 8, 13799-13812	О
52	Atomic-scale origin of the low grain-boundary resistance in perovskite solid electrolyte Li0.375Sr0.4375Ta0.75Zr0.25O3. 2023 , 14,	О
51	Effect of magnon-magnon interaction on ferromagnetism in hexagonal manganese pnictide monolayers. 2023 , 107,	0
50	Bulk Synthesis and Transport Properties of Rocksalt-Type Ti1\(\text{MMgxN} \) Solid Solution. 2023 , 62, 5951-5960	О
49	Hydrogen anion as a strong magnetic mediator for obtaining high-temperature ferromagnetic semiconductors: The case of hydride double perovskites. 2023 , 107,	0
48	Robust half-metallicity and topological properties in square-net potassium manganese chalcogenides. 2023 , 107,	O
47	Competition between phonon-vacancy and four-phonon scattering in cubic boron arsenide by machine learning interatomic potential. 2023 , 7,	0
46	Topotactic hydrogen forms chains in ABO2 nickelate superconductors. 2023 , 107,	О
45	Effects of fission product doping on the structure, electronic structure, mechanical and thermodynamic properties of uranium monocarbide: A first-principles study. 2023 ,	0
44	Influence of alkaline-earth metals (B = Be, Mg, Ca) doping on the structural, electronic, optoelectronic, thermodynamic, and core-level spectroscopic studies of CsBCl3 halide perovskites. 2023 , 58, 6656-6676	О
43	Magnetic bond-order potential for iron-cobalt alloys. 2023, 7,	0
42	Potential high-temperature superconductivity in the substitutional alloy of (Y,Sr)H11 under high pressure. 2023 , 107,	O
41	Revealing stability origin of Dion-Jacobson 2D perovskites with different-rigidity organic cations. 2023 ,	0
40	Exploring the High-Temperature Stabilization of Cubic Zirconia from Anharmonic Lattice Dynamics.	O
39	Computational simulation of self-cleaning carbon-based membranes with zeolite porous structure for desalination. 2023 , 136, 109925	0
38	Artificial Intelligence Guided Studies of van der Waals Magnets.	O
37	Stacking effect on the electronic structures of hexagonal GaTe.	0
36	Electrical tuning of robust layered antiferromagnetism in MXene monolayer. 2023, 122, 162403	O

35	Ab initio derived force field potential for the accurate simulation of thermal transport in AlN. 2023,	О
34	Structural transitions at high pressure and metastable phase in Si0.8Ge0.2. 2023, 170180	Ο
33	MatHub-2d: A database for transport in 2D materials and a demonstration of high-throughput computational screening for high-mobility 2D semiconducting materials.	0
32	Superior hydrogen storage capacity of Vanadium decorated biphenylene (Bi+V): A DFT study. 2023 ,	O
31	Two-dimensional T?-phase MA2N. 2023 , 157256	O
30	Probing the effect of ordered carbon vacancy on the thermophysical properties of VC1-x: A comprehensive first-principles calculations. 2023 ,	O
29	Weak Electron-Phonon Renormalization Effect Caused by the Counteraction of the Different Phonon Vibration Modes in FeS2.	0
28	Impact of Vacancies in Monolayer \$1mathrm{T}-text{TiTe}_{2}\$ for Optoelectronic and Spintronic Applications: A First-Principles Study. 2023 ,	O
27	Effect of crystal field engineering and Fermi level optimization on thermoelectric properties of Ge1.01Te: Experimental investigation and theoretical insight. 2023 , 7,	O
26	Strain-Induced Medium-Temperature Thermoelectric Performance of Cu4TiSe4: The Role of Four-Phonon Scattering. 2023 , 19,	O
25	Electronic properties and photocatalytic water splitting with high solar-to-hydrogen efficiency in a hBNC/Janus WSSe heterojunction: First-principles calculations. 2023 , 107,	O
24	Tunable Schottky contacts in graphene/XAu4Y (X, Y = Se, Te) heterostructures.	O
23	Distinct ferrovalley characteristics of the Janus RuClX ($X = F, Br$) monolayer.	O
22	A first principles study on physical properties of Nb-doped LiCoO2 for memristor (CM-3:IL02). 2023 ,	O
21	High-Throughput Design of Magnetocaloric Materials for Energy Applications: MM·X alloys.	0
20	Optimizing Superconductivity: From Cuprates via Nickelates to Palladates. 2023 , 130,	O
19	Magneto-optical Kerr Effect in Ferroelectric Antiferromagnetic Two-Dimensional Heterostructures.	0
18	Resonant Exciton Scattering Reveals Raman Forbidden Phonon Modes in Layered GeS. 3986-3994	O

CITATION REPORT

17	Characterizing Grain Boundary Effects on Mg2+ Conduction in Metal Drganic Frameworks.	0
16	Unconventional Charge-Two Weyl Phonons in High-Symmetry Lines.	O
15	Full optimization of quasiharmonic free energy with an anharmonic lattice model: Application to thermal expansion and pyroelectricity of wurtzite GaN and ZnO. 2023 , 107,	O
14	First-principles study on the high-pressure physical properties of orthocarbonate Ca 2 CO 4.	O
13	Efficient separation and recovery process of Pd(II) based on sintering-leaching method by silica-based aluminum hexacyanoferrate. 2023 , 410, 137290	0
12	Tunable electronic and optical properties of MoTe2/InSe heterostructure via external electric field and strain engineering. 2023 , 35, 315501	O
11	Theoretical Study of Stability of Halogen-Defective Trihalide Monolayers: Cases of Ali $\bf 3$, Asi $\bf 3$, and IrBr $\bf 3$.	0
10	Non-Centrosymmetric 2D Nb 3 Sel 7 with High In-Plane Anisotropy and Optical Nonlinearity.	O
9	Ternary GePdS3: 1D van der Waals Nanowires for Integration of High-Performance Flexible Photodetectors. 2023 , 17, 8743-8754	0
8	Ab initio study of phononic thermal conduction in ScAgC half-Heusler. 2023, 96,	O
7	Janus monolayer TaNF: A new ferrovalley material with large valley splitting and tunable magnetic properties. 2023 , 18,	0
6	A two-dimensional kagome magnet with tunable topological phases. 2023 , 30, 101566	O
5	Role of anharmonicity in phonon-mediated superconductivity of quasi- van der Waals layered XP2 (X´=´As, Sb, Bi) structures: Insight from first-principles calculations. 2023 , 959, 170440	0
4	Pressure-induced antiferromagnetic-tetragonal to nonmagnetic-collapse-tetragonal insulator-metal transition in ThMnAsN.	O
3	Li-ion transport in solid-state electrolyte of Li1₪Al1₪Si2+xO6: an ab initio study.	0
2	Elastemp IA workflow to compute the quasi-harmonic temperature dependent elastic constants of materials. 2023 , 226, 112223	O
1	Accurate prediction of short-range order and its effect on thermodynamic, structural, and electronic properties of disordered alloys: exemplified in archetypical Cu3Au. 2023 , 106214	0